Structural Analysis and Design of Floating Wind Turbine Systems

By

Joshua Di Pietro

B.S. Naval Architecture and Marine Engineering United States Coast Guard Academy, 2005

Submitted to the Department of Mechanical Engineering in Partial Fulfillment of the Requirements for the Degrees of

Master of Science in Mechanical Engineering
Master of Science in Naval Architecture and Marine Engineering
at the
MASSACHUSETTS INSTITUTE OF TECHNOLOGY
JUNE 2009

Author:.....

LTjg Joshua M Di Pietro
Department of Mechanical Engineering
May 8,2009

Certified by:.....

Paul D. Sclavounos
Professor of Mechanical Engineering and Naval Architecture
Thesis Supervisor

Certified by:.....

Trent R. Gooding
Associate Professor of the Practice
Naval Construction and Engineering Program (Course 2N)
Thesis Reader

Accepted by:.....

David E. Hardt
Professor of Mechanical Engineering
Chairman, Committee on Graduate Students

Page Intentionally Left Blank

Structural Analysis and Design of Floating Wind Turbine Systems

By

LTjg Joshua M. Di Pietro, USCG

Submitted to the department of Mechanical Engineering

on May 8, 2009 in partial fulfillment of the

Requirements for the degrees of

Master of Science in Mechanical Engineering
and
Master of Science in Naval Architecture and Marine Engineering

Abstract

As oil supply rates approach potential maximums and the global detrimental effects of carbon emitting energy technology are becoming more comprehensively understood, the world is searching for environmentally benign energy technology which can be reliably and economically harvested. Deep water offshore wind is a vast, reliable and potentially economical energy source which remains globally untapped. In order to harvest this resource, potential floating turbine systems must be analyzed and designed for economic production and deployment, reliable operation, and adequate service life.

The Laboratory of Ship and Platform Flow (LSPF) has created trusted hydrodynamic modeling software used to perform a Pareto Optimization which resulted in an optimized Floating Wind Turbine (FWT) design which is a Tension Leg Platform (TLP); hereto called MIT TLP-1. This thesis details the structural design aspects of Floating Wind Turbines (FWT) in a rationally based optimization approach for incorporation into existing LSPF hydrodynamic optimization approaches. A steel structural design is created based on the geometry and loading of the MIT TLP-1 for a 10m significant wave height. The design is based on similar system analysis, classic linear structural theory, American Bureau of Shipping rules and American Petroleum Institute recommended practices. The design is verified using Finite Element Analysis (FEA). The results of this work show that the MIT TLP-1 design is technically feasible from a structural integrity, performance and producibility standpoint.

Thesis Supervisor: Paul D. Sclavounos

Title: Professor of Mechanical Engineering and Naval Engineering

Page Intentionally Left Blank

1 Acknowledgements

I would like to express my sincere gratitude to my thesis advisor, Professor Paul D. Sclavounos for his guidance and the wealth of knowledge he imparted on me during this research project. His energy and enthusiasm for such a wonderful project are contagious. I am grateful to have had the opportunity to work with a man who has had so much influence on marine hydrodynamics and the current state of offshore wind.

My education at MIT was made possible by my employer the United States Coast Guard. I consider myself blessed to be associated with an organization which invests so much in its people, and believes in the value of higher education.

My friends and colleagues at the Laboratory for Ship and Platform Flow have been tremendous. Sungho Lee has been instrumental in so many parts of this work and has constantly offered his help, expertise and general good will throughout my time at the Laboratory for Ship and Platform Flow. I would like to thank Per Einer Ellefsen for his support and assistance throughout the long hours of research. Ned Carpenter has been a tremendous UROP, I am grateful for the investments he has made in this work, often times at the detriment of his required undergraduate classes.

2 Table of Contents

Introduction

3.1 Introduction and Motivation

As oil supply rates approach potential maximums and the global detrimental effects of carbon emitting energy technology are becoming more comprehensively understood, the world is searching for environmentally benign energy technology. This alternative energy must be reliably and economically harvested. Over the last 10 years wind power has been the fastest-growing clean energy technology. [6]

Wind energy's rapid growth during the current decade reflects its fulfillment of societies' modern energy needs. Wind energy, and especially offshore wind energy is currently one of the most environmentally benign forms of energy generation. It is a free, inexhaustible, environmentally friendly, utility scale and cost effective energy source.

As wind energy continues to grow, onshore resources located close to population centers with wind profiles substantial enough to become economical are becoming scarcer. National Renewable Energy Lab (NREL) preliminary studies indicate a total U.S. offshore wind potential exceeding 1TW. [5] Much of this wind resource is located in water depths of over 50m, which is not economical for current offshore wind technology, which relies on monopole structures driven into the seafloor.

This vast wind resource located in deep water has many desirable attributes which offset the potential increases in costs associated with a more complex wind turbine system. A brief list of the benefits of offshore wind are listed in Table 3.1

Wind a rapidly growing, free, inexhaustible, environmentally friendly, utility scale and cost effective energy eource
Vast offshore wind resources with higher and steadier wind speeds in deeper waters
Over 75% of worldwide power demand from coastal areas
Wind power output increases with cube of wind speed
Lower offshore wind turbulence – longer farm life ~ 25-30 years
Connection to electric grid by sub sea AC or HVDC cables
Experience of oil industry essential for the development of safe and cost effective spar and tlp wind turbine floaters
Floating wind turbines provide infrastructure for arrays of wave energy converters in waters depths over ~ 40m with significant wave power density

Table 3.1-Benefits of Floating Wind

In addition to the benefits listed in table 3.1, a major benefit of far offshore deepwater wind turbines is that there is a lower barrier to entry in many cases. One major barrier to entry in the offshore wind turbine industry is environmental regulation due to concerns over marine migratory bird mortality due to blade strikes. In order to get building permits, currently most sites will require expensive bird strike studies. As farms are pushed farther away from the coast, the presence of migratory birds, which travel along the coast, disappears, alleviating much of the bird strike concern.

Coastal communities reject many of the recently proposed projects that are considered unsightly blemishes on their pristine coastal horizons. Far offshore, deepwater wind turbines alleviate this form of resistance from the community. If placed far enough off of the coast they disappear from the horizon, due to the curvature of the earth. Equation 3.1 may be used to calculate the distance from shore required for the NREL 5 MW turbine to be below the horizon.

(3.1)

L Distance from Shore for Turbine to be Invisible
H Max Height of Turbine Blade Tip (90 + 65=155 m)
R Earth Radius (~ 6,370,000 m)

$$L = \sqrt{2HR}$$

L = 28 miles (45 Km) (H=155m - Blade Tip)
L = 21 miles (34 Km) (H=90m -Hub)

The Massachusetts Institute of Technology Floating Wind Turbine Project, (MIT FWT), began in response to the desirable attributes of the deep water FWT, listed above, and the current lack of any utility scale floating wind farms. The project has been developed by Professor P.D. Sclavounous and his graduate students in the laboratory for Ships and Platform Flow (LSPF). The goals of the MIT FWT project are to create the optimal design of a Floating Wind Turbine in terms of cost and performance, to be used in locations whose water depths exceed the threshold depth for which fixed monopole structures are economical.

3.2 Previous Work

This structural design study of the MIT TLP-1 is one of the last steps in an elaborate project aimed at the optimal design of deep offshore wind. The principle dimensions, motions and hydrodynamic loads of the FWTs which form the input for the present study were yielded from the research of previous LSPF students. The general aim and results of each of the founding works are briefly presented below.

3.2.1 National Renewable Energy Lab

The National Renewable Energy Lab (NREL) Wind Energy Division, worked closely with the MIT FWT project throughout the life of the project. The results of NREL's studies have often provided valuable information that allows the direction to the MIT FWT project to adapt as the project evolves and the design space changes. For the purposes of brevity, the entirety of those studies will not be discussed here. One of the key studies which MIT's FWT project is based on is NREL's estimation of probable attributes of a 5 MW wind turbine. The NREL 5 MW wind turbine model will be presented in the Design Inputs chapter of this work.

3.2.2 Coupled Dynamics and Economic Analysis of Floating Wind Turbine Systems, Elizabeth Wayman [3]

This thesis took some of the first steps towards the optimization of FWT platform shapes designed to support the NREL 5 MW turbine. Designs were considered for 30-300 meter water depths. The first iteration of a tool used to analyze the coupled hydrodynamic and aerodynamic loading of the FWT was presented. This analysis tool integrated the effects of gyroscopic effects from the turbine rotor, with the aerodynamic and hydrodynamic effects of the structure. The analysis tool was applied to several different types of structures. These structures were evaluated on dynamic performance in various environmental conditions, and their installation cost

3.2.3 Parametric Design of Floating Wind Turbines, Christopher Tracy [4]

This thesis used the method developed and discussed in [3] to conduct a parametric study of the design of FWT. Its baseline parent hull designs came from the offshore oil and gas industry which were adapted in order to support the 5 MW NREL turbine. The work also studied the effects of different mooring systems on the FWT design. A Pareto analysis was used to determine the best designs in terms of RMS acceleration and cost. The cost was roughly calculated, for comparison purposes only, from the displacement of the structure and the total mooring line tension.

3.2.4 Dynamic Response Analysis of Spar Buoy Floating Wind Turbine Systems, Sungho Lee [5]

This work presented the Pareto design of a synthetic mooring system for spar buoy floating wind turbines functioning in shallow water depths. A code was developed in order to capture the unique behaviors of synthetic mooring lines. The location of the mooring line was also varied. The design objectives were the minimization of nacelle acceleration and the static and dynamic tensions acting on the anchors. The limiting case which the designs were subjected to was the 100-year hurricane condition.

3.2.5 Floating Offshore Wind Turbines: Responses in a Sea State Pareto Optimal Design and Economic Assessment; Paul Sclavounos, Chris Tracy, Sungho Lee. [6]

This paper was published in the Proceedings of the 27th Offshore Mechanics and Arctic Engineering OMAE 2008 Conference on June 15-20, 2008 in Lisbon, Portugal. This article was the culminating work based off the findings of [4] and [5]. It presented two Tension Leg Platform (TLP) designs and two Spar buoy designs which were the result of extensive Pareto studies. The findings of this paper are the closest published systems to those studied in the present paper. The designs presented in [6], were updated and enhanced based on the published findings. The details of these updated designs will be presented in following chapters of this work.

3.3 Goal of Present and Future Work

As the MIT FWT project has matured, the designs studied have started to converge on a few high performing designs. The operational environment dictates which designs are best suited for a specific project. The goal of the present paper is to create a reasonable structural design for the most promising FWT design discovered to date, the MIT TLP-1. This work will allow for a more detailed estimate of the amount of structural steel required for the FWT along with the amount and complexities of the welds. This work will also provide information on the structural response of the FWT to loads.

The FWT design was broken into three distinct sections which were then structurally designed. These sections are the tower, the pontoon, and the cylindrical section, and can be seen in figure 3.1.

At the completion of all structural design studies, the information yielded from this work will allow a project on detailed cost estimation to take place. This cost information is extremely important to the FWT project, and will determine its economic viability in industrial power generation.

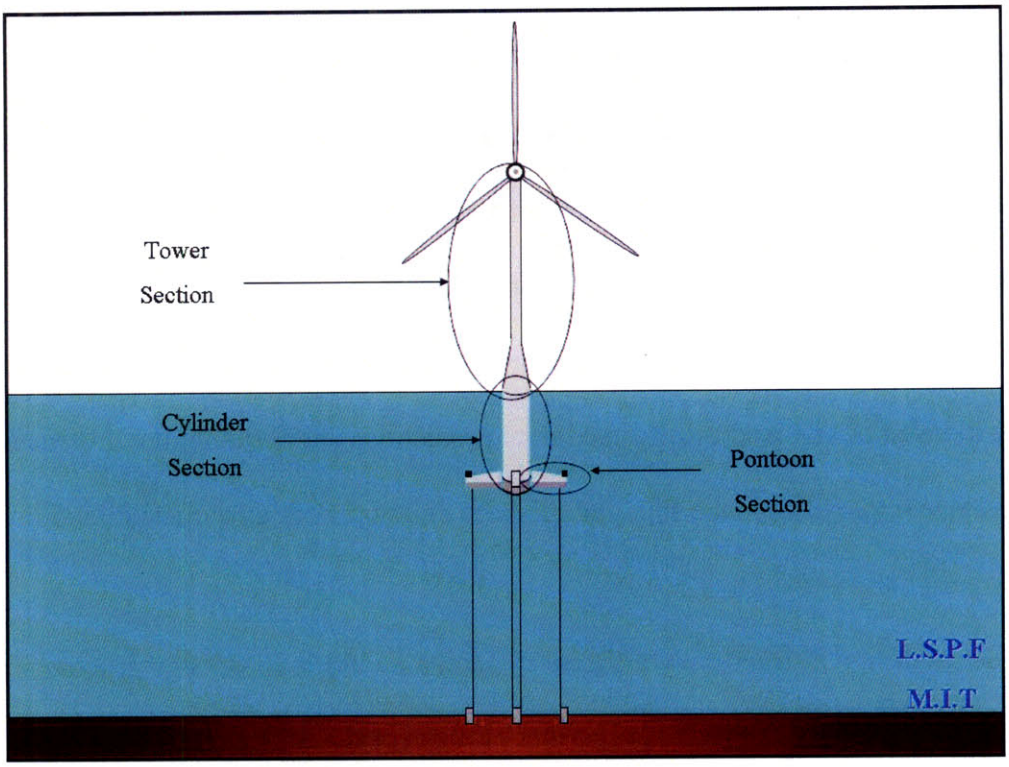

Figure 3.1- Sections for Design

4. Background

4.1 Structural Design of Marine Systems

Ships and offshore structures are the largest mobile structures ever built by man. The structural design of a ship or offshore structure is created after the general shape of the structure is already chosen based on hydrodynamic, operational, and sea keeping considerations. Since the shell plating is a major strength member of the system, and its shape is already selected prior to the beginning of structural design, the structural designer does not control all elements of the structural makeup. Additionally the structural performance of a given design is difficult to analyze due to the complex interactions that occur between the various components of the structure. Since the offshore system has to support its own structural weight, initial predictions have to be made which are used as the starting point of the design. Once the design stage is complete it has to be checked against the initial predictions and rerun until convergence occurs. These design complexities make ship and offshore structural design a difficult and iterative process.

In order to design a structurally efficient system, a multiple step design process is usually undertaken. Key steps in the structural design of offshore systems are presented below with brief explanations. This section is not intended to be an exhaustive instruction on the structural design process. It is intended to present the basic ideals behind the method of structural design used in this project.

4.1.1 Similar System Analysis

In order to ensure a reasonable and buildable design, a design baseline is first determined. In Offshore Engineering the first step of this design is called "similar system analysis." In order to conduct similar system analysis, a proven and successful design with similar attributes to the current design is selected. Once the similar system is selected, key non-dimensional numbers are pulled from the existing design. These non-dimensional numbers are then used to predict end values for the current design. Similar system analysis is best conducted on the same type of structure, for instance a spar buoy used for oil storage compared to another spar buoy used for the same purpose. Even when the system, or in this case, entire industry is completely new, similar system analysis still may be extremely helpful in the early stages of design. The key to similar system analysis for brand new systems is properly identifying which elements of the legacy system are pertinent. If elements of the legacy system are not entirely pertinent, or have slightly different drivers, those non-dimensional numbers can be modified to be more applicable to the current design.

4.1.2 Rules Based Design

Classification societies such as Lloyd's, Det Norsk Veritas (DNV) and American Bureau of Shipping (ABS) promote the security of life, property and the environment through the development of standards for design, construction and operation of marine systems. These standards are commonly referred to as rules. Every major offshore system is designed to meet the rules published by one of the Classification Societies. With the increased competition between classification societies which came from the appearance of "flags of convenience" in

the 1960's, classification societies have increasing pressures to relax the requirements of rules, and obtain rules which help achieve more efficient design. Despite these pressures on the rules, classification society rules are not written to help design optimum structures, they are written with the sole goal of providing safe and reliable structures. Rules are often times derived from first principles and closed form solutions, especially in the area of structural design. In some cases however, empirical evidence, historic best practices and conservative safety margins are incorporated into the rules. In order to save construction cost and increase payload, most major offshore projects currently built use the rules in conjunction with other more complex analysis techniques. In structural design this is because the possible failures are numerous, complex, and interdependent. With the simplified formulas provided by the rules, the failure margins are largely unknown and it is difficult to distinguish structural adequacy with over-adequacy. Despite the inefficiencies of designs based solely on rules, these designs are safe, will perform and can be completed with less man hours of design, hence the rules based design usually forms the preliminary design of an offshore system, and is later enhanced during detail design via enhanced design techniques.

4.1.3 Rational Design

Owen Hughes of Virginia Polytechnic Institute and State University has written the seminal work on modern ship structural design entitled Ship Structural Design: A Rationally-Based, Computer-Aided Optimization Approach [19]. In his book he describes "rationally based structural design" as:

> "Design which is directly and entirely based on structural theory and computer-based methods of structural analysis and optimization, and which achieves an optimum structure on the basis of a designer-selected measure of merit."

The section presented herein is done so with the goal of generally informing the reader of the idea of rational design. Rational design is a complex and lengthy subject which would not be fit to describe in adequate detail in this thesis. Hughes' book is extremely well laid out and very illustrative; it should be consulted for a more detailed understanding of rational design.

Rational design was first developed for the aerospace industry based on the high premium of structural weight and the large payout of any structural weight reduction. It involves a thorough analysis of all factors affecting the performance, and a synthesis of this compiled information with the objective the structure is intended to achieve. This process is much more computationally intense than rules based design, and is conducted in a semi-automatic fashion. It cannot be an automatic or "black box" technique because the designer must make preliminary decisions for criteria, objectives and constraints based on initial estimations which will be validated/invalidated by the technique. The semi-automatic nature of the design allows the designer to constantly update the criteria, objectives and constraints based on the intermediate results of the analysis.

Since the rational design is a much more involved process requiring more man hours for design, but yields a more efficient design, the choice for rational design versus rules based design must be based on the relative premium paid for design objectives (in this case weight savings) versus design cost. In fact careful and concerted coordination of

these two complimentary design techniques is best suited for initial design of novel structures.

5. Design Inputs

5.1 Introduction

The MIT FWT project has multiple proposed designs for the FWT system. Currently the most promising designs being considered are mini TLP's with thin steel shell pontoons and mini TLP's with tubular truss structure pontoons. The size and proportions of these designs vary with the potential location of the project.

The structural design concentrated primarily on the MIT FWT-1. MIT FWT-1 principle dimensions, cable tensions and ballasting are the result of a Pareto optimization for a system designed to support a 5 MW NREL turbine in 200m water depth with optimal performance in seas with a significant wave height of 10m. This design has two main sections, the center cylindrical section and the pontoons.

This preliminary design considers all components of the FWT system to be built of mild steel with the properties:

Density (ρ)	7800 kg/ m^3
Modulus of Elasticity (E)	200 GPa
Yield Stress (σ_y)	250 MPa

By conducting this preliminary design in mild steel, future design and feasibility studies will have a stable, low cost and conventional material to compare with.

5.2 The Wind Turbine

As discussed in the introduction section, the NREL baseline 5 MW turbine was used in the present FWT analysis. This model is the predicted representative attributes of a 5 MW, three-bladed, upwind turbine resulting from a NREL study of all existing industrial wind turbines combined with conceptual studies of proposed machines. The details and rationale for this model are given by NREL in [7]. Its general specifications have been tabulated and are presented in Table 5.1.

Properties		As-designed	Units
Hub height		90	m
Hub diameter		3	m
Rotor diameter		126	m
Total mass		700	metric tons
Center of gravity	X	-0.2	m
	Y	0	m
	Z	64	m
Wind speed		11	m/s
Turbine thrust		80	metric tons
Turbine moment		7200	metric tons-m
Maximum tip speed		80	m/s
Maximum rotor speed		12.1	rpm

Table 5.1 The NREL baseline 5 MW wind turbine specifications

Figure 5.2 shows the characteristics of the turbine over the operational wind speed envelope. The NREL 5 MW turbine is a variable pitch machine, which adjusts the pitch of the blades such that the rated power of the turbine is constant after a certain wind speed threshold called the rated wind speed. At speeds higher than 25m/s, the turbine feathers its blades and locks the rotor. The Rotor thrust can be seen in purple in Figure 5.2, and can be seen to peak to a value of 80 tons at

the rated wind speed. At this wind speed the thrust acting on the tower due to bluff body resistance is less than 1 ton and acts with a much smaller moment arm than the thrust acting on the blades. The tower resistance at 25 m/s is roughly 3 tons, yet the rotor thrust has dropped roughly 50 tons from the maximum thrust. Hence, the worst case scenario for wind thrust acting on the wind turbine system is at the rated wind speed, at this wind speed the tower resistance is negligible compared to the turbine resistance. This means that the highest wind thrust generated on the turbine tower system is approximately equal to the rated thrust of 80 metric tons. Therefore the maximum generated torque about the free surface is 7.2 X 10^7 N*m.

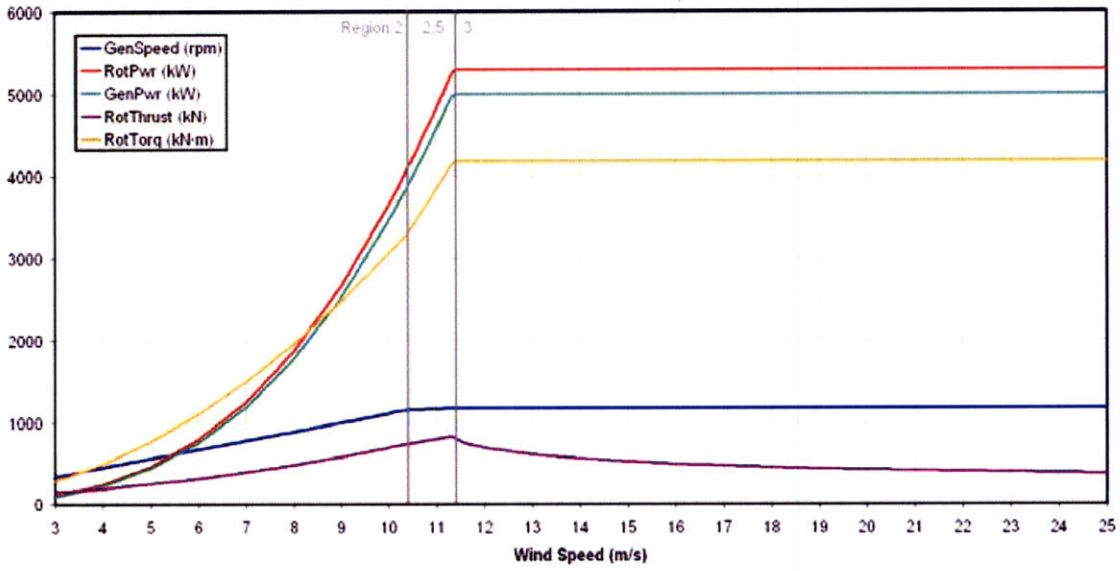

Figure 5.2-Operational Characteristics of NREL 5 MW turbine

The mass, damping, and restoring matrices for the NREL 5 MW wind turbine as evaluated by the program Fatigue, Aerodynamics, Structures, and Turbulence (FAST) are shown below. These values are key in calculating the coupled equations of motion for the FWT system.

(5.1)

$$M_{WT} = \begin{bmatrix} 0.7 & 0 & 0 & 0 & 44.3 & 0 \\ 0 & 0.7 & 0 & -44.3 & 0 & 6.6 \\ 0 & 0 & 0.7 & 0 & -6.6 & 0 \\ 0 & -44.3 & 0 & 3499 & 0 & 0 \\ 44.3 & 0 & -6.6 & 0 & 3560 & 0 \\ 0 & 6.6 & 0 & -513.3 & 0 & 101.2 \end{bmatrix} \times 10^6$$

$$B_{WT} = \begin{bmatrix} 0.04 & 0 & -0.01 & -0.25 & 4.00 & 0.08 \\ 0 & 0 & 0 & -0.11 & -0.18 & -0.05 \\ -0.01 & 0 & 0 & -0.04 & -0.92 & -0.33 \\ 0.27 & -0.10 & 0 & 16.17 & 50.30 & 13.88 \\ 3.42 & 0.06 & -1.00 & -23.92 & 400.10 & 59.01 \\ 0.05 & -0.02 & 0.22 & 11.08 & -52.60 & 101.2 \end{bmatrix} \times 10^6$$

$$C_{WT} = \begin{bmatrix} 0 & 0 & 0 & 0.3 & 0.2 & 0 \\ 0 & 0 & 0 & -0.1 & 0.3 & -0.07 \\ 0 & 0 & 0 & -0.3 & -0.4 & 0 \\ 0 & 0 & 0 & 8.5 & -22.4 & 59.7 \\ 0 & 0 & 0 & 26.8 & 28.9 & -4.1 \\ 0 & 0 & 0 & -1.2 & 1.1 & -4.8 \end{bmatrix} \times 10^6$$

5.3 The Platform - MIT FWT1

The general arrangement of this FWT design can be seen in Figure 5.3. The pontoons in this design are thin shell, stiffened structures. The pontoon legs were made volumus in order to house the required ballast. This ballast can be in the form of conventional concrete or some more progressive ballast options such as olivine sand.

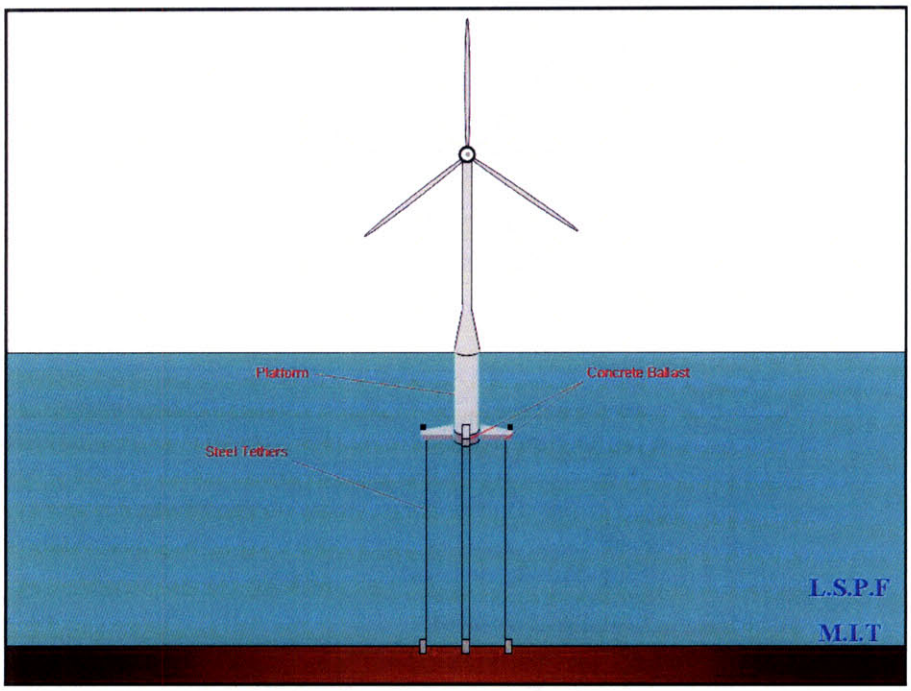

Figure 5.3-MIT TLP-1

As stated above, the principle dimensions, cable tensions and ballasting are the result of a Pareto optimization for a system designed for a 200m water depth with optimal performance in seas with a significant wave height of 10m. The principle dimensions of the MIT TLP-1 are summarized in Table 5.3. The centers of gravity, concrete mass and concrete height are all initial estimates which will be corrected as the structural design iterates. During hydrodynamic analysis, the MIT TLP-1 is modeled as a rigid symmetrical cylinder/pontoon system with tensioned rigid mooring lines attached at the end of the each pontoon to provide the stability and stiffness on the entire system. It is assumed that the platform is connected to the seabed by four mooring anchors spreading out by 90 degrees with respect to each other.

Platform	Cylinder Radius [m]	5
	Cylinder Length [m]	40
	Pontoon Radius [m]	30
	Pontoon Height at Cylinder [m]	10
	Pontoon Height at End [m]	5
	Width of Pontoon [m]	4
	Total Displacement [metric tons]	6291
Concrete Ballast	Concrete Mass [metric tons]	4288
	Concrete Height [m]	4.2
Center of Gravity [m]		-28.06
Center of Buoyancy [m]		-27.57
Sea condition	Water depth [m]	200 / 70
	Significant Wave Height [m]	6/10/2014
Mooring System	Type	TLP steel tethers
	Fairlead Arm, L [m]	25
	Fairlead Position, [m/m]	-0.5 ~ 1.0
	Pre-tension [metric tons]	300 ~ 500

Table 5.3 Key Attributes of MIT TLP-1

The initial pre-tension is calculated with no environmental load on the system hence mooring line tensions are all equal. Once wind thrust is applied, a quasi-static equilibrium offset of the entire system due to wind thrust is determined by iteration analysis. The effective initial pre-tension at this position becomes non-uniform between the legs. The corresponding forces from the tension legs at the initial or quasi-static equilibrium position are calculated. These are then combined, under a finite water depth condition, with the Wave Analysis at Massachusetts Institute of Technology (WAMIT) output of the wave exciting forces including the diffraction effects at the initial position. The seabed and the free surface are assumed parallel to each other. Vortex Induced Vibration (VIV) and other viscous effects including sea currents are not considered in this analysis.

5.4 The Equation of Motions and Sea Spectrum

As presented in previous LSPF publications [4], the equations of motions which represent the coupled FWT TLP system are listed below in Equation 5.2.

(5.2)

$$M(w)\ddot{\xi}(t) + B(w)\dot{\xi}(t) + C\xi(t) = aX(w)e^{iwt}$$

$M(w)$ = Total mass matrix [6x6]
$B(w)$ = Total damping matrix [6x6]
C = Total stiffness matrix [6x6]
$X(w)$ = Vector of wave induced exciting forces and moments [6x1]
$\xi(t)$ = Vector of system's displacement [6x1]
$\dot{\xi}(t)$ = Vector of system's velocity [6x1]
$\ddot{\xi}(t)$ = Vector of system's acceleration [6x1]
w = Incident wave frequency

The 6 X 6 matrix for the above equations is a result of the six degrees of motion for sea systems. Figure 5.4 shows the method of numbering for these six modes as used in this paper.

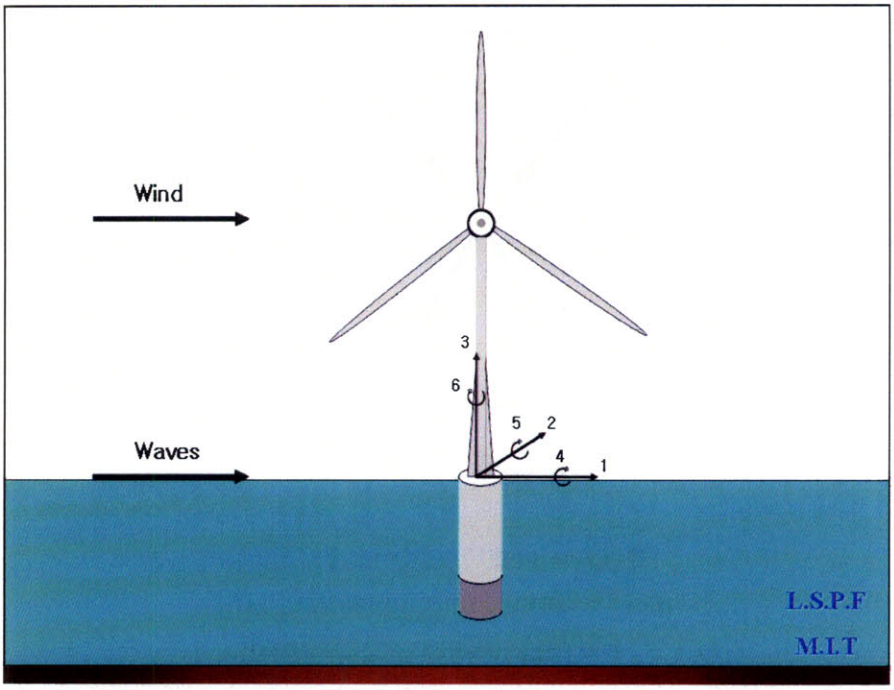

Figure 5.4 Six modes of motion

The total mass, total damping and total stiffness matrix consists of multiple components which are shown below in equation 5.3. These dynamic properties were evaluated via proven numerical analysis codes including WAMIT and Lines, which were developed and extensively tested in the MIT LSPF for previous projects and FAST, which was developed by NREL. Figure 5.5 shows which calculated property corresponds to which numerical analysis technique.

(5.3)

$$M(w) = M_{platform} + M_{windturbine} + M_{added}(w)$$
$$B(w) = B_{windturbine} + B_{platform}(w)$$
$$C = C_{platform} + C_{windturbine} + C_{mooring}$$

$M_{added}(w)$ = Added mass matrix [6x6]

$B_{platform}(w)$ = Wave damping matrix [6x6]

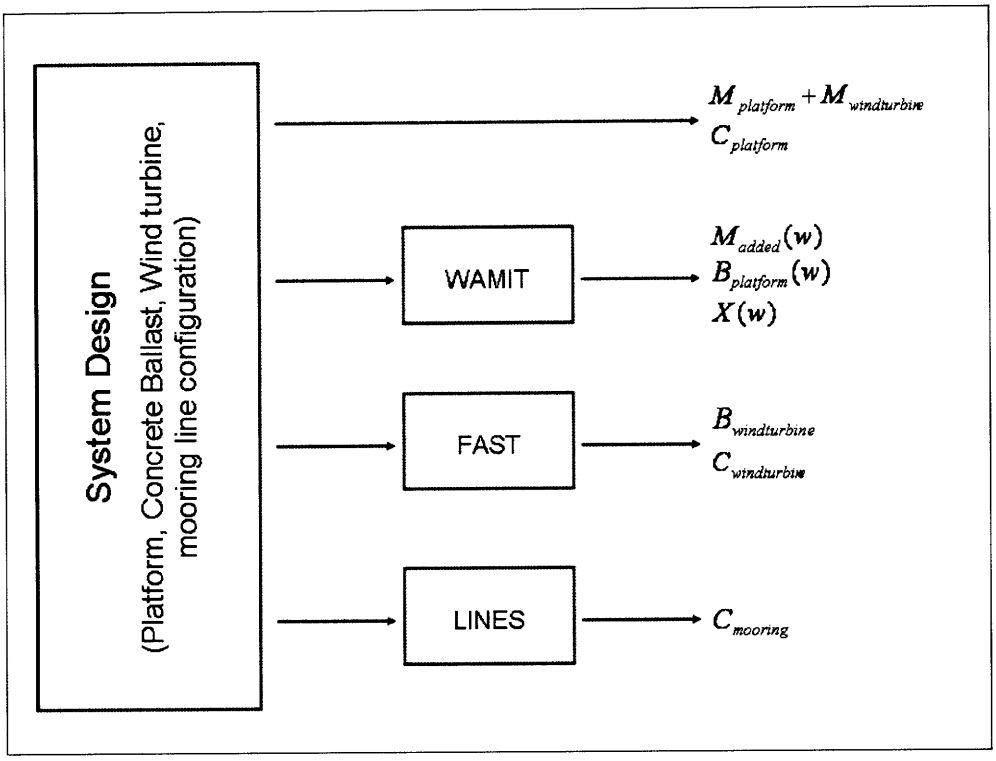

Figure 5.5 System Properties Corresponding to Numerical Codes[4]

Since the wave induced exciting force acting on the system is sinusoidal as a function of time, the resulting motion becomes sinusoidal as well. For convenience the equations of motions are expressed in the frequency domain, this is achieved by expressing the sinusoidal function in a complex form and substituting it back into the equation of motion. This enables the entire system response to be expressed in matrix form in the frequency domain as shown below in equation 5.4.

(5.4)

$$\begin{pmatrix} RAO1(w) \\ RAO2(w) \\ RAO3(w) \\ RAO4(w) \\ RAO5(w) \\ RAO6(w) \end{pmatrix} = [-w^2 M(w) + iwB(w) + C]^{-1} \begin{pmatrix} X1(w) \\ X2(w) \\ X3(w) \\ X4(w) \\ X5(w) \\ X6(w) \end{pmatrix}$$

5.4.1 Sea Spectrum

The International Towing Tank Conference (ITTC) accepted spectral density function is presented below in equation 5.5.

(5.5) $$S(w) = H_s{}^2 T_1 \frac{0.11}{2\pi} \left(\frac{wT_1}{2\pi} \right)^{-5} e^{-0.44\left(\frac{wT_1}{2\pi}\right)^{-4}}$$

Where;

H_s = Significant wave height defined as the mean of the 1/3 highest waves

T_1 = Mean wave period in the above spectral density function

The RAOs calculated via equation 5.4 can be combined with the ITTC spectral density function above via equation 5.5 to yield a Root Mean Square (RMS) of the system motions and tensions. These RMS values will be used for the calculation of loads applied to the design of the structure.

(5.6) $$\sigma_i^2 = \int_0^\infty RAO_i(w)^2 S(w) dw$$

5.5 RMS Values

The Root Mean Squared (RMS) values are caluculated by integrating the Response Amplitude Operators (RAO) over the prescribed sea spectrum. Using the methods developed in the LSPF and presented in ref [1, 3, 4, 5, 9] and above, the RMS values for the motions and forces acting on the MIT TLP-1 were predicted. Figure 5.7 shows key RMS values for sea states with 6, 10 and 15m significant wave heights.

Key RMS Input Values for FWT Design			
Hs [m]	15	10	6
RMS Nacelle Acceleration [g]	**0.047**	**0.034**	**0.021**
RMS Surge Motion [m]	**2.6921**	**2.175**	**1.004**
RMS Tension Per Each Side [tons]	**39.646**	**27.499**	**19.678**
RMS Moment at Tower Base [tons.m]	**29340.817**	**21354.238**	**12891.423**

Figure 5.7

The information provided in the above figure along with the wind turbine loads presented in above sections comprise the entire necessary RMS values required to design the tower and pontoon sections of the MIT FWT TLP-1.

In addition to the above information, RMS values for cylinder bending moment as a function of depth were required for the structural design of the cylindrical section of MIT TLP-1. Figure 5.8 presents the bending moment acting on the cylinder due to a combination of the dynamic loading from surge motion and the pitch exciting moment. The three specific lines correspond to 6, 10, 15m significant wave height sea states. The 10m significant wave height sea state bending moment is combined with the bending moment due to the maximum wind thrust to define the design bending moment. The x-axis refers to the non-dimensional vertical location along the cylinder, where 0 is at the waterline and 1 is at the maximum draft.

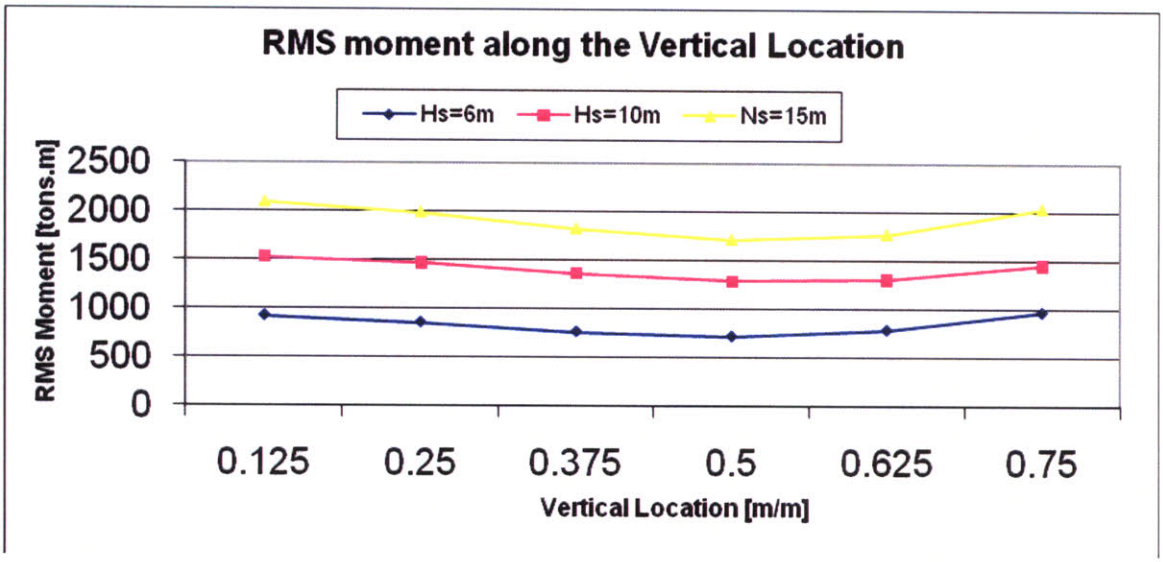

Figure 5.8

The dip in the above cylinder RMS moment results from phase cancelation of the dynamic bending moment by the pitch bending moment. This is best illustrated by the below series of graphs of RAO moment versus ω for specific cylinder heights. The leftmost and sharpest peak is mainly due to the surge natural frequency of the cylinder. This results from the surge inertial properties multiplied by ω^2. Since the peak inertia component occurs at a ω which is below 1, the peak is reduced when multiplied by ω.

While the ω increases above 1 the surge inertial component decreases asymptotically to zero, which accounts for the second hump. The right most hump results from the pitch moment. The trough between the two rounded crests results from phase cancellation of the surge inertial components and the pitch moment.

The RAO graph is then multiplied by the sea state in order to obtain the RMS cylinder moment. The cylinder vertical locations which have the sea state peak located at the same ω as the trough resulting from surge and pitch moment phase cancellation will have a smaller RMS

value. This accounts for the shape of the RMS moment graph presented in figure 5.9.

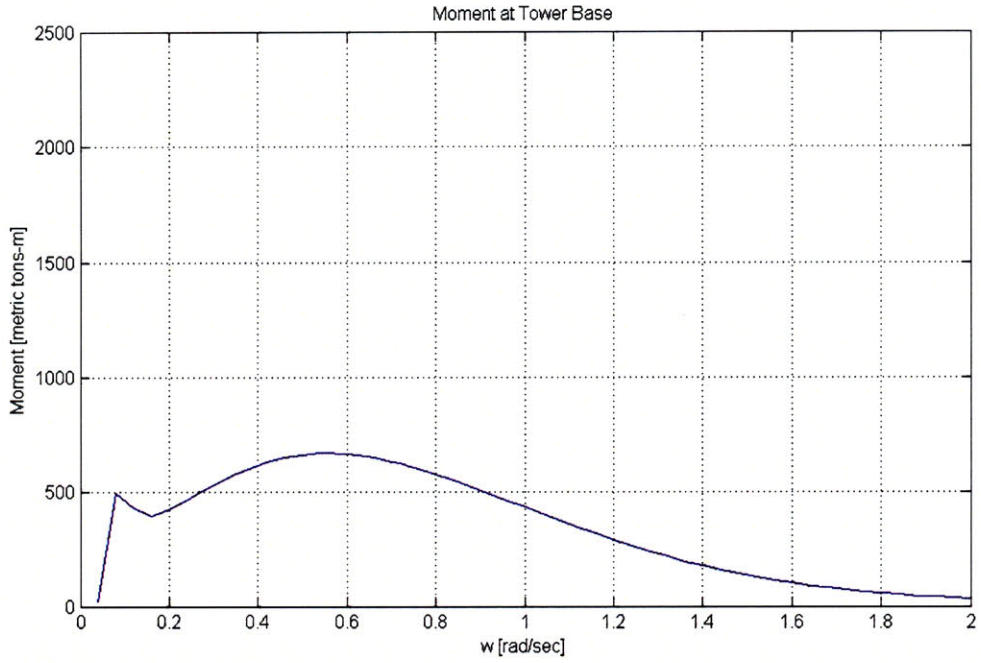

Figure 5.9-Moment at 5m Cylinder depth

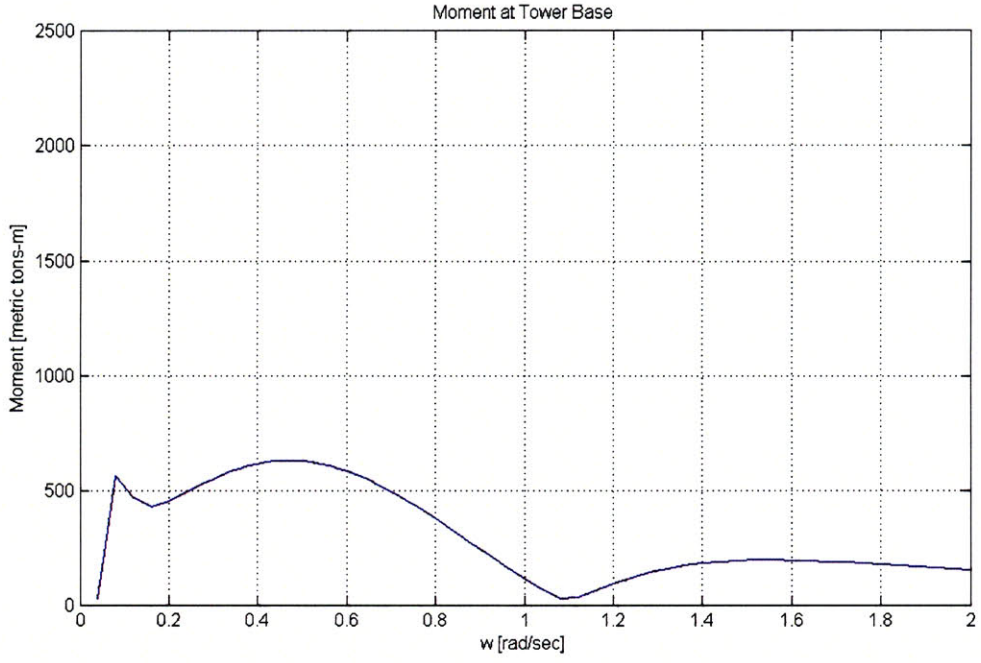

Figure 5.10-Moment at 10m Cylinder depth

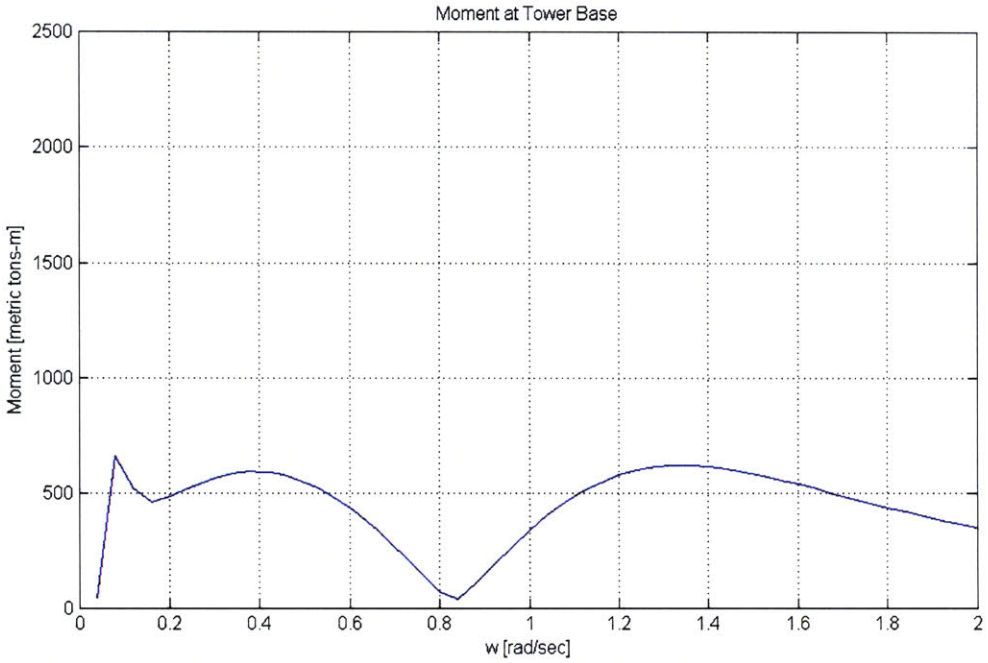

Figure 5.11-Moment at 15m Cylinder depth

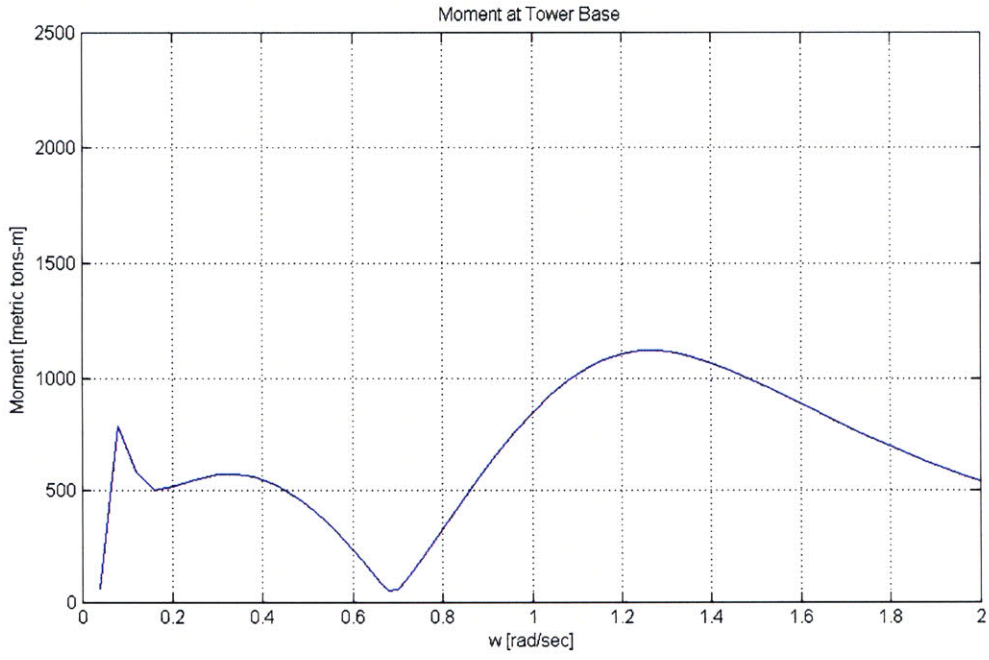

Figure 5.12-Moment at 20m Cylinder depth

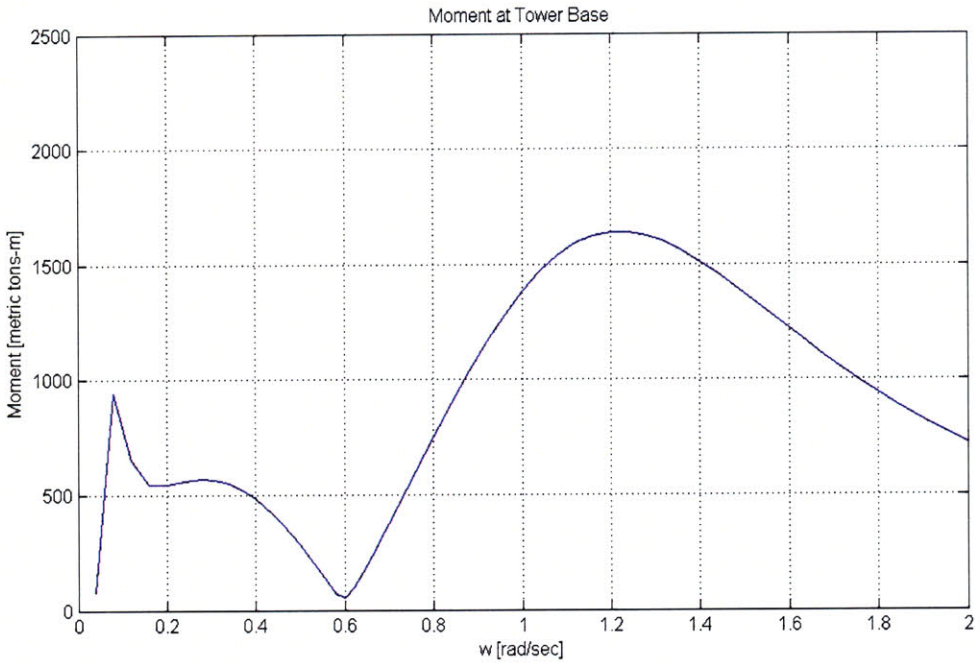

Figure 5.13-Moment at 25m Cylinder depth

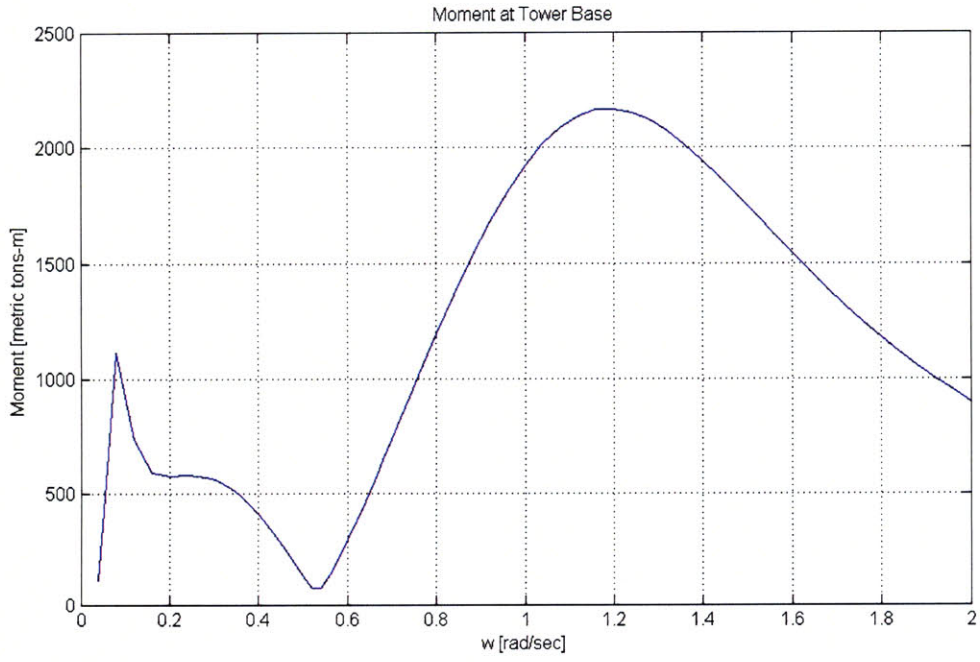

Figure 5.14-Moment at 30m Cylinder depth

The RMS moment was combined with the maximum wind moment to produce the total moment as a function of cylinder depth, which is included as figure 5.15.

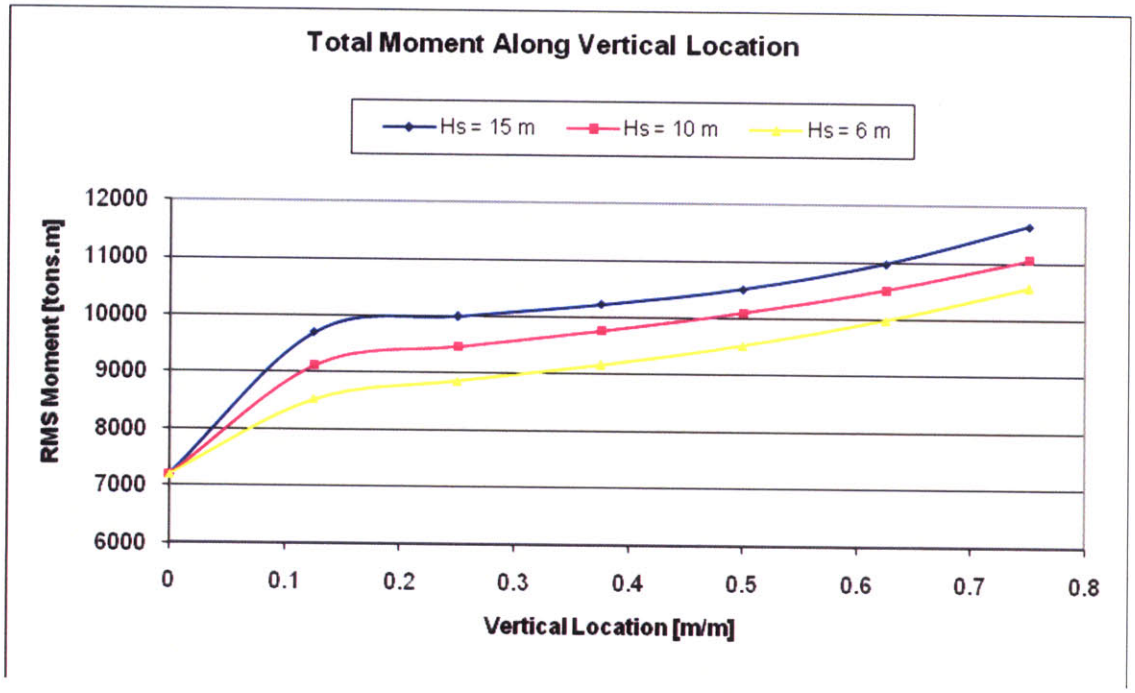

Figure 5.15

6. Feasibility Study, Dynamic Ballast System

6.1 Introduction

The magnitude of the pre-tension required in the MIT TLP-1 tension legs is a major cost driver for the FWT system. The tension legs prevent the MIT TLP-1 from pitching or heaving by acting as rigid legs while they are in tension. The pre-tension is set in order to ensure that no loading condition causes the TLP tension legs to go slack. If the tension legs cease to be in tension, the platform will undergo unwanted motion, and the tension leg could potentially fail.

A key goal of the LSPF FWT project has been to reduce the required pre-tension through hydrodynamic Pareto optimization of the platform shape. The optimized shape reduces the wave excitation forces acting on the platform, and hence reduces the required pre-tension.

The other major external load which drives pre-tension is the wind moment acting on the tower and nacelle. Since the tower and nacelle properties for this thesis are already set by the NREL 5 MW turbine assumptions, the wind moment transmitted to the platform cannot be changed.

Though the wind moment cannot be changed, it can be counteracted. If the wind moment is counteracted, the tension legs would not have to create the counteracting force, and hence the pre-tension could be reduced.

A dynamic ballast system is one way to counteract the wind moment. This system would use pumps and controls to ballast the windward pontoon of the platform with seawater until the wind moment is counteracted.

6.2 Methodology and Results

There are many forces which dictate the required leg pre-tension. These forces are linearly superimposed to create the final required pre-tension. For the purposes of this feasibility study, only the pre-tension due to wind will be considered, since the presence of a dynamic ballasting system does not counteract other pre-tension drivers. Figure 6.1 shows the results of wind forces on tension legs for the un-ballasted and ballasted scenarios.

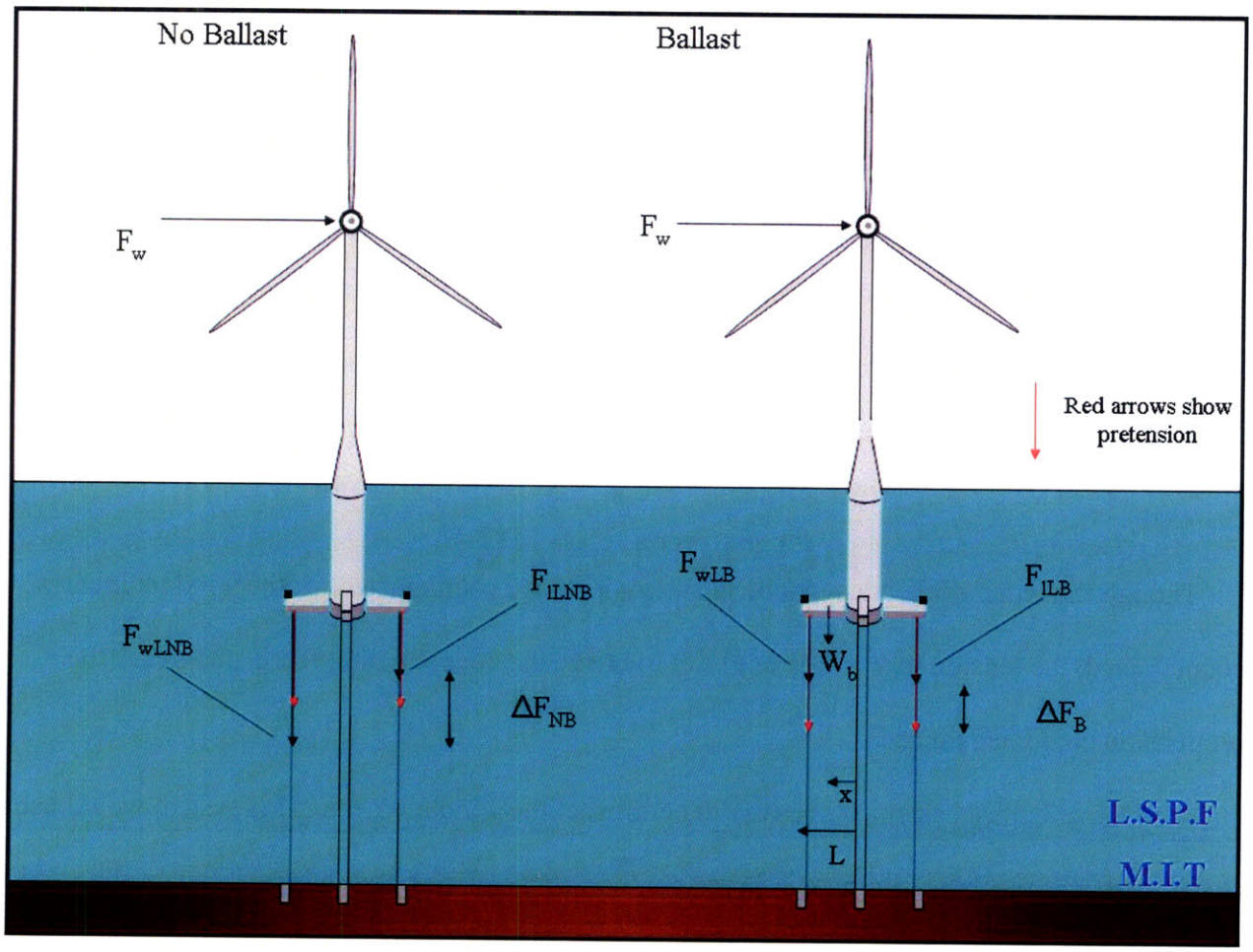

Figure 6.1-Change in leg tension due to wind forces

This feasibility study considers the four legged MIT TLP-1 for the analysis, but the results of the study are equally valid for a pontoon with any number of floaters. In a four pontoon FWT design which does not use dynamic ballasting, a difference between the windward and leeward tension leg tensions must exist to counteract the wind moment. The windward leg tension will increase by a certain magnitude which is equal to the decrease in tension on the leeward side. Since the pre-tension for wind, F_{PT}, must be set in order to ensure that it is never slack, the F_{PT} will be equal to that decrease of tension on the leeward pontoon, ΔF_{NB}. A static analysis of the sum of forces and moments acting on the platform results in equation 6.1. Where M_w represents the wind moment and L is the length of the pontoon. This equation is used to set the pre-tension due to wind in the non-ballasted design.

$$F_{PT} = \Delta F_{NB} = \frac{M_w}{2L} \tag{6.1}$$

The ΔF_{NB} in this design is created solely to counteract the wind moment. In the ballasted case, the wind moment is completely counteracted by the moment created by the ballast moment. This is equal to the weight of the ballast water multiplied by the distance from platform centerline to the center of gravity of the ballast water. This negates any de-tensioning of the leeward tension leg due to a wind moment. Unfortunately there is still de-tensioning experienced in the legs, which is due to the added weight of the ballast water. The added weight of the ballast water consumes the reserve buoyancy which created the tension acting on the leg in the first place. Equation 6.2 shows the tension reduction associated with additional weight due to ballasting to counteract the wind moment. It was obtained through a summation of the forces

and moments acting on the platform. X is equal to the location of the ballast center of gravity non-dimensionalized by pontoon length.

(6.2) $$F_{PT} = \Delta F_B = \frac{M_w}{4xL}$$

By comparing Equations 6.1 and 6.2, it can be seen that the pre-tension force required will be smaller for a ballast system only when the location of the ballast center of gravity is greater than ½ the length of the pontoon.

The threshold length for the pontoon above which a ballast system is associated with a reduction in pre-tension is presented in figure 6.2 It was found by combining the Ballast center of gravity equation, ballast displacement equation, and requirement that the center of gravity is equal to ½ the pontoon length, then varying the pontoon length. The proportions of the pontoon were assumed to remain the same regardless of the pontoon length. The assumed proportions are that of the MIT FWT1. The pontoon permeability was assumed to be 95%. The threshold length is equal the pontoon length when the ballast system counteracting moment is equal to the wind moment, which is 10400 tons-M for MIT TLP-1.

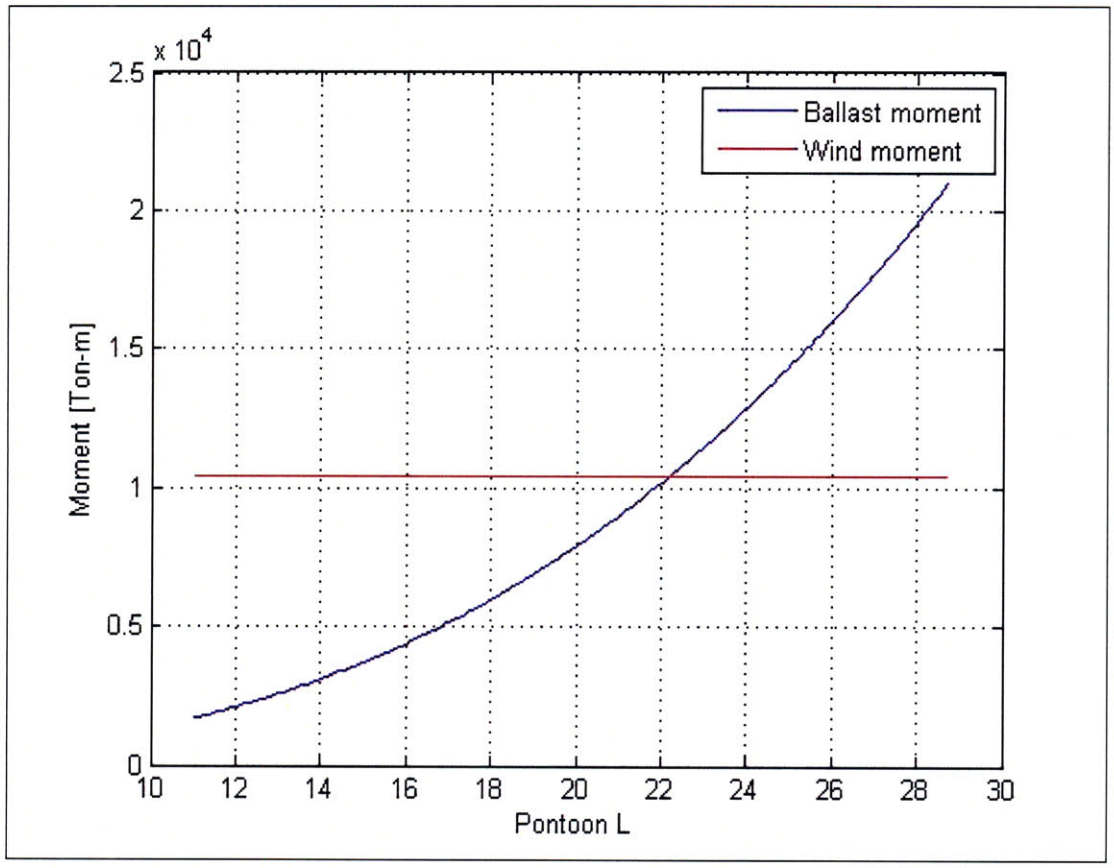

Figure 6.2 Ballast Moment versus Wind Moment

At the threshold length, almost the entire pontoon is ballasted. The threshold length is associated with the highest amount of required ballast weight. As the length of the pontoon increases above the threshold length, ballast moment arm increases while ballast weight decreases. This is captured in figure 6.3 where Lr is equal to the reserve length of the pontoon, and Lb is the ballasted length.

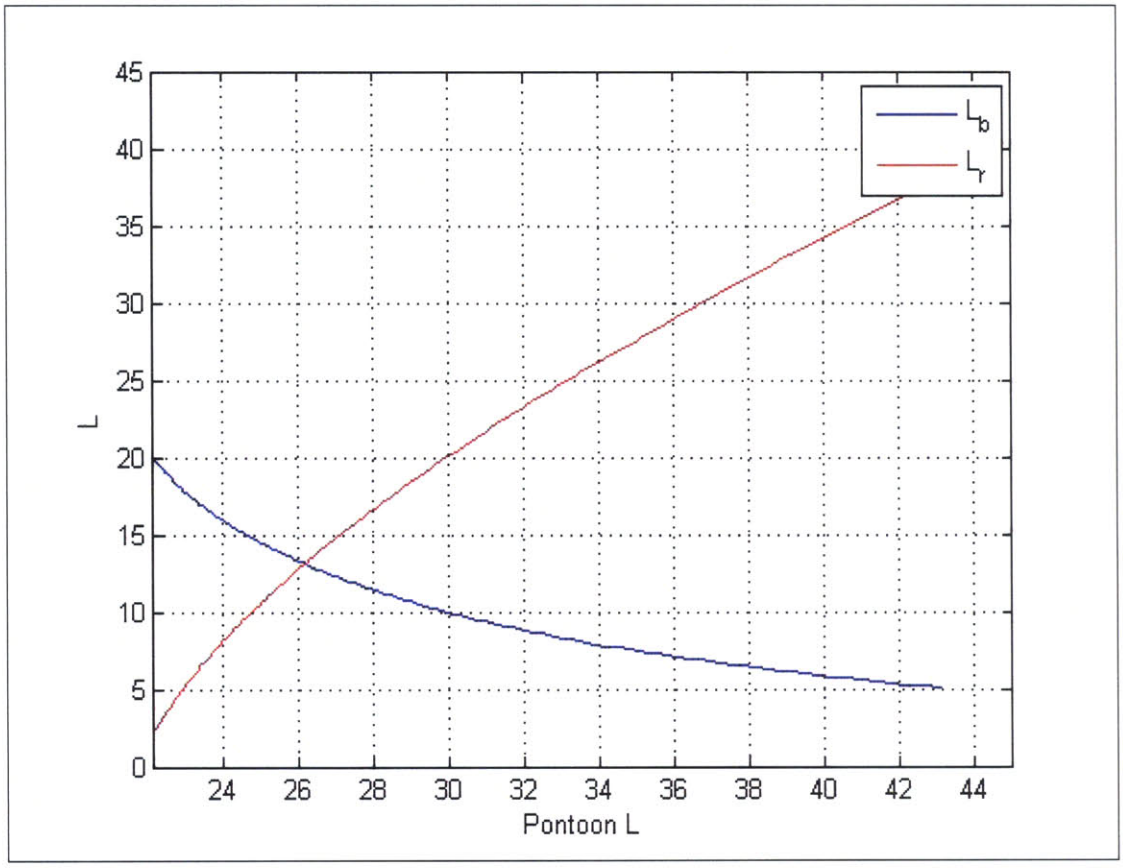

Figure 6.3 Reserve Length versus Ballasted Length of Pontoon

Both the non-ballast and ballast design experience a reduction in the required pre-tension as the pontoon length increases as can be seen in Figure 6.4. The reason that the required pre-tension remains smaller for the ballasted versus non-ballasted design can be seen by comparing equations 6.1 and 6.2. Since x increases with L, and x and L are in the denominator of equation 6.2, the L term in the denominator is of a higher order than that in equation 6.1

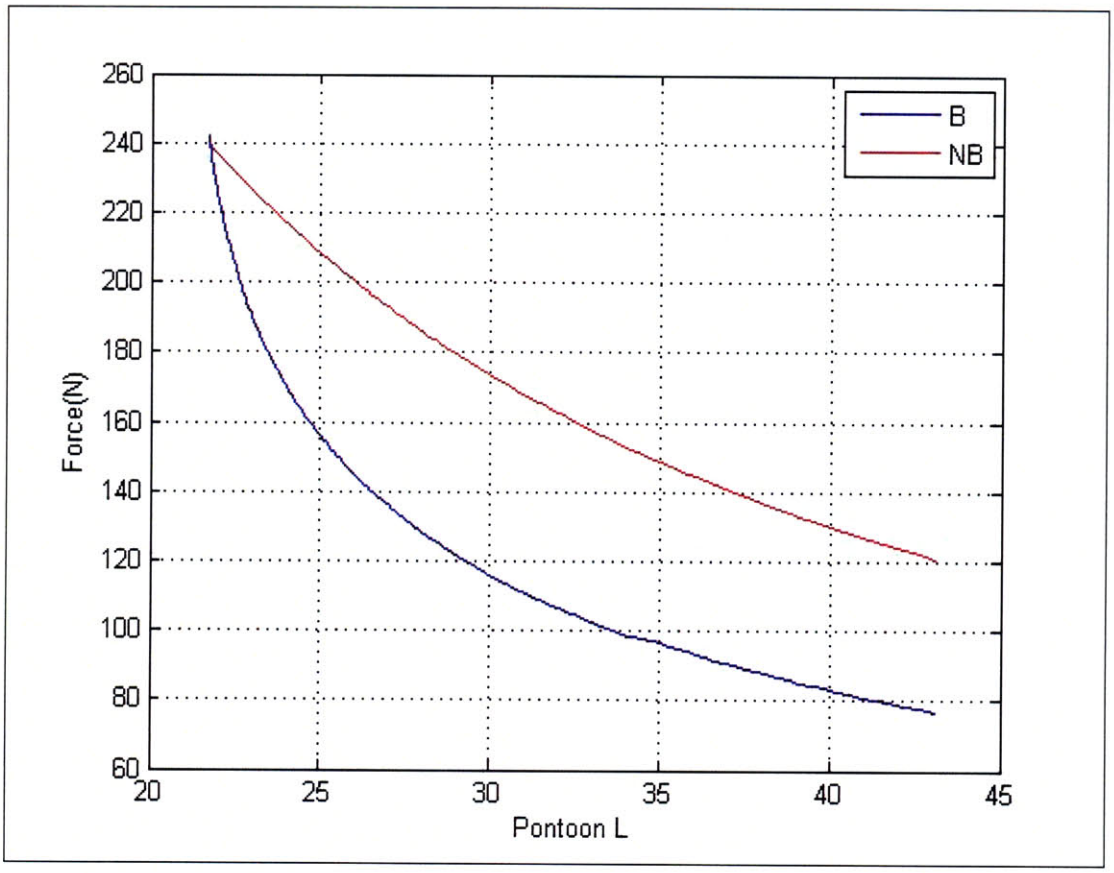

6.4 Required Pre-tension for Ballasted and Non Ballasted Platforms

The pre-tension is set to ensure that leeward side tension leg never goes slack; it is the windward side, though, that determines the required size of the tension legs and mooring system. It may be more beneficial to consider the maximum tension vice the pre-tension. In the non-ballasted system the windward side tension due to wind is equal to twice the required pre-tension. In the ballasted system design the windward side is equal to all other tension legs and is less than the required pre-tension. If the maximum tension is considered vice the pre-tension, ballasting potentially becomes desirable at lower pontoon lengths. For this reason the ballasted system may have cost savings over the non-ballasted side even before the threshold pontoon length is achieved.

Even if the entire windward pontoon is pressed completely full with ballast, the wind

moment cannot be completely compensated until a pontoon length of 21.7m. So for pontoon lengths less than approximately 22 meters, the tension will be a function of the wind moment not counteracted by the ballast, and the ballast weight. Since the results of Pareto hydrodynamic analysis yield a pontoon length of 25m, and the ballast analysis shows that increasing length decreases required pre-tension, pontoon lengths less than 22 meters are not considered. Figure 6.5 shows the maximum tension versus pontoon length for ballasted and non ballasted designs.

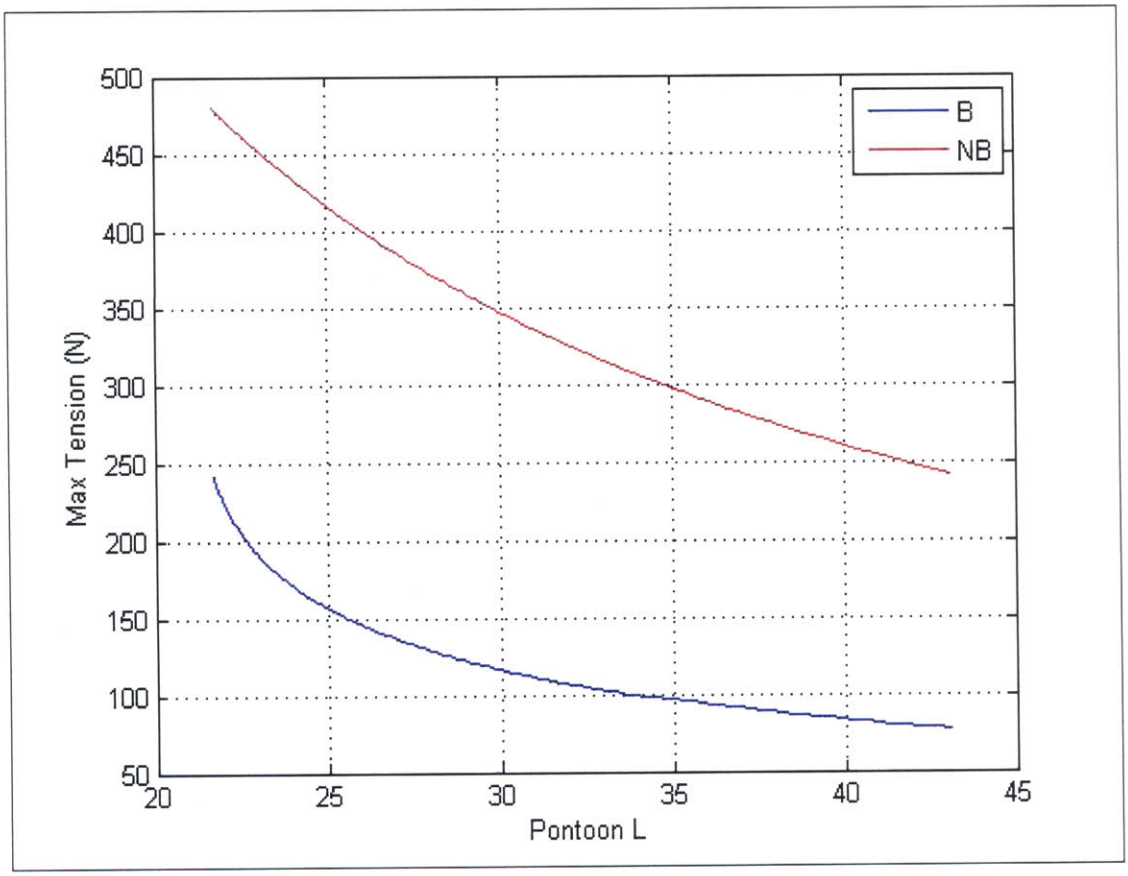

Figure 6.5 Maximum tension versus Pontoon Length

6.3 Conclusion

This feasibility study shows that for the MIT TLP-1 pontoon proportions and lengths exceeding 22.16m, active dynamic ballasting will reduce the required wind pre-tension. Tension drives the structural steel requirements of the pontoons, the strength of the tension legs, and the size of the mooring system. All of these contribute to the cost of the FWT system. The maximum tension will be reduced significantly for all pontoon lengths which exceed the threshold length, and even be reduced, albeit less significantly, for lengths not above the threshold.

Cost estimation is needed in order to determine if this pre-tension and maximum tension reduction are economical given the additional system complexity of an active ballasting system. In order to conduct this cost estimation, it is important to have an initial structural design of the platform in order to determine how the structural demands may be decreased with the ballasting system. Subsequent chapters of this thesis will design the structure for a non-ballast system. Once this design is completed, the validity of the ballasting system can be assessed from a cost standpoint, at which point a new structural design will be undertaken.

7. Design of Tower System

7.1 Introduction

Though the general properties of the 5 MW NREL turbine are already assumed, the specific structural attributes of the actual tower are not. In order to more fully investigate the structural and fatigue response, producibility and cost of the FWT system, a preliminary design of the tower was required. The structural design of the tower was not meant to be an optimization, since the overall weight and geometry characteristics must remain the same for continuity with past and current FWT projects. The preliminary structural design was conducted in conjunction with the cylindrical section design and used the environmental loads and accelerations presented in chapter 5.

7.2 Initial Design

The selection of the stiffening type was the most important design decision for the structure of the tower. Though stiffened cylinders are almost exclusively more weight efficient than monocoque cylinders, monocoque cylinders of reasonable thickness are much cheaper to produce because of the man hours saved by not welding stiffeners. Since the cylinder is not subject to hydrostatic loading, and only subject to wave loading near the base, and since the expected accelerations associated with the MIT TLP-1 design were so small, it was initially assumed that the tower could be built as a monocoque cylinder.

For structural simplicity, strength and fatigue life, the base radius of the tower was set equal to the diameter of the cylindrical section. Since the tower height, base radius, material density

and weight were already known, there were only two remaining parameters. These were wall thickness and top radius. Based on available plate thicknesses and current wind tower proportions, these variables were chosen at 20mm thickness and 3m top radius.

7.2.1 Rules Based Design

Though there is currently no specific classification society guidance for floating wind turbines, there are certain general common rules and recommendations put out by classification societies which can be applied to the tower with little to no adaption. For large diameter to thickness ratio cylindrical shells, the most applicable ABS offshore structural rules (Mobile Offshore Drilling Units, MODU, Floating Production Instillations, FPI) refer to the American Petroleum Institute's Bulletin 2U on Stability Design of Cylindrical Shells, ref [25].

The initial structural design was subjected to the analysis procedure set forth in Bulletin 2U. A brief explanation and complete calculations for the tower from this procedure can be found in Appendix 1.

Bulletin 2U is based on classical linear theory for bifurcation buckling which is modified by reduction factors which account for the effects of imperfections. Since this theory applies ubiquitously to wide cylinders, there is no required modification for the specific scenario of the FWT.

For the Buckling portions of the Bulletin 2U analysis procedure, the tower was assumed to be a cylinder with radius 4m vice the actual truncated cone design. This assumption is valid via classical linear theory for small cone angles. For this turbine the cone angle is 1.3 degrees. Another classification society, Det Norsk Veritas (DNV) states that the cone should be adjusted to an effective cylinder via equations 7.1 and 7.2 below. Due to small angle theory, it may be

assumed that the effective tower height remains the same and the effective radius equals the average radius.

(7.1) & (7.2)

$$r_e = \frac{r_t + r_b}{2\cos\alpha}$$

$$l_e = \frac{l}{\cos\alpha}$$

The full API Bulletin 2U procedure for the monocoque cylinder can be seen in Appendix 1. The as designed tower exceeded all requirements of Bulletin 2U with a large margin. Some key calculations from Bulletin 2U are listed below:

Maximum Combined Axial and Bending Stress	73 MPa
Elastic Buckling Stress F_{xeL}	362 MPa
Local Shell Critical Buckling F_{xcL}	192 MPa
Elastic Column Buckling $F_{\phi eC}$	413 MPa
Additional margin for Maximum Allowable Stress	2

7.2.2 FEA Analysis

FEA via ABAQUS was run in conjunction with the API Bulletin 2U design analysis. The FEA yields stress outputs which were used to check against threshold requirements for the API Bulletin 2U calculations. The FEA also has the capacity to calculate bifurcation buckling which serves as a check on the requirements of API Bulletin 2U, since bulletin 2U is more of a design procedure where as the FEA is better suited for very detailed structural analysis. FEA also allows detailed calculation of the structural natural frequencies which is extremely important for

the tower section since it will be subjected to oscillating loads, requires a long service life and is a very slender body.

ABAQUS was used to mesh, load, calculate and process the results of the Finite Element Analysis. The tower and the nacelle were both modeled in ABAQUS.

The present work did not deal with the structural design of the nacelle. Consequently the nacelle was modeled as a three-dimensional rigid continuum element. The density properties were manipulated to ensure that the NREL 5 MW turbine model weight was equal to the nacelle weight modeled in ABAQUS.

The tower was modeled as a 3-D deformable shell. The material properties were that of mild steel which have been presented elsewhere in this paper. The base of the cylinder was assumed to be clamped in all six degrees of motion. It is assumed that the detail design of the connection of the tower to the cylinder section of the floater will be sufficiently rigid in order to choose this boundary condition. This same detailed design assumption is required to justify the connection of the tower to the nacelle, which was connected via the TIE function in ABAQUS. The TIE function links the nodes of the two different meshes along the contact of the two different parts.

7.2.2.1 Analysis Steps

7.2.2.1.1 Weight

The first step was the weight step; this was conducted as a general static analysis. The base boundary condition and the nacelle to tower tie were created in this step. The only load applied in this step was gravity. The loads, ties, and boundary conditions created in this step were propagated to all subsequent steps.

7.2.2.1.2 Acceleration

The motions of the tower were accounted for quasi-statically which allowed this step to also be a general static analysis step. The accelerations were added as a gravity load in their corresponding direction which allows the program to calculate the dynamic induced stresses with less computational cost. This load was propagated through all subsequent steps.

7.2.2.1.3 Wind

This step was run as a general static analysis. The maximum possible wind load for the tower was modeled as a uniform pressure load acting on the windward surface of the tower. Additionally the maximum possible rotor load due to wind was modeled on the windward face of the nacelle as a uniform pressure load. This load was propagated to all subsequent steps.

7.2.2.1.4 Axial Buckling Load

This step was run as a linear perturbation buckling analysis. The Lanczos eigenvalue extraction method was used to determine the eigenvalue of the buckling load associated with the bifurcation point. This step was run on the deformed shape resulting from the previous general static steps. The purpose of this step was to ensure that that the bifurcation point had not already been exceeded, and determine what additional axial load would result in the tower buckling. The load was modeled as a uniform pressure load acting in the vertical direction by placing the load on the top face of the nacelle.

7.2.2.1.4 Bending Buckling Load

This linear perturbation buckling analysis step was run in exactly the same manner as the above axial buckling load. The load was modeled as a uniform pressure load acting in the horizontal direction by placing the load on the windward face of the nacelle. This potentially simulates the situation of an additional load associated with an un-feathered turbine blade in high wind conditions.

7.2.2.1.5 Natural Frequency Extraction

The last step investigates the natural frequencies of vibration of the tower via the linear perturbation frequency extraction step. This uses a linear perturbation Lanczos eigenvalue extraction technique. All eigenvalues for all natural frequency modes were extracted from 0-90 rad/sec.

7.2.2.2 Mesh Convergence Test

The tower was meshed with the element type SR4; these are rectangular linear 4-node doubly curved elements with reduced integration and hourglass control. There were five integration points through the thickness of the shell. Figure 7.1 is a close up view of the chosen tower mesh.

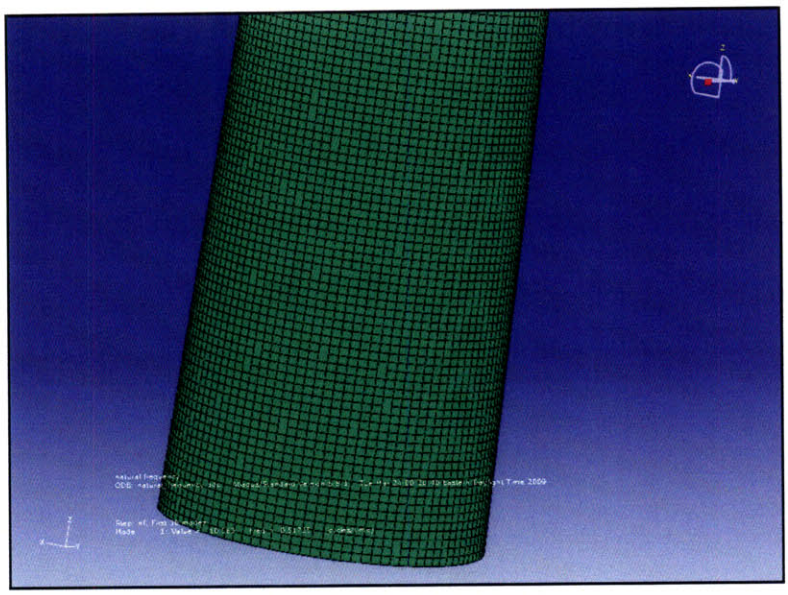

Figure 7.1 Sample Tower Mesh

The mesh density was varied with the buckling eigenvalue for each mesh recorded. Figure 7.2 plots the total number of elements against the eigenvalue resulting from the analysis for each mesh. From the figure it can be seen that the mesh is dense enough for the results of the analysis to converge. The final mesh had a global seed size of .03658 which corresponds to a total of 9350 nodes.

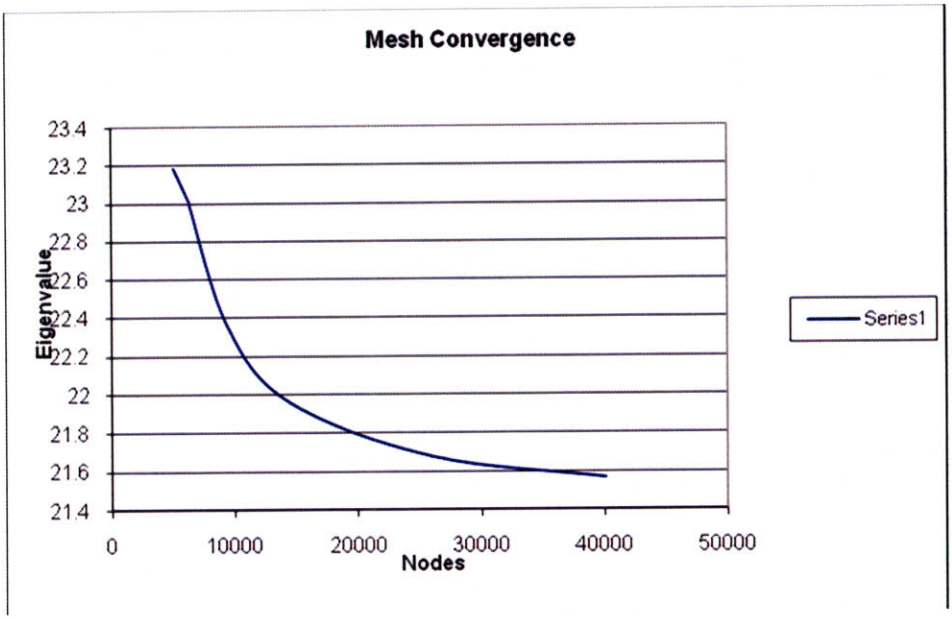

Figure 7.2 Mesh Convergence Test

7.3 Results and Discussion

The ABAQUS analysis results supported those of the API Bulletin 2U in that the structural design is adequate for the expected environmental loads. Presented below are the results of each step of this analysis.

7.3.1 Gravity

The maximum stress due to gravity is located at the tower to nacelle connection, this is due to the out of plane stresses resulting from the nacelle gravity acting along the z axis and the shell oriented at an angle relative to the z axis. Another peak in the stresses is seen at the bottom of the tower, where the clamped boundary condition is applied, once again this is due to out-of-

plane stresses resulting from the angle of the truncated conical cylinder. Figure 7.3 shows the tower stress distribution due to gravity. The stresses further away from the nacelle and boundary connections act solely in plane and are subsequently much smaller; the minimum stress is at the top of the tower with a magnitude of 9 MPa and maximum is at the bottom of the tower with a magnitude of 14 MPa.

This design assumes a simple clamped connection of the tower to the nacelle with no additional stiffening. Any final design would most likely require a detail design and analysis for the tower to nacelle connection. Since this is impossible without knowing the exact make up of the nacelle, and the analysis passed as is, this detail design was not undertaken in the current project.

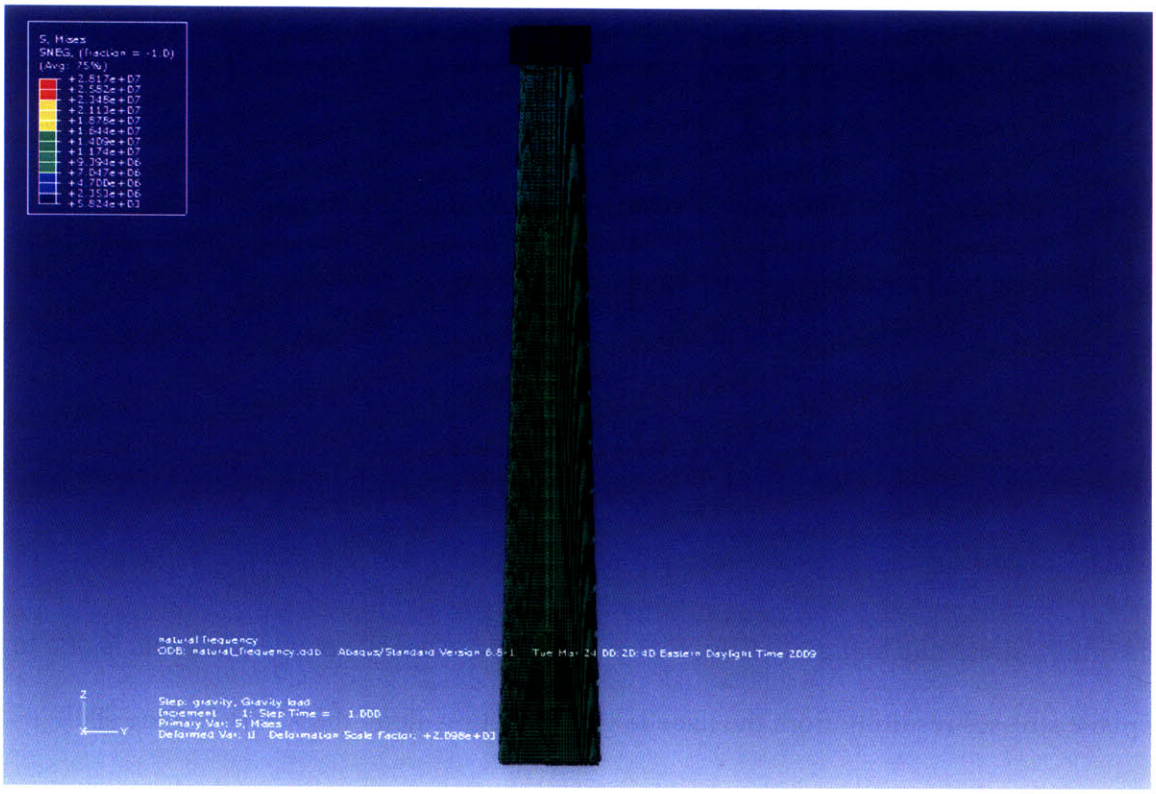

Figure 7.3 Gravity Load Output

7.3.2 Wind

The maximum stress observed due to the rotor wind thrust was 62.4Mpa which was located at the leeward base of the tower as seen in figure 7.4.

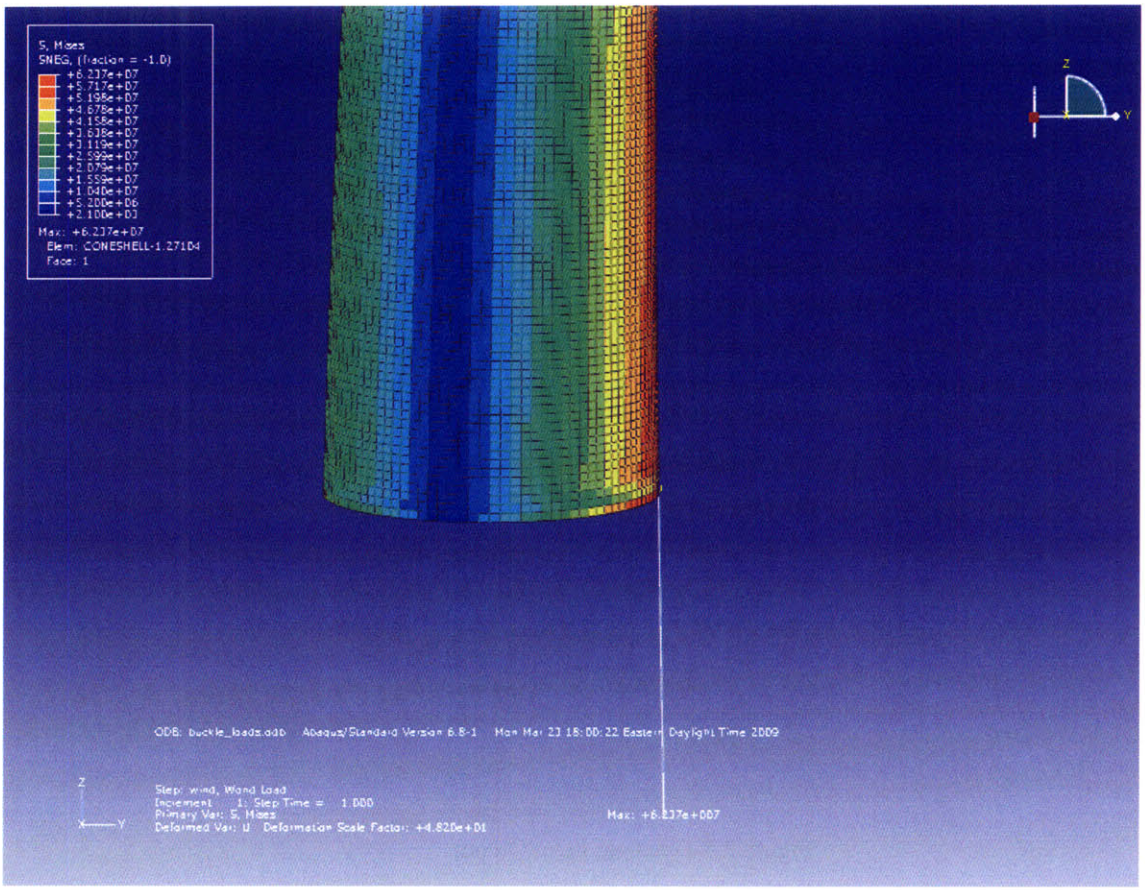

Figure 7.4-Wind Load Output

7.3.3 Dynamic

The maximum stress observed due to dynamic loads from acceleration was 73.0 MPa located at the leeward base of the tower as seen in Figure 7.5.

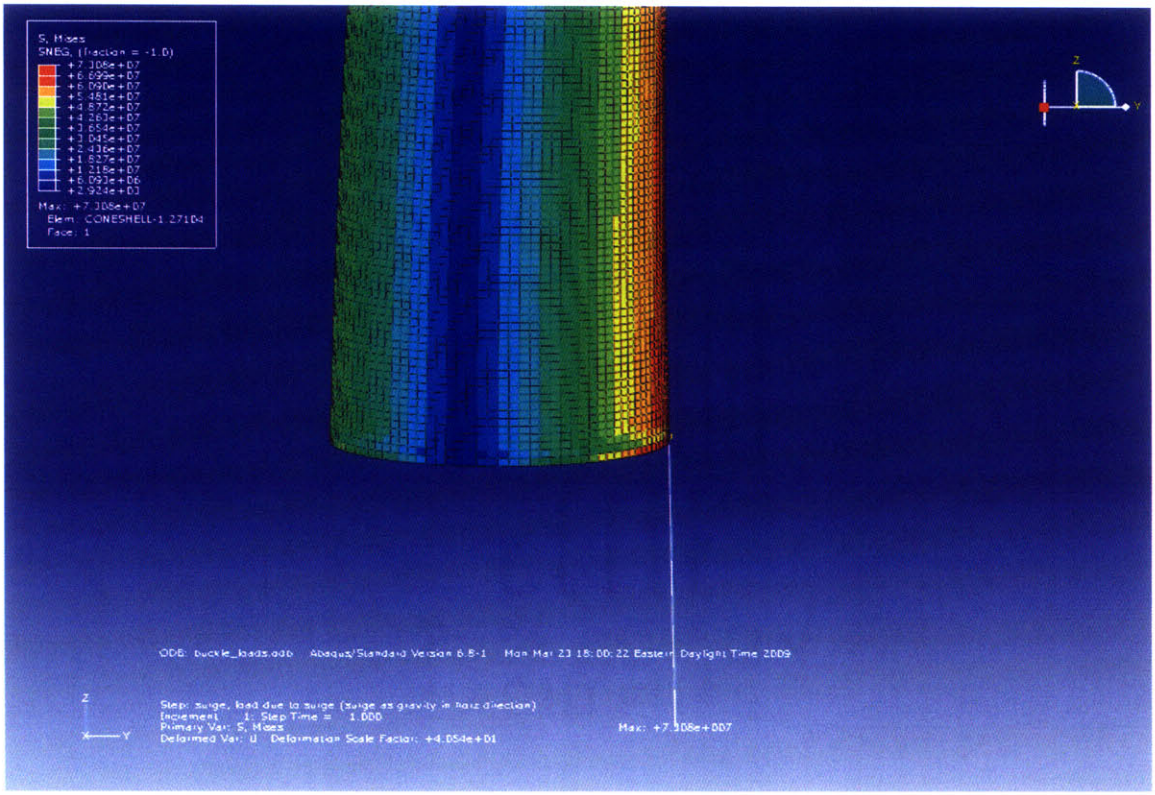

Figure 7.5-Dynamic Load Output

7.3.4 Axial Buckle

The lowest eigenvalue for axial buckling was 5286, which when multiplied by the magnitude of the buckling load means that the reserve axial buckling load of the loaded tower is approximately 266MN. The buckling occurs in the same location as the maximum stresses shown in the sections above.

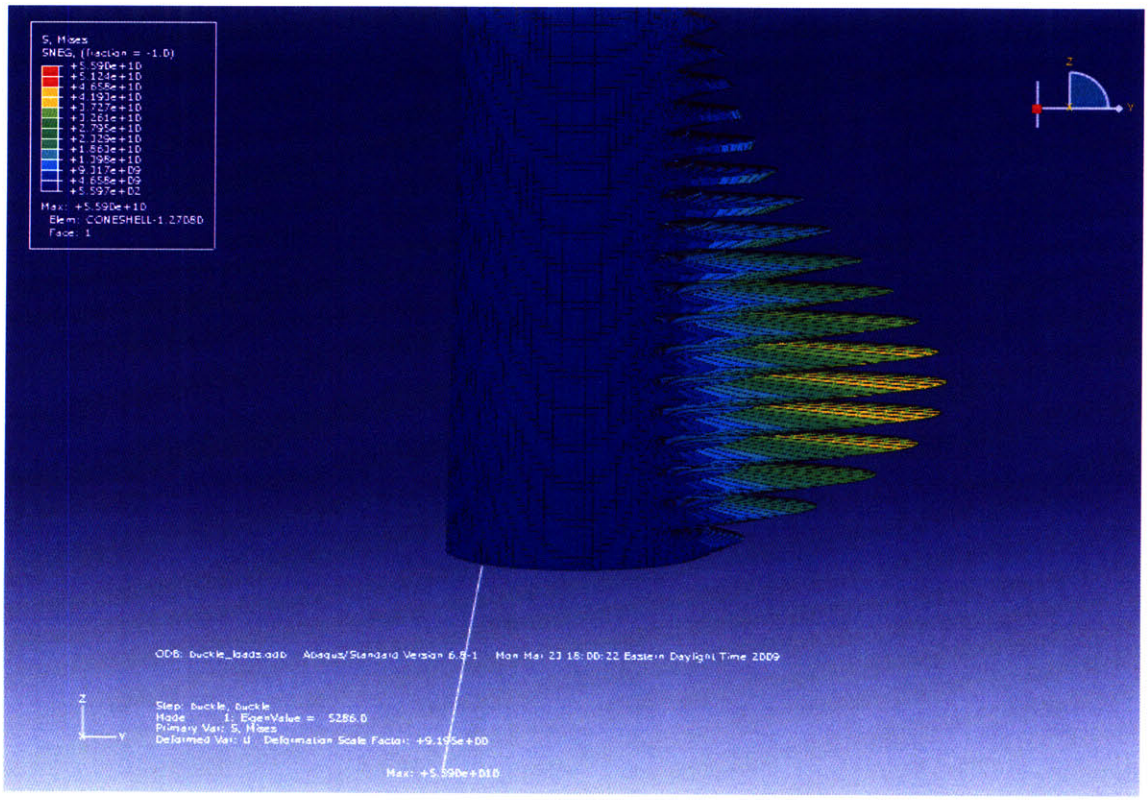

Figure 7.6-Axial Stress Buckling Load

7.3.5 Bending Stress Buckle

The lowest eigenvalue for axial buckling due to bending stress from rotor thrust was 244. When multiplied by the applied buckling load acting on the nacelle face, this means that the reserve rotor load for buckling of the loaded tower is approximately 12.2 MN.

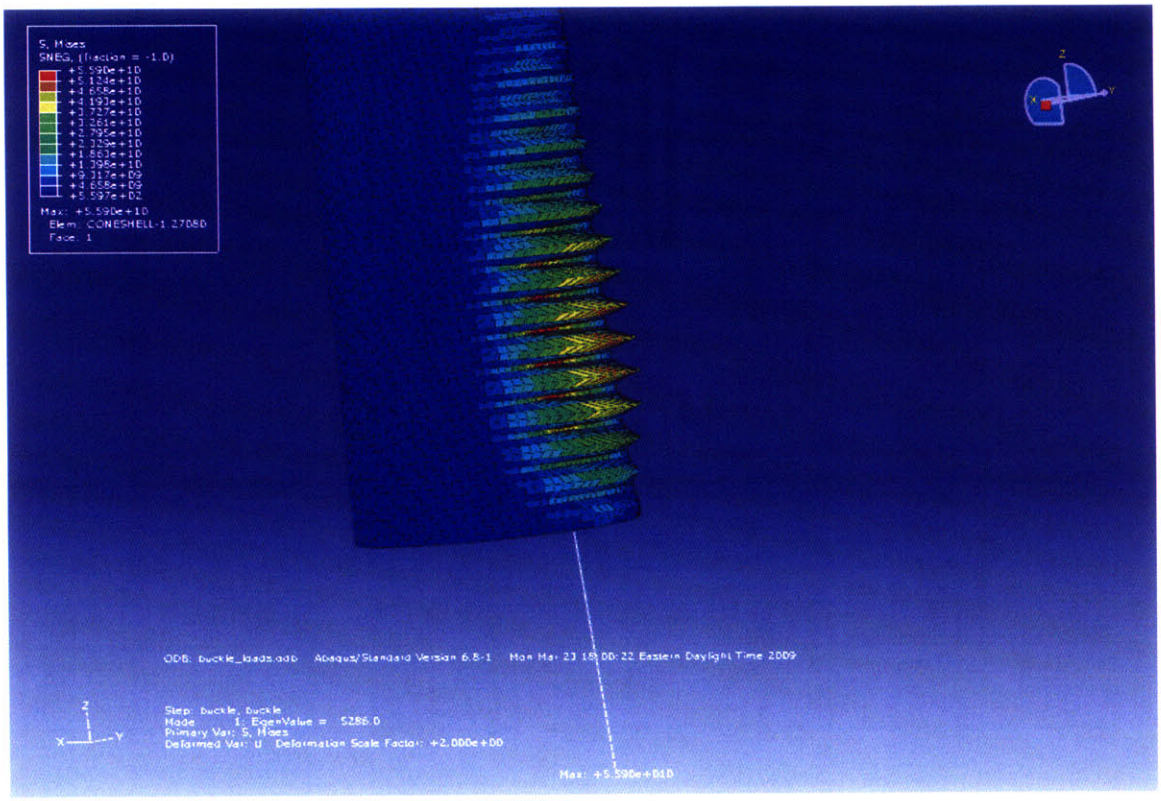

Figure 7.7-Bending Stress Buckling Load

7.3.6 Natural Frequency

All natural frequency modes between 0 and 90 rad/sec were calculated and the first 15 are presented below in Table 7.1. The frequency range of typical sea spectra is 0-2 rad/sec. The lowest frequency mode of natural frequencies from the ABAQUS analysis was 3.80 rad/sec, which is well outside of the range of sea spectra, so wave excitations at the natural frequencies are highly unlikely.

EIGENVALUE OUTPUT				
MODE NO	EIGENVALUE	FREQUENCY (RAD/SEC)	FREQUENCY (CYCLES/SEC)	GENERALIZED MASS
1	10.563	3.25	0.51725	3.84E+05
2	10.563	3.25	0.51725	3.84E+05
3	184.13	13.569	2.1596	84573
4	184.13	13.569	2.1596	1.69E+05
5	258.52	16.078	2.559	72109
6	258.52	16.078	2.559	72662
7	534.27	23.114	3.6787	60340
8	534.27	23.114	3.6787	60801
9	651.08	25.516	4.061	60554
10	651.08	25.516	4.061	51632
11	751.67	27.417	4.3635	1.58E+05
12	751.67	27.417	4.3635	1.58E+05
13	994.89	31.542	5.02	48932
14	994.89	31.542	5.02	57392
15	1126.6	33.564	5.3419	80442

Table 7.1-First 15 Natural Frequency modes

The other key oscillating exciting force which must be considered is the cyclic loading due to the passage of the rotor blade over the tower. The maximum speed of the rotor is 12.1rpm. Since the turbine is 3 bladed this means that the maximum exciting frequency is 3.8 rad/sec.

This exciting frequency is 3.25 rad/sec, which is smaller than the lowest two natural frequency modes. Additionally the natural frequency vibration directional components and the

excitation directional components each act in the X_{44} or X_{55} direction, therefore resonance does pose a significant problem. Table 7.2 shows the participation factors for the first 15 modes; it can be seen that mode 1 and 2 vibrate principally about the X or Y axis.

The best way to avoid resonance problems is to make the structure stiffer and raise the lowest natural frequency modes above any environmental excitation frequencies. For the monocoque tower system, the stiffest possible structure while maintaining the NREL 5 MW design weight would result from a cylinder with the maximum possible diameter. The plate thickness would have to decrease as the diameter increases, for a cylinder diameter of 10 meters, the plate thickness would become 1.5 centimeters.

A natural frequency extraction analysis was conducted for a cylinder with a diameter of 10 m and thickness of 1.5 cm. This represented the stiffest possible structure (in the global X_{44} or X_{55} direction), given the 5 MW NREL specified tower weight, and the maximum diameter (based on the floater cylindrical section). The analysis doesn't consider any of the requirements specified by the API Bulletin 2U. Its main purpose was to determine if it was possible to increase the lowest natural frequency mode above the blade passage frequency. The lowest natural frequency, resulting from this potential tower was 3.32 rad/sec, which is still below the blade passage frequency. From this analysis it can be seen that large changes in the overall cylinder geometry, which do not increase tower weight, do not reflect a substantial enough change in the tower's lowest natural frequency to exceed the blade passage frequency.

PARTICIPATION FACTORS						
MODE NO	X-COMPONENT	Y-COMPONENT	Z-COMPONENT	X-ROTATION	Y-ROTATION	Z-ROTATION
1	-7.75E-04	1.1462	-1.15E-12	-96.534	-6.53E-02	-2.80E-11
2	1.1462	7.75E-04	1.39E-13	-6.53E-02	96.534	-7.92E-12
3	-1.20E-12	9.34E-13	1.22E-05	-4.09E-11	-1.45E-10	2.42E-13
4	-1.51E-13	-4.45E-13	-3.24E-12	5.27E-11	-2.47E-11	3.21E-07
5	-2.56E-07	1.81E-12	-3.59E-14	-1.73E-10	-8.81E-06	2.58E-13
6	-1.93E-13	7.67E-07	1.11E-14	-3.04E-05	-1.21E-10	4.30E-13
7	-9.25E-06	-4.25E-12	4.37E-14	6.21E-11	-2.72E-04	9.94E-13
8	2.14E-12	7.00E-06	1.15E-14	-2.07E-04	-8.96E-11	-5.67E-13
9	2.98E-12	1.03E-12	-2.96E-11	-2.24E-11	6.80E-11	7.48E-07
10	3.72E-12	-3.38E-12	-5.67E-08	7.63E-11	8.29E-11	-4.59E-10
11	0.7766	-4.86E-06	-9.61E-13	1.28E-04	20.512	5.45E-12
12	4.86E-06	0.77662	-1.25E-13	-20.512	1.28E-04	1.74E-11
13	7.19E-12	-3.44E-12	2.96E-07	1.08E-10	2.36E-10	7.97E-10
14	-7.07E-13	-8.33E-13	5.48E-11	2.43E-11	-2.22E-11	-3.69E-06
15	2.27E-12	-2.29E-12	-5.70E-05	8.98E-11	8.34E-11	1.97E-12

Table 7.2-First 15 Natural Frequency Participation Factors

7.4 Conclusion

The API Bulletin 2U and ABAQUS analysis agree in predicting that the tower structure as designed exceeds structural requirements. The maximum stresses for the design are well below the allowable stresses for all failure modes. Eigenvalue frequency extraction analysis shows that the lowest natural frequency mode is below any expected excitation frequency due to typical sea spectrum; however blade passage frequency is higher than the lowest natural frequency mode. Concept design study shows that it is not possible to design a structure with the specified weight given the designed cylindrical section diameter used for this paper. This concept design study also suggests that drastic monocoque cylinder diameter changes alone will not result in a structure which avoids this particular potential resonance issue.

Since the blades will reach their fullest pitch at the same time as the maximum blade frequency is obtained, further work is needed to determine if the blade passage corresponds to an

appreciable environmental load on the tower. If this is not the case, then the as designed structure is sufficiently stiff in terms of all other structural metrics and should be considered as a viable design.

This analysis and design was not meant to optimize the tower section since many current and past designs used the weight and center of gravity properties of the 5 MW NREL turbine. Instead the current chapter strove to show a potential structural design for the 5 MW turbine. Before any studies into the optimization of the tower structure are conducted, a full iteration of the complete floating wind turbine system should be considered, including cost estimation. This will allow any future optimization to properly weight the two optimization variables, weight and costs.

8 Design of Cylindrical Floater Section for TLP

8.1 Introduction

As discussed in References [1, 2, and 3] there are many potential methods in which to support the tower and nacelle. Sight specific properties and continuing research will evolve the current floater designs. Despite a potential transitioning of shapes and properties of floater designs, all designs presented thus far and foreseeable future designs incorporate a cylindrical shell section. Based on the superior structural efficiency of orthogonally stiffened cylinders over monocoque cylinders, any cylindrical shell section appearing in the floater of a wind turbine design will be orthogonally stiffened.

Terebushko [21] showed that cylinders stiffened with typical stiffener geometric parameters and spacing usually achieve a structural weight which is 1.5 times lighter than the corresponding monocoque cylinder of equal overall dimensions. The significant weight savings shown by Terebushko is not associated with optimal design. The analysis presented below attempts to improve on this expected weight savings by conducting a parametric weight optimization study.

The analysis presented in this chapter will go through a design process with the goal of a cylindrical section with maximum weight efficiency. There are many foreseeable floater designs which will rely on cylindrical sections. The design process for all of these cylindrical sections will be virtually the same. The parametric stiffener design algorithm was developed so that any cylindrical section general geometry of future floater designs could be analyzed with this algorithm.

8.2 Methodology

8.2.1 Initial Design

8.2.1.1 Subdivisions

All modern steel floating structures are subdivided by bulkheads into water tight compartments. One reason for this is damaged stability; this ensures that a failure in water tight integrity of one section of the structure will not results in the loss of the structure. In the MIT FWT cylindrical section, bulkheads serve the additional purpose of strengthening the cylinder.

The more subdivisions a structure has the less likely it is to have a catastrophic failure if it sustains damage which affects the watertight integrity of the structure. However, each additional bulkhead added to the structure requires more steel and increases the weight and cost of construction. In naval architecture a common design requirement is that a ship must be able to withstand open sea damage which extends over a length of 10% of the overall design waterline line and still maintain positive stability. As the cylindrical section is oriented vertically while the major axes of ships are oriented horizontally, the ship is exposed to much more damage along the waterline than the spar. For this reason a more reasonable requirement for the cylindrical section will be set that states the cylinder must be able to remain stable and buoyant after it sustains damage extending from the waterline to 10 meters below the waterline. This distance was chosen as it seems that most allisions with floating or even partially submerged objects incur damage which extends no more than 10 meters below the waterline.

Since the cylindrical section design has so many potential variations on its use in different floater and mooring schemes, it would be difficult and unduly time consuming to conduct a full damaged stability calculation on all potential cylinder design variations. In the specific case of the MIT FWT project there are some unique attributes of the system which allow for some

damage stability robustness and enable the designer to make a few general subdivision rules which will conservatively ensure adequate damaged stability for all foreseen MIT FWT designs.

The first important attribute of the MIT FWT is that the blades of the wind turbine can be feathered in case of emergency, which reduces the induced wind moment. The NREL 5 MW wind turbine has a stated maximum thrust of 80 tons; this maximum is achieved at a wind speed of 11.5 m/s, and decreases even as wind speeds increase to 25m/s, by adjusting the pitch of the blades. At 25 m/s the blades are feathered and the rotor stops. Once the blades are feathered it is assumed that the thrust on the rotors are negligible and the only wind thrust acting on the system is due to flow over the bluff tower body. For the given geometry of the NREL 5MW turbine and a wind speed of 25m/s this resulting thrust is easily calculated via equation 8.1.

$$Ct = \frac{T}{1/2\rho v^2 A} \tag{8.1}$$

Whereas the wind thrust due to an operating turbine is assumed to be at the hub height, the thrust due to viscous effects on the tower acts at the centroid of the surface area of the tower. This height is approximately 37m from the waterline. This means with a cylinder depth of 40m, the total moment with blades feathered in 25 m/s wind speeds is 132 tons-m compared to the 10400 tons-m associated with 12m/s winds with blades pitched for rated power.

The significance of this finding is that in cases of damage and flooding the blades can be feathered which reduces the pitching moment significantly. This reduces the requirements for stability during damaged conditions. Normally, naval architects calculate required damaged stability by considering the reduction in overall stability due to flooding. In this case it is more convenient, useful and universal to consider a worst case scenario pitching arm due to flooding.

The worst case scenario for cylinder damage is if the top section of the cylinder was flooded. For our case we will show that even if the top 1/3 of the cylinder (which would be a flooded length of 13.33 m) was flooded solid, the maximum potential healing arm is still much smaller than the healing arm reduction resulting from feathering the turbine blades. In order to determine a shift in a center of gravity, due to a flooded section, equation 8.2 can be used.

$$cg = \frac{\sum w_1 cg_1}{\sum w_1} \tag{8.2}$$

The maximum vertical shift for flooding occurring in the top third of the section via equation 8.2 is 0.083L. All designs considered thus far in the FWT project have had cylindrical sections whose diameter to length ratios have exceeded 0.1. So even for the impossible case of the cylinder healing 90 degrees, the shift in the center of gravity resulting from a hypothetical top $^1/_3$ flooding of the cylindrical section would not even exceed the moment arm of any tension leg attachments. Also if the case of the 5 MW turbine is considered with a cylindrical section of 40 meters in length, the most extreme example, this hypothetical healing moment would be roughly equal to the reduction of healing moment created by feathering the blades.

These conservative calculations show the effects of the design requirement presented above which allows damage to extend ten meters below the water line. For this design requirement, positive stability in damaged conditions is not a concern as long as chosen subdivisions of the cylinder ensures that there is no individual compartment greater than $^1/_3$ the total length of the cylinder.

8.2.1.2 Similar System Analysis

In order to ensure a reasonable and buildable design, a design baseline was first determined. In naval architecture the first step of this design is called "similar ships analysis." In order to conduct a similar ships analysis, a proven and successful design with similar attributes to the current design is selected. For the Floating Wind Turbine Project the Sea Star mini TLP was chosen.

Atlantia Marine first developed the Sea Star TLP in 1992. The target market of this structure was to reach a deepwater segment of the offshore oil market where the majority of discoveries were small, but plentiful. The Sea Star was able to make these smaller field discoveries profitable due to the lower acquisition and maintenance cost of the mini TLP versus full size TLP and Spar designs at the time.

The FWT floater has an almost identical design space, namely that the resource is plentiful but relatively small. In order to compete with conventional energy sources, the structure used in any floating wind turbine must be economical and reliable.

The Sea Star TLP has one element of the design which must be disregarded and should not be propagated into the MIT FWT design. The Sea Star has a large cylindrical section passing through the center of the cylinder called the "Tree" which is used for the passage of oil pipes and drilling equipment. This is standard because all mini TLP's built to date are intended for oil production. All TLP's have this specific attribute, so selecting a similar design for the MIT FWT without the "Tree" is impossible.

Once the Sea Star mini TLP was selected as a similar platform, dimensions and properties were harvested from publically available resources released by Atlantia. The general dimensions and loads of the Matterhorn field example of the Sea Star mini TLP are listed in Table 8.1

Matterhorn was Atlantia's first dry-tree TLP, and it was the first deepwater structure in the Gulf of Mexico to be built on a full turnkey EPCI contract.	
Location	Mississippi Canyon, Block 243
Water depth	2820 feet
Project award	September 2001
Platform installation	August 2003
First oil	November 2003
Payload	16,850 kips
Column diameter	84 feet
Column height	125 feet
Draft	104 feet
Pontoon radius	179 feet
Pontoon height	42 feet
Deck/facilities weight	13,350 kips
Deck dimensions	140 x 140 feet

Table 8.1

The loads of the Sea Star were converted to a nominal average axial stress by dividing by cross sectional area as given by the plate thickness multiplied by the circumference. This average load was compared to the average axial load of the 40m draft MIT TLP-1, which is presented in the Design Inputs section. The ratio of axial loads between the two TLP designs will remain relatively constant along the Z axis as the moment and weight generally vary linearly along the Z axis in both designs. Consequently the average axial load ratio can be taken as the local axial load ratio at every point considered in the design of the cylindrical section.

As discussed in the Section 8.2.1.1, the cylindrical section will be required to be broken up into subdivisions. The baseline design places bulkheads in such a way as to create subdivisions which are of the same proportion of those seen in the Sea Star TLP. Due to differences in the geometries between the Sea Star and the MIT TLP-1 pontoons, a slight modification to the bulkhead arrangement had to be made in the MIT TLP-1. Since the rigidity of the cylinder

section-to-pontoon connection is an extremely important design aspect, it is desirable to locate a cylinder section bulkhead coincident with the top connection of the pontoon; this same design attribute can be seen in the Sea Star TLP. The MIT TLP-1 pontoons reach proportionally higher from the bottom of the cylindrical section than that of the Sea Star. Whereas the Sea Star TLP lowest cylinder section is the same height as the pontoon, the corresponding cylinder section for the MIT TLP-1 would be too large. Consequently an additional bulkhead was located halfway between the bottom of the cylinder section and the top of the pontoon. This additional bulkhead placement brings the total bulkheads expected on the baseline design to be equal to seven for a total of six cylinder sections.

While the axial load ratio can be considered to be constant throughout the cylinder section. The second load considered, hydrostatic load, obviously varies with depth. Consequently the hydrostatic pressure ratio between the two systems was calculated for each cylinder section. For simplicity the hydrostatic pressure ratio was taken to be the ratio of the heights of the sections. The hydrostatic load contributes to two specific structural stresses, in plane horizontal stress due to hoop compression, and lateral pressure. Excessive hoop stress will manifest itself in plate buckling waves oriented in the horizontal direction. Excessive lateral pressures act out of plane and will create bending stress on the plate and stiffeners. Both of these structural responses dictate the size and spacing of the ring stiffeners, as these are the main structural members responsible for resisting these stresses.

8.2.1.3 Plate Aspect Ratio

In thin walled stiffened shells, the stiffeners act as simple supports for the plates that lie in between the stiffeners. The plates subtended by the stiffeners have specific aspect ratios dictated

by the spacing of the longitudinal (or verticals in this case) stiffeners and the ring stiffeners. The aspect ratio of a plate is an extremely important element in determining the buckling stress of the plate. This buckling stress results from in-plane stresses which are created by the axial stress and the hoop compression stress discussed above. Proper selection of plate aspect ratio for the combined loading of a structure will result in increased structural efficiency.

Plate stiffening should always be in the direction of the principal in-plane stress. Reference [18] provides an excellent proof of this concept and shows that for unidirectional stiffening, stiffeners which lay in the same direction as the principle axial stress result in a buckling stress which is four times higher than if the stiffeners were laid orthogonal to the direction of stress.

The scantling spacing of the Sea Star can be seen in Figure 8.2; this spacing was obtained from Reference [20]. The scantling spacing was used to determine an aspect ratio for the plating of the Sea Star. This aspect ratio was then modified to efficiently withstand the particular stresses experienced by the MIT TLP-1 cylindrical section.

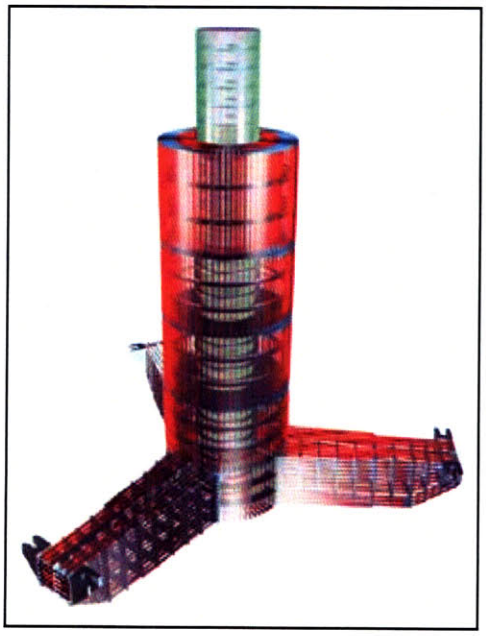

Figure 8.2

In this specific design, there are two orthogonal stresses: ring compression stress due to hydrostatic pressure, and axial stress due to the wind and wave moment plus the weight of the structure. For this stress profile an orthogonally stiffened design will be the most structurally efficient. The Sea Star TLP achieved success on the efficiency of its stiffener layout. The designers of the Sea Star TLP completed time consuming detailed structural analysis to ensure the aspect ratio of the plate was efficiently laid out for the particular stresses experienced by the Sea Star TLP. Since this design is already efficient, this layout will be adjusted for the MIT FWT cylinder section baseline to attempt to start the design process with a buildable design. Equation 8.3 was used to modify the Sea Star plate aspect ratio to the baseline MIT FWT aspect ratio.

$$\frac{SS_{AR} R_A}{R_L} = WT_{AR} \tag{8.3}$$

Where

SS_{AR}	Sea Star plate aspect ratio	
WT_{AR}	MIT TLP-1 plate aspect ratio	
R_A	Axial stress ratio	(SS/WT)
R_L	Lateral stress ratio	(SS/WT)

Since the aspect ratio of the Sea Star plate was efficient based on stress distribution and modified via these ratios, we would expect that the aspect ratios discovered for the MIT TLP-1 would be reasonably efficient enough to act as a baseline design. Table 8.2 shows key similar system analysis parameters.

Similar System Analysis		
Axial Stress Ratio	Lateral Stress Ratio	Sea Star FWT1 Aspect Ratio
1.2	1.054.320988	3.424113
1.2	1.12	3.086422
1.2	1.062.777778	2.193414
1.2	1.092.469136	1.890965
1.2	1.171.851852	1.320427
1.2	1.171.851852	1.320427

Table 8.2

8.2.1.4 Plate Thickness

The plate thickness of the FWT cylindrical section was set equal to 20mm. This thickness was chosen because that was the thickness of the tower section for the 5 MW NREL turbine. Since the tower section was 20mm thick and would sit on the floater's cylindrical section, the floater thickness should be equal to or greater than the tower thickness, in order to decrease complex stress and fatigue effects on the cylinder/tower joint.

The producibility of potential cylinder designs was taken into account throughout the design process. In this phase of the design, producibility considerations limited the maximum thickness of the plate. Special welding techniques, which are more expensive, must be used on plate thicknesses which exceed 25mm. Since the tower thickness was already close to 25mm and the cylinder section thickness could not be less than 20mm as discussed above, a set cylinder thickness of 20mm was chosen. This thickness choice has the added benefit of a continuous plate thickness through the floater cylinder to tower interface.

8.2.1.5 Rules Based Design

The selection of the FWT plate aspect ratio and plate thickness form the required inputs for a rules based structural design of the cylindrical section. The American Bureau of Shipping (ABS) Classification Society rules for Floating Production Instillations (FPI) and the rules for Mobile Offshore Drilling Units (MODU) were used for the preliminary design. There are no rules which explicitly deal with floating wind turbines. After research into all classification society rules, these ABS rules seemed the closest to covering the particular floating wind turbine situation. The rules state that TLP should first be designed for the local load effects as these loads are most likely the limiting case. The subsequent design should then be verified to withstand global loads.

For local loading, the plate and stringers can be assumed to be flat for preliminary design estimations. This allowed the design to initially consult both the FPI and MODU rules as the wind turbine design lays somewhere near both of these types of vessels. Eventually both rules refer to the Section 3-2-2 of the MODU rules titled Common Structures. Paragraph 9.3 of the Common Structures section provides an equation for the thickness of plating which can be seen below as equation 8.4

(8.4) $$t = sk\sqrt{(qh)} / 254 + 2.5mm$$

Where

t	thickness in mm
s	stiffener spacing, in mm
k	$(3.075\,\alpha - 2.077)/(\alpha + 0.272)$ for $1 \leq \alpha \leq 2$ 1.0 for $\alpha > 2$
α	aspect ratio of the panel (longer edge/shorter edge)
q	$235/Y$ ($24/Y$, $34{,}000/Y$)
Y	specified minimum yield point or yield strength, in N/mm2 (kgf/mm2, psi), or72% of the specified minimum tensile strength, whichever is the lesser
h	greatest of the following distances, in m (ft), from the lower

edge of the plate to:
i) a point located two-thirds of the distance from the top of the tank to the top of the overflow;
ii) a point located 0.91 m (3 ft) above the top of the tank;
iii) a point representing the load line;
iv) a point located at two-thirds of the distance to the freeboard deck.

Since the aspect ratio and plate thickness were already set upon entering into Equation 8.4, the equation was used to calculate the spacing of the stiffener. Since the h (already known from selection of bulkhead height see, 8.2.2.1) and α vary depending on the section, the required spacing will vary as well. Table 8.3 shows the calculation for required stiffener spacing for all sections of the MIT TLP-1. For structural strength and better fatigue performance, it was determined that the vertical stiffeners should run continuously up the entire length of the cylinder, though they will be allowed to change their cross section at each bulkhead. For this reason, the smallest required stiffener spacing resulting from Equation 8.4 was used as the stiffener spacing for all sections of the FWT cylindrical section.

Stiffener Spacing						
Inputs	Section 1	Section 2	Section 3	Section 4	Section 5a	Section 5b
alpha	3.42	2.31	2.19	1.89	1.32	1.32
h (m)	15	23	29	35	40	45
t (mm)	20	20	20	20	20	20
k	1	1	1	0.994701793	0.9146275	0.914627498
Y (N/mm^2)	250	250	250	250	250	250
s (mm)	1353	1093	972	890	906	854

Table 8.3

The aspect ratio of a plate is defined as the long edge divided by the short edge. The spacing presented in Table 8.3 is for the edge of the plate, the minimum spacing is .972 meters. In the similar ship design presented above, the short edges for all sections were always the edge

between vertical stiffeners, so multiplying the minimum spacing (.972m) between the vertical stiffeners by the aspect ratio will give the spacing between ring stiffeners for each section. Equation 8.5 is the Section Modulus calculation for stiffeners and beams, in our case these are the vertical stiffeners.

(8.5) $$SM = fchsl^2$$

Where

f	7.8 (0.0041) 0.9 for stiffeners having clip attachments to decks or flats at to the ends or having such attachments at one end with the other end supported by girders 1.00 for stiffeners supported at both ends by girders
h	greatest of the distances, in m (ft), from the middle of l to the same points to which h for plating is measured (see 3-2-2/9.3)
s	spacing of stiffeners, in m (ft)
l	length, in m (ft) between supports; where brackets are fitted at shell, deck or bulkhead supports, and the brackets are in accordance with 3-2-2/Table 2 and have a slope of approximately 45 degrees, the length l may be measured to a point on the bracket located at a distance from the toe equal to 25% of the length of the bracket.

The Section Modulus is a convenient way to specify the required strength for scantlings; it is equal to the moment of inertia divided by the distance to the extreme fiber. In this calculation, l the length between supports, is equal to the ring stiffener spacing for a given cylinder section. The required section modulus for each cylinder section can be seen in Table 8.4.

Stiffeners and Beams						
Inputs	Section 1	Section 2	Section 3	Section 4	Section 5a	Section 5b
f	7.8	7.8	7.8	7.8	7.8	7.8
c	1	1	1	1	1	1
h (m)	7.5	14.0	21.0	27.0	31.0	35.0
s (m)	0.890	0.890	0.890	0.890	0.890	0.890
l (m)	3.049	2.058	1.953	1.684	1.176	1.176
SM req (cm^3)	484.07	411.56	557.09	532.34	297.77	335.98
SM req (in^3)	29.540	25.115	33.996	32.485	18.171	20.503

Table 8.4

Once the required Section Modulus is known, published manuals for steel construction can be consulted in order to choose standard stiffener cross sectional geometry. For the purposes of this design the American Institute of Steel Construction (AISC) Manual for Steel Construction was used. A structural T cut from "W" shapes was selected as the type of stiffener shape considered for the vertical stiffeners. The table of Dimensions and Properties for Structural T's was entered into with required section modulus. For each section the T which had the smallest weight per length and a Section Modulus which exceeded the required section modulus was selected. Table 8.5 shows the selected cross section type, and some key properties for the vertical stiffeners of each of the sections.

Vertical Stiffener Properties						
	Section 1	Section 2	Section 3	Section 4	Section 5a	Section 5b
Weight (kg/m)	73.71	73.71	87.86	80.41	73.71	62.54304
web height (cm)	37.66	37.66	41.73	37.88	37.66	33.92
web thickness (cm)	1.32	1.32	1.40	1.38	1.32	1.17
flange width (cm)	26.54	26.54	29.16	26.61	26.54	25.30
flange thickness (cm)	1.70	1.70	1.88	1.93	1.70	1.63
I (cm^4)	13403	13403	19521	14526	8991	8991
SM (cm^3)	492	492	642	524	359	359

Table 8.5

The Ring Stiffeners obviously could not be assumed to be flat; hence a more involved initial

calculation process must be undertaken. The ring stiffener Section Modulus requirements are large enough to dictate cross sectional dimensions which are not listed in the Manual of Steel Construction tables. The ring stiffener cross section dimensions were chosen as a custom design built up from two plates of common thickness. The practice of using built up stiffeners is common in ship building. In order to ensure reasonable cross sections were used, criterion published in AISI, Cold-Formed Steel Design Manual, 1983 Edition were applied to all potential stiffener dimensions. These criteria ensure that the ring stiffener will fail from yield prior to failing from buckling, which is common practice in ship and offshore system design. The ring sizing procedure put forth in API Bulletin 2U was used to size the rings. Broad ranges for the rings web and flange thickness and heights were set. Any combinations of properties which did not meet compactness criteria were instantly thrown out. The stress in the ring was calculated for each combination of the ring properties. A ring was deemed acceptable if the ring stress divided by a safety factor of 1.25 was less than the yield stress. The passing ring which minimized weight was then selected as the design ring. Table 8.6 shows key properties of the custom girders selected to serve as ring stiffeners.

Ring Stiffener Properties						
	Section 1	Section 2	Section 3	Section 4	Section 5a	Section 5b
Weight (kg/m)	174	210	230	240	220	224
web height (cm)	51	66	66	66	66	66
web thickness (cm)	2.86	3.49	3.49	3.49	3.49	3.49
flange width (cm)	15.24	7.62	12.70	15.24	10.16	12.70
flange thickness (cm)	5.08	5.08	5.08	5.08	5.08	4.44
I (cm^4)	7.08E+04	1.26E+05	1.48E+05	1.57E+05	1.37E+05	1.40E+05
SM (cm^3)	2017	3298	3619	3747	3471	3508

Table 8.6

With the selection and calculation of ring stiffener properties, all required dimensions for

the shell stiffening are known. This does not constitute a full buckling analysis. This is just a preliminary analysis which is conservatively selected in order to have a reasonable starting point for future analysis which will be presented in following sections.

The next step in the baseline design of the cylindrical section is the design of bulkheads. The calculation of bulkhead scantlings is very similar to the calculations presented above, for the purposes of brevity will not be presented. The equations used for the calculation of the bulkhead scantlings can be found in ABS MODU rules 3-2-2/9. The plate thickness used for the bulkheads was set equal to that of the shell plating for simplicity of design and build. The aspect ratio of the plate was optimized for total weight reduction for each of the bulkheads. Table 8.7 shows some key attributes of the baseline design bulkheads.

Bulkhead Properties							
	Top Blkhd	Blkhd 1	Blkhd 2	Blkhd 3	Blkhd 4	Blkhd 5	Bot Blkhd
Plate aspect Ratio	1	2	2	2	2	2	2
Spacing (mm)	2987	1353	1093	972	886	829	781
Stiffener/Beam SM (cm^3)	31.7	35.4	34.8	36.7	35.8	33.6	31.8
Girder/Web SM (cm^3)	2601	7070	10656	14240	16689	17908	19051
Nbr Stiffeners	2	6	8	9	10	11	12
Nbr Girders	2	3	4	4	5	5	5

Table 8.7

The scantling design of the baseline cylinder section serves as a reasonable starting point for the initial iteration of the structural optimization code to be discussed in later sections. The scantling design also serves as a reasonableness check during the creation of the code and during the vetting of the optimization code.

8.2.1.6 Structural Weight of Baseline Design

Once the scantling design presented above was completed, the structural weight of the cylindrical section could be calculated. This weight calculation is extremely useful in future steps of the optimal design; it gives a reasonable estimate of the structural weight of the cylinder for given depths, which will be used in the optimization code to be discussed later. The structural weight also serves as a metric to compare the weight savings produced through the design yielded by the optimization code. The type of steel assumed to be used in this design is mild steel; this selection was made based on the ease of construction for mild steel and the economic price of mild steel. The assumed mild steel density was 7800kg/m^3. Table 8.8 lists the weights of the different components at each section of the cylindrical cylinder.

	Weight of Components						
	Section 1	Section 2	Section 3	Section 4	Section 5a	Section 5b	Total
Stiff/ Beam Weight (kg)	878	642	681	573	365	365	
Stiff/ Beam number	31	31	31	31	31	31	
Stiff/ Beam Tot Weight (ton)	27.23	19.91	21.11	17.76	11.31	11.31	108.62
Ring weight (kg)	13635	16481	18061	18851	17271	17563	
Ring Number	2	3	2	2	3	3	
Ring Total Weight (ton)	27.27	49.44	36.12	37.70	51.81	52.69	255.04
Plate weight (ton)	49.00	39.14	29.88	29.01	24.50	24.50	196.03
Total Section Weight (ton)	103.50	108.49	87.10	84.48	87.62	88.50	559.69

Table 8.8

Bulkhead weights of the baseline design are also extremely important. The weight of each bulkhead changes with the depth of that bulkhead, due to hydrostatic pressure. Since each compartment formed by a bulkhead is designed to be a void compartment, the corresponding bulkhead must be designed to withstand the full hydrostatic pressure at the given depth, this is to ensure that in a damaged scenario, the bulkhead resists progressive damage. Table 8.9 lists the

weights of each component of each of the seven bulkheads.

	Weight of Components							
	Top Blkhd	Blkhd 1	Blkhd 2	Blkhd 3	Blkhd 4	Blkhd 5	Bot Blkhd	Total
Stiff/ Beam Weight (kg)	439	439	439	439	439	439	402	
Stiff/ Beam number	2	6	8	9	10	11	12	
Stiff/ Beam Tot Weight (ton)	0.88	2.64	3.51	3.95	4.39	4.83	4.82	24.15
Girder weight (kg)	677	1226	1840	2448	2859	3064	3258	
Girder Number	2	3	4	4	5	5	5	
Girder Total Weight (ton)	1.35	3.68	7.36	9.79	14.29	15.32	16.29	66.73
Plate weight (ton)	1.22	1.22	1.22	1.22	1.22	1.22	1.22	7.30
Total Section Weight (ton)	3.45	7.53	12.09	14.96	19.90	21.37	22.33	98.18

Table 8.9

The total weight of the cylindrical section TLP-1 baseline design can be seen to be 657 tons. This weight is much higher than the final design will become after it has been optimized via the method described below.

8.2.2 Shell Optimization

In order to perform any structural optimization an objective function is required. In typical ships that objective function combines weight reduction (for purposes of increased cargo capacity) and initial cost. Since the FWT will not have any cargo, only the initial cost must be taken into account. The initial cost is a function of both the amount of steel and the labor required for fabrication. The weight of steel is extremely easy to measure, while labor cost for a new type of structure are difficult to obtain, and ever changing with the advent of new techniques. Since this is a novel structure, and no cost estimation has been preformed for the structure, attempting to estimate the labor rates and times would be challenging and potentially inaccurate. For this reason, the objective function for optimization of this initial structural design

only included the weight of the structure. The influence of labor on the cost of the structure was preliminarily taken into account by imposing reasonable design limits, for example the number of vertical stiffeners was limited to 32 to reduce weld lengths. Once the preliminary structural design is complete, the requisite information for full cost estimation will be known. After this is completed, an optimization function which includes weight and labor can be created.

The parametric optimization process varied the bulkhead spacing, number of compartments, stiffener spacing, plate aspect ratio, and stiffener and ring sizing. The bulkhead spacing and number of compartments were first varied subject to a minimum spacing of 5m and maximum spacing of L/3 (from damage stability considerations presented above). The number of vertical stiffeners and bulkhead spacing of every compartment was selected parametrically, then the remaining variables were varied for the given bulkhead spacing. This was continued for all acceptable bulkhead spacing and number of vertical stiffener combinations. For each bulkhead and stiffener combination, the structural design which passed all required tests (discussed below) and was the lowest weight was retained. The test results of each bulkhead spacing and number of stiffener combination were then compared to determine the lowest weight design which passed all yield buckling and hierarchy requirements.

The section of the cylinder which attaches to the tension leg was not included in the optimization analysis. The design of this section will require detailed stress analysis at the connection points and full fatigue analysis studies. Some rough order approximations about the structural weight of this section will be possible, however, based on results of this optimization study.

The shell optimization process used the baseline design presented above as the initial starting point for stiffener spacing, plate aspect ratio, and stiffener and ring sizing. The initial values

were varied by 50% in either direction. If, during the optimization run, any range limit was selected as an optimal value for a variable, that variable range was increased. In some cases maximum and minimum variable values were set, not by what the optimization process indicated, but by practical design limitations.

ABS MODU rules were used in conjunction with American Petroleum Institute Bulletin 2U "Bulletin on Stability Design of Cylindrical Shells" to determine if a particular design was acceptable. This bulletin is intended for design of cylindrical shells with a D/t ration which is greater than 300. The D/t of the baseline design presented above is 500. The buckling equations and design requirements presented in Bulletin 2U are the results of classical buckling equations, proven test data and analytical studies [25]. The buckling limits of the cylindrical shells are based on classical equations reduced by reduction factors in order to account for imperfection and non-linearity effects in the boundary condition as well as the geometry. The reduction factors used in Bulletin 2U were determined through tests conducted on fabricated cylinders [25]. The optimization procedure relies heavily on the work presented in Bulletin 2U which is a compilation of many works dealing with the structural analysis of cylindrical shells. The optimization procedure uses too many equations and symbols to list in this work. The reader is referred to Bulletin 2U for any calculation of buckling unless otherwise specified below.

Figure 8.3 outlines the API Bulletin 2U process to which each design was subjected.

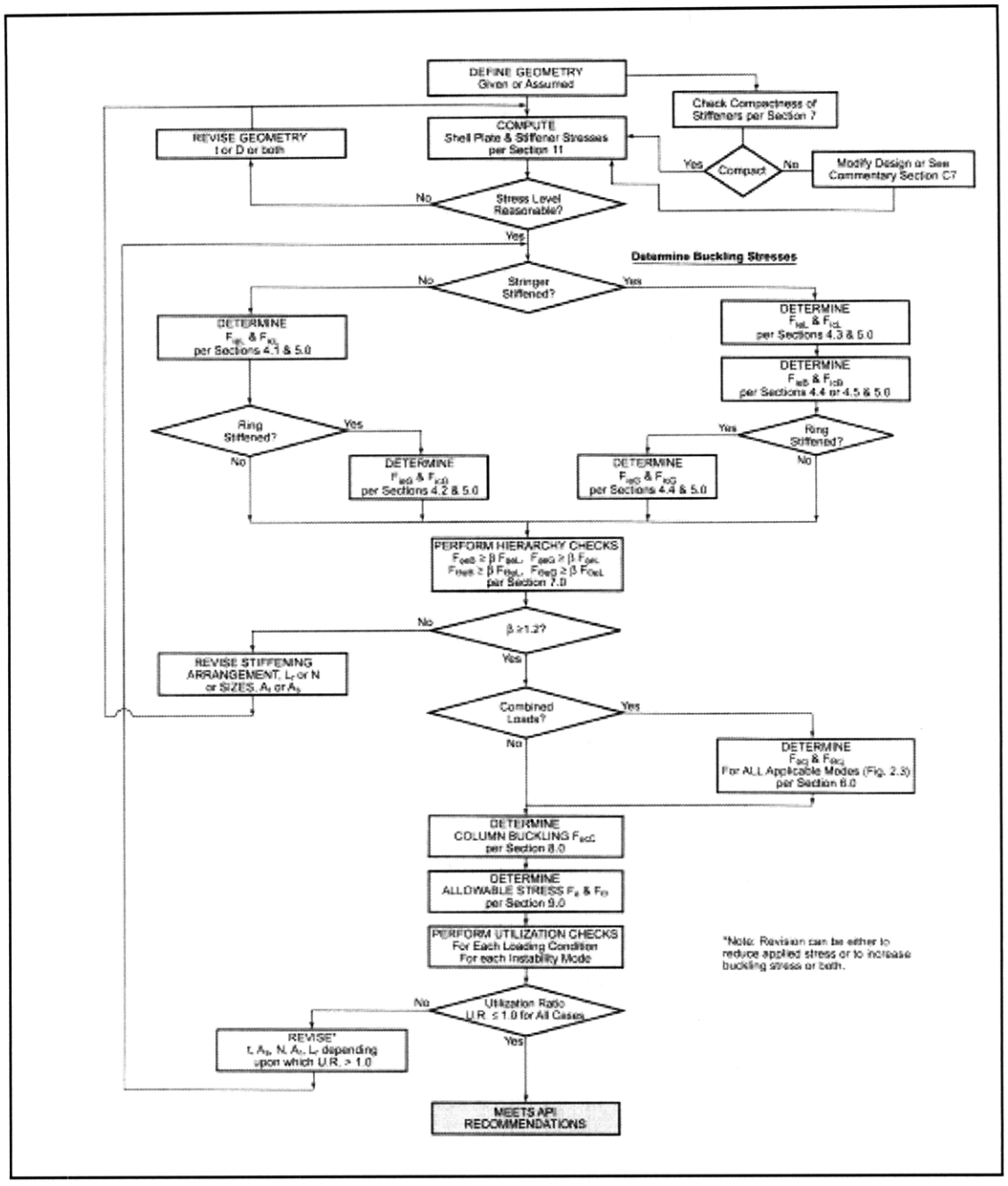

Figure 8.3-Flow Chart for Meeting API Recommendations [25]

As stated in previous chapters the MIT TLP-1 is assumed to be an orthogonally stiffened cylinder, hence the ring and stringer stiffened design procedure must be followed in Bulletin 2U.

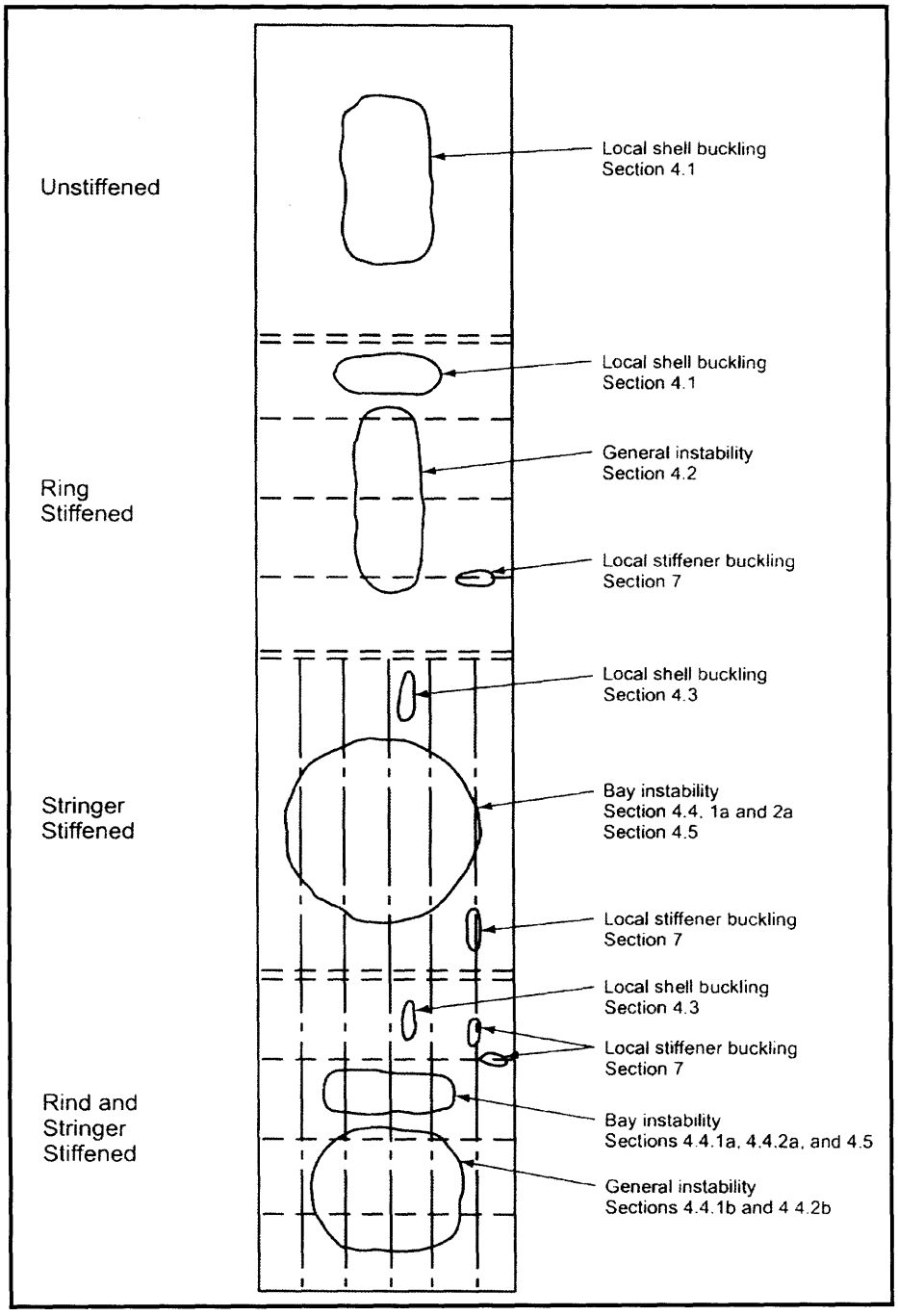

Figure 8.4-Shell Buckling Modes for Cylinders [25]

Figure 8.4 shows the four ways that a ring and stringer stiffened cylinder can fail, and details the chapter of Bulletin 2U which ensures the adequacy of the structure for each failure.

The first type of failure is the local stiffener buckling. This is the most undesirable type of

failure as it provides no warning and will precipitate total catastrophic failure of the cylinder. In order to prevent this type of failure, the stiffeners are required to be "compact." A compact cylinder meets AISI requirements put forth in the AISI Cold-Formed Steel Design Manual, 1983 Edition. These requirements ensure that the stiffener will yield before the buckling stress is reached.

The local shell buckling calculation calculates the bifurcation point for two loads, axial and external pressure. The local shell buckling calculation procedure assumes that the rings and stringers provide adequate rigidity and hence, the cylinder can be treated as a series of curved plates supported along all four edges. Two independent works by Batdorf and Kollbrunner both show that the buckling coefficient can be taken as 4 for this case. The coefficient is then utilized in the classic curved plate buckling equation. API validated this method with the results of a 1983 test conducted by C.D. Miller entitled "Interpretive Report of the Conoco/ABS Test Program"

The bay instability and general instability were tested via the simply supported orthotropic shells method presented in [26]. This method assumes the effective membrane thickness in the longitudinal direction is equal to the area per unit length of the shell and the bending rigidity is based upon the effective moment of inertia per unit length of shell. For the bay instability the cylinder length was set equal to the ring spacing. The cylinder length for general instability was found by setting the cylinder length equal to the length between bulkheads. Bifurcation values for both external pressure as well as axial stress were calculated via this method. The orthotropic shell method is only valid when number Vertical Stringers is less than three times the number of hoop buckling nodes, n. If this condition was not met by a given design, an alternative method was used to determine bay and general buckling stress. The

alternative bay buckling stress calculation is based on the procedure proposed by Faulkner, et al [27]. Faulkner's work is based on the formulation of a collapse mechanism. The alternative method for general instability is based on the assumption that widely spaced vertical stringers provide no stability to ring stringers. The alternative method uses the method laid out in 2U for general buckling of ring stiffened cylinders.

Once local, bay and general stability are known, hierarchy checks are performed. Hierarchy checks ensure that there is no buckling mode interaction which might occur if bay or general buckling stress approaches local buckling stress. This is because local buckling was calculated assuming the stiffeners acted as simple supports. As general and bay instability buckling stresses are approached, this simply supported assumption becomes less valid. An example of the hierarchy requirement recommended by Bulletin 2U is presented below in equation 8.6.

$$F_{\theta cB} > \beta F_{\theta cL} \tag{8.6}$$

Though the mode interactions can be mitigated by the use of Beta, interactions still exist between axial and radial loads of a given mode. For this reason 2U requires the designer to predict buckling stresses due to combined loads. The local, bay and general buckling stresses for axial load and external pressure are entered into the equations presented in Chapter 6 of Bulletin 2U. These equations come from interaction test results presented in "Collapse Tests of Ring Stiffened Cylinders under Combinations of Axial Compression and External Pressure" by Miller and Groove.

Once the buckling stresses are calculated for all modes, a factor of safety is applied to each mode. The partial factor of safety depends on the proximity of the calculated value to yield

force. The partial factor of safety is calculated via Equation 8.7.

$$\psi = \begin{cases} 1.2 & F_{icj} \le 0.50F \\ 1.4 - .4F_{icj} / F_y & F_{icj} \le 0.50F_y \le F \\ 1.00 & F_{icj=}F_y \end{cases} \tag{8.7}$$

This partial factor of safety is then multiplied by the design safety factor which was selected as 1.25. The selection of the safety factor value is addressed in Chapter 9. The allowable stress is found by dividing each buckling stress by the total safety factor. This allowable stress is then compared to the actual stress in a utilization check; if the allowable stress is greater than the actual stress the design passes.

The final results of the optimization program are listed below in Table 8.9 below. Design constraints were placed on the cylinder in addition to the design requirements listed above, and the recommended practices put forth in Bulletin 2U. The value of the vertical stringer web height and thickness was required to be less than or equal to the web height of the vertical stringer of the section below. This ensured that loads in the vertical stringers could be fully transferred to the vertical stinger of the below compartment. Additionally, for the sake of producibility, only standard steel plate thicknesses were used for all stringers and plates. Though this reduces the refinement of the optimization, it is a practical limitation, and while its effect increases the steel required in the structure, it also increases the actual safety factor above the target safety factor.

The total mass of the cylinder, including bulkheads designed via the method outlined in the similar system analysis section above, was 342 tons. This represents a nearly 1/3 reduction in

structural weight as compared to the design yielded from similar systems analysis.

Optimized Properties				
Parameter	Section			Unit
	Bottom	Middle	Top	
Mass/Length	12404.65	10058.99	8594.23	kg/m
Section Mass	78562.78	103942.9	114589.8	kg
N of Vert Stiff	32	32	32	
Vert Flng Thick	0.030	0.030	0.030	m
Vert. Wb Thick	0.015	0.015	0.015	m
Vert Flng Wdth	0.300	0.225	0.150	m
Vert Wb Hght	0.413	0.413	0.413	m
N of Rng Stiff	3	3	3	
Rng Flng Thick	0.020	0.020	0.020	m
Rng Wb Thick	0.020	0.020	0.020	m
Rng Flng Wdth	0.200	0.250	0.200	m
Rng Wb Hght	0.551	0.551	0.551	m
Compartment L	6.333	10.333	13.333	m
Shell thickness	0.020	0.020	0.020	m

Table 8.9- Optimized Cylinder Properties

8.2.3 FEA Analysis via ABAQUS

The optimized cylinder design was then evaluated via the FEA program ABAQUS to ensure the structural adequacy of the design. The analysis was a quassi static analysis run in ABAQUS Standard. All elements were entered into ABAQUS as thin shells. All elements were linear quadratic 4 –node with reduced integration and hourglass control. The material was assumed to be mild steel, the properties of which are presented in Chapter 5. The assembly consisted of 10 parts: shell, bulkhead, vertical stringer web, vertical stringer flange, ring web, ring flange, bulkhead girder web, bulkhead girder flange, bulkhead stiffener web and bulkhead stiffener flange. These parts were connected to the tower as designed in Chapter 7. These different

structural elements were connected via the Tie keyword, with 5 degrees of freedom. The approximate global size of each element was .15625 meters.

The cylinder was loaded from the environmental load results presented in Chapter 5. The environmental loads were included in six distinct steps during the analysis.

8.2.3.1 Analysis Steps

8.2.3.1.1 Gravity Load

This was a static step with the self weight of the structure acting on the entire model. There was one boundary condition imposed in this step at the cylinder depth of 30 meters, this was a clamped boundary condition at the bottom of the cylinder shell and vertical stringers. This is done so as not to consider the cylinder to pontoon connection which will be designed in future work. The assumption is made that subsequent detailed design of the structural connection will be significantly rigid to justify this boundary condition assumption. The loads and boundary condition created in this step, as with all general static analysis steps, propagated to all future steps.

8.2.3.1.2 Quasi Hydrostatic Load

The quasi hydrostatic load step was also run as a static step. The loads from the previous step were propagated. A quasi static significant wave crest height was imposed on the cylinder, which meant the total calculated hydrostatic load was equal to the significant wave height plus the draft at a given point. This accounts for one element of the hydrodynamic loading,

separating the hydrostatic loading into different elements is an acceptable approach [2]. By separating hydrostatic and hydrodynamic loads, the computational time in ABAQUS is greatly reduced.

8.2.3.1.3 Wind Load

The wind load was run as a static step. A pressure was applied to the face of the nacelle which created a total thrust on the nacelle of 80 tons. This wind thrust acts in the same direction as the surge acceleration.

8.2.3.1.4 Dynamic Load

There are two elements which contribute to the dynamic load, surge loading from incident waves, and bending moment due to surge acceleration. There exists significant phase cancelation between these two loads. The total moment due to each element taken separately is approximately three times greater than the two loads taken together due to phase cancellation. Inputting these two separate loads at the correct phase angle into ABAQUS would be time consuming, difficult and computationally intense. Instead two separate runs were undertaken in ABAQUS, in each case all of the loads in above sections were propagated into the dynamic load.

The motions of the cylinder and tower were accounted for quasi-statically which allowed this step to also be a general static analysis step. The RMS accelerations presented in Chapter 5 were added as a gravity load in their corresponding direction which allows the program to calculate the dynamic induced stresses with less computational cost. This load was propagated through to the axial buckling load.

The second method included a quasi static pressure load which was set equal to the RMS

pressure from hydrodynamic wave loading and added mass in the surge direction. The RMS hydrodynamic pressure in the surge was calculated via SWAN, and is one component of the total moment acting on the cylinder presented in Chapter 5. This load was propagated through to the hydrostatic buckling step, as the load was a pressure which could participate in causing hydrostatic buckling.

The total quasi static loading resulting from the first four steps can be seen in Figure 8.5.

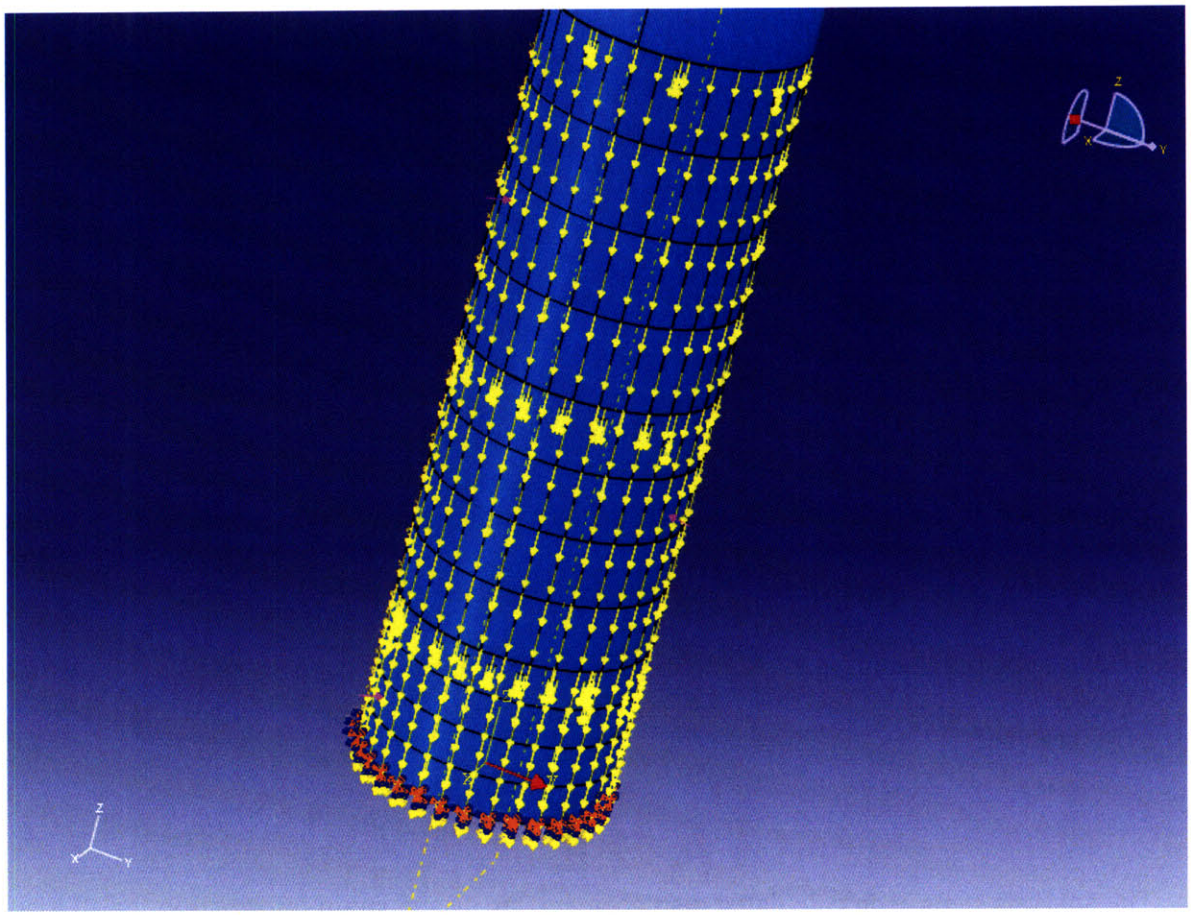

Figure 8.5-Quasi-statically Loaded Cylinder

8.2.3.1.5 Buckling

The next two steps were the buckling steps. In these steps the cylinder, loaded with the above mentioned loads was subjected to a linear perturbation step. In this step an Eigenvalue buckling analysis using the Lanczos method was conducted. The two buckling steps investigated the onset of buckling due to two separate buckling loads which were applied as axial and hydrostatic pressure. The first buckling step applied an axial buckling load at the tower to cylinder seat. The second buckling step applied hydrostatic load. The buckling steps serve as a check to ensure that the buckling loads were not exceeded when the cylinder was loaded with the maximum environmental loads, and to determine the additional load, above the maximum loads, required to initiate buckling.

8.2.3.1.6 Natural Frequency Extraction

The last step investigates the natural frequencies of vibration of the cylinder and tower via the linear perturbation frequency extraction step. This uses a linear perturbation Lanczos eigenvalue extraction technique. All eigenvalues for all natural frequency modes were extracted from 0-70 rad/sec.

The analysis steps each calculated displacement, stress and strain information for all loads which will be presented in the results section below.

8.3 Results/Discussion

Once all components were added, connected and subjected to boundary conditions and loads, the analysis was run. The mesh was refined in a mesh convergence test, in the same manner as described in the Tower Design chapter. The mesh was determined to be converged and the average global element size of .175m was used. The initial model built was designed via classical buckling formulation, latest available test data and analytical studies ABS rules and API recommended practices. The required safety factor was 1.25. This safety margin was chosen based on the relatively smaller consequences of structural failure of a wind turbine as compared to the loss of a petroleum handing manned platform. The ABAQUS analysis predicts that the actual achieved safety factor is much greater than the minimum required safety factor of 1.25. The total mass of the optimized cylinder was 342 tons.

The maximum loading of each component in each of the quasi static conditions is presented below. Bulkhead components are not included as they do not experience stresses above 10Mpa unless there is a hull breach.

	Max Global Component σ (Mpa)				
Load Case	Stiffener Flange	Stiffener Web	Frame Flange	Frame Web	Shell
Gravity	10.3	19.2	2.2	2.0	14.5
Hydrostatic	37.0	48.6	53.3	53.4	99.5
Wind Load	36.1	104.3	57.0	55.7	122.8
Hydrodynamic	70.0	120.6	58.4	56.8	132.0
Surge Acceleration	70.4	83.6	54.8	51.59	131.5

Table 8.9

The sections below present a summary of the stresses of the deformed cylinder for each loading condition.

8.3.1 Gravity Load

The maximum gravity load stress is 13.2 MPa; this is experienced in the tower shell. This stress is located at the bottom of the tower shell plating.

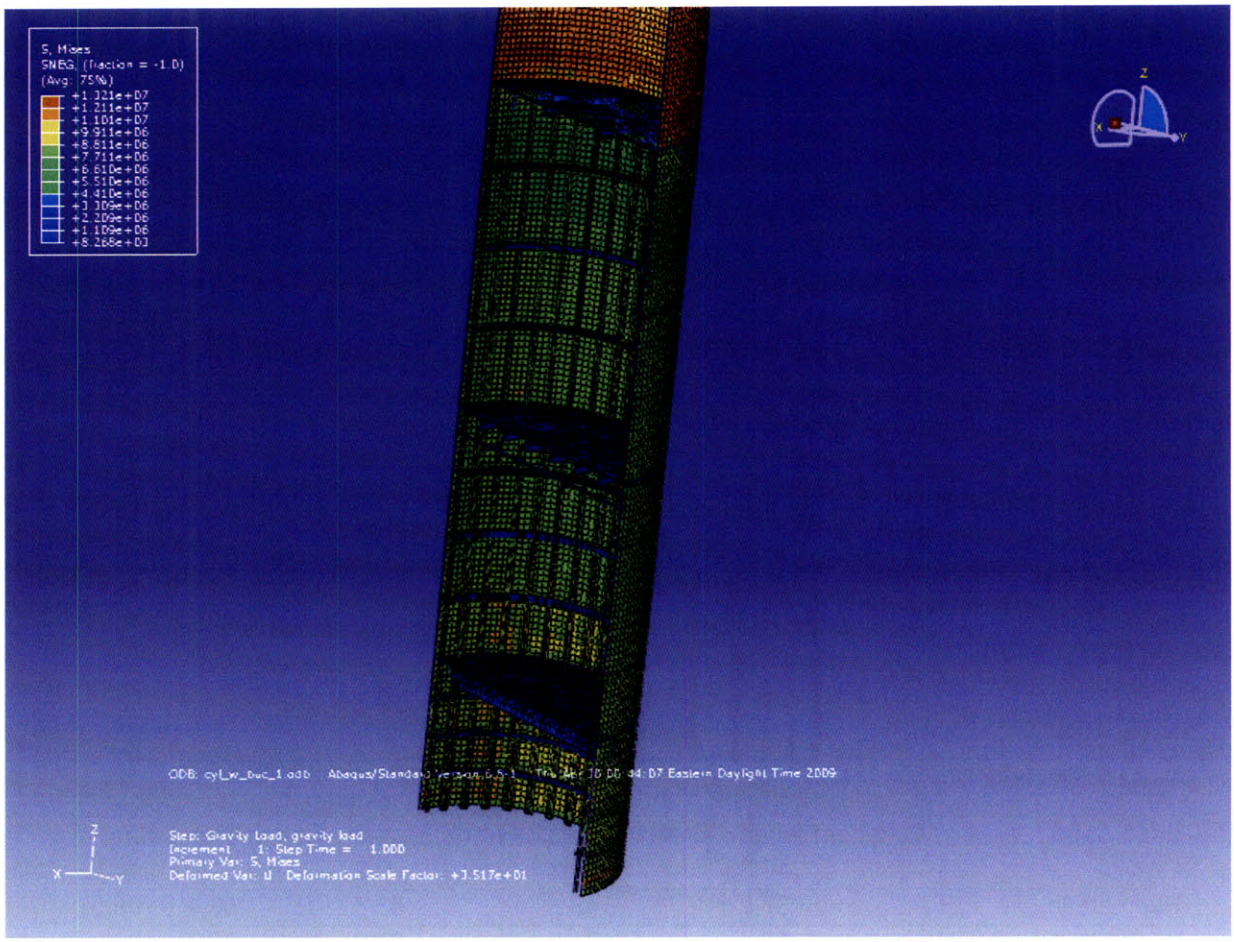

Figure 8.6-ABAQUS Rendering of Mises Stresses for Gravity Load

8.3.2 Quasi Hydrostatic Load

The maximum hydrostatic and gravity load stress is 107.2 MPa; this is experienced in the cylinder shell. This stress is located between the last ring of the bottom compartment and the boundary condition connection; it occurs in the shell at the location of vertical stiffeners.

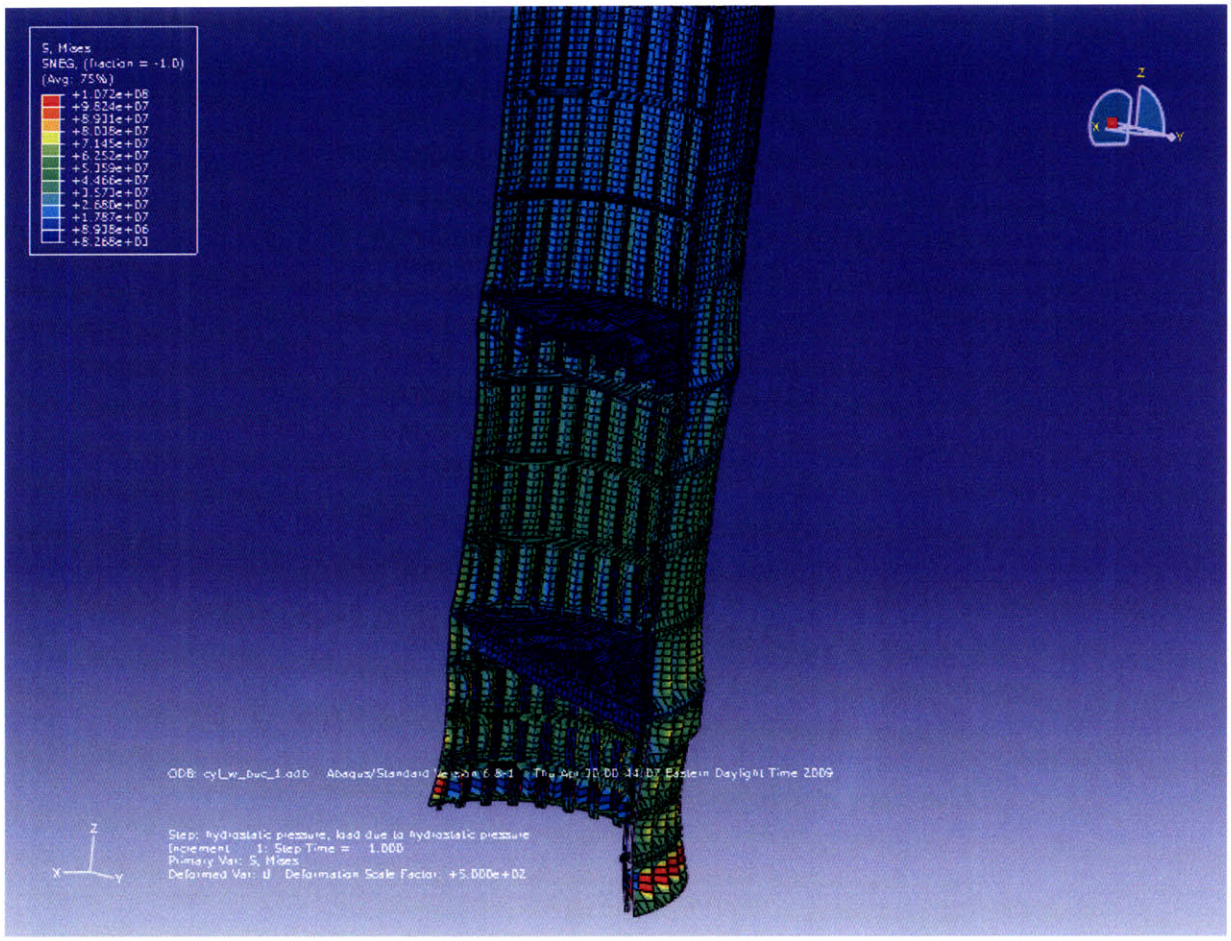

Figure 8.7-ABAQUS Rendering of Mises Stresses for Hydrostatic Load

8.3.3 Wind Load

The maximum stress due to gravity and hydrostatic loading on the nacelle is 125.2 MPa. It is experienced in the shell at the same location as maximum hydrostatic load on the leeward side of the tower.

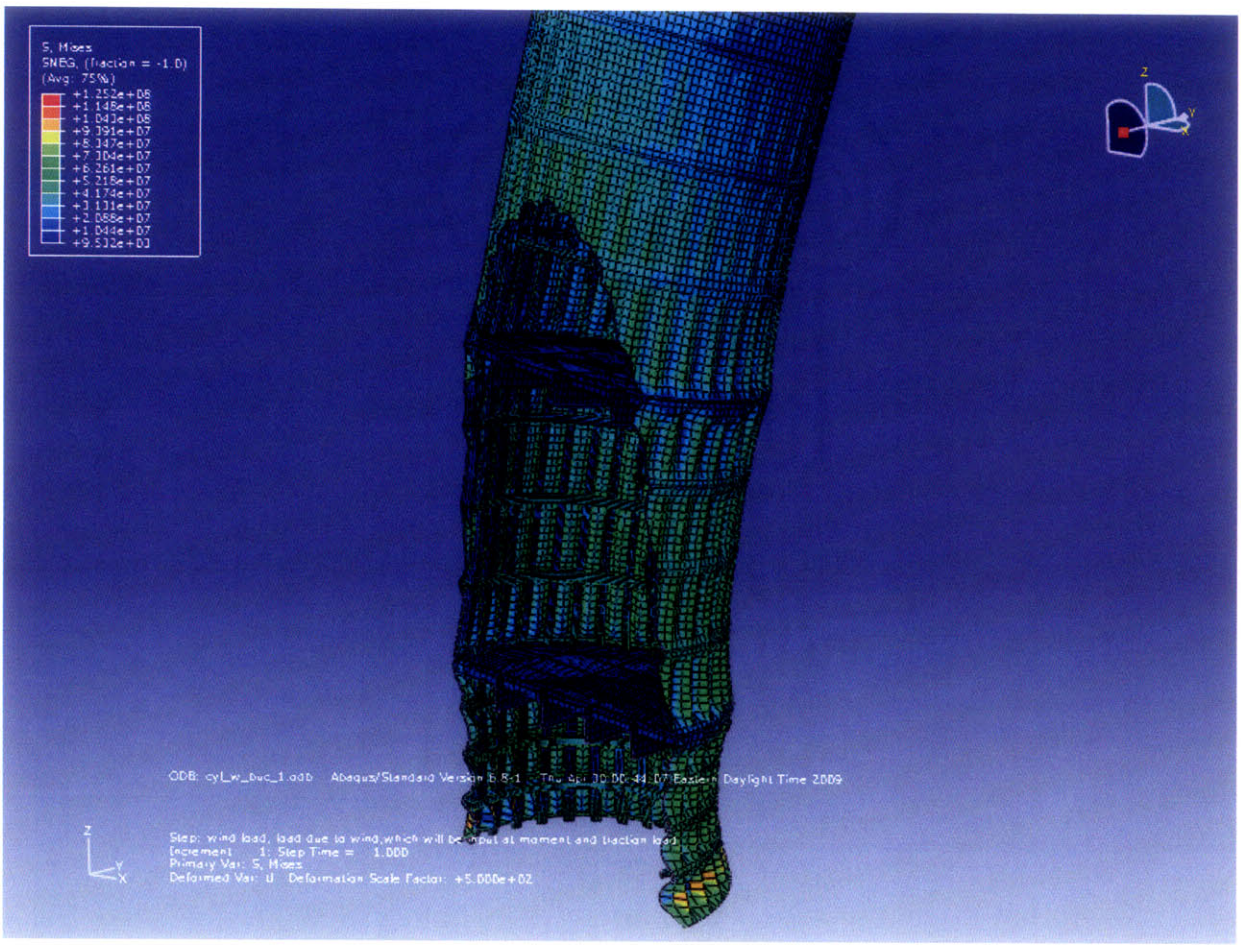

Figure 8.8-ABAQUS Rendering of Mises Stresses for wind load

8.3.4 Dynamic Load

The maximum stress due the above previous loads and surge motion is located at the bottom of the cylinder, between the lowest ring and the boundary condition, in the shell at the leeward vertical stiffener. The maximum stress is 132 MPa.

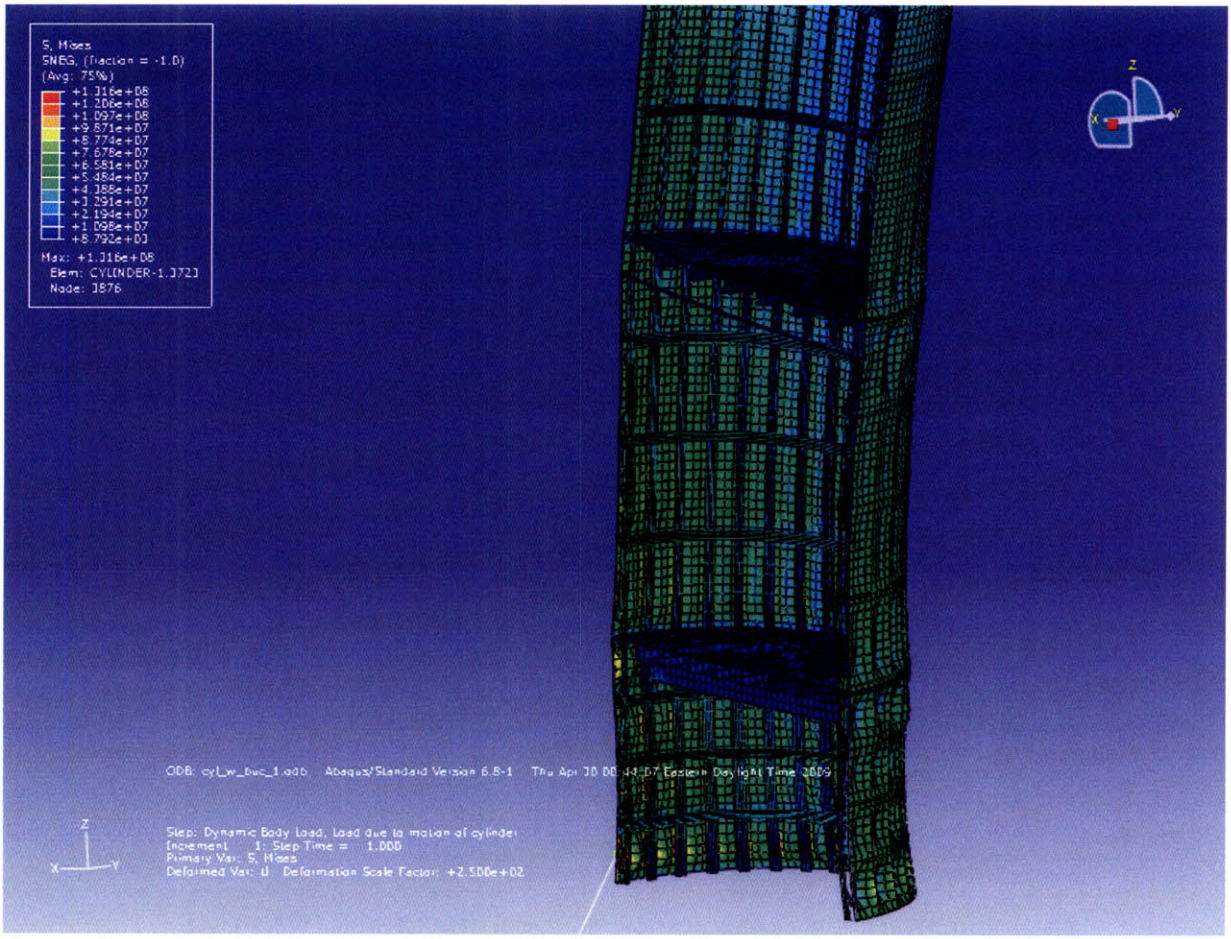

Figure 8.9-ABAQUS Rendering of Mises Stresses for Surge load

The maximum load due to gravity, hydrostatic, wind, and hydrodynamic wave load acting on the cylinder is 132 MPa. This is located at the same location as the maximum stress due to surge motion.

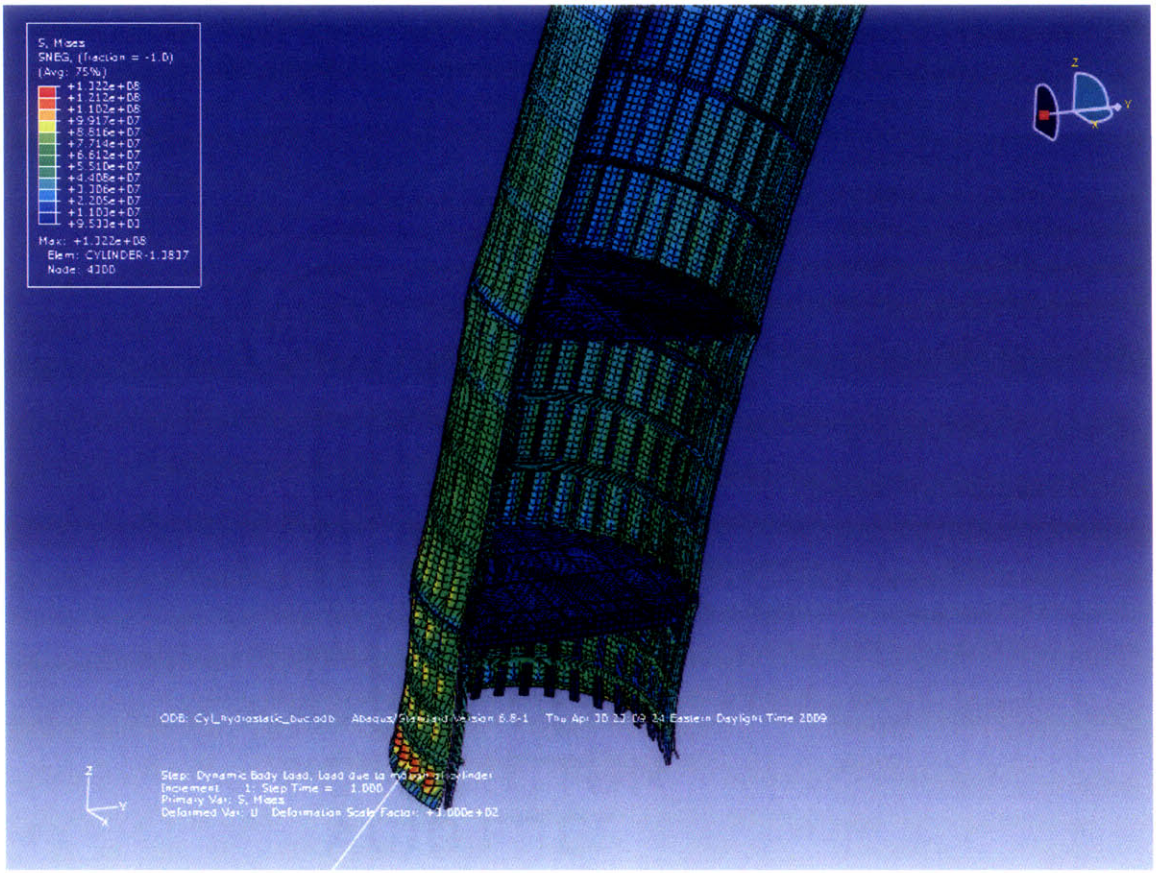

Figure 8.10-ABAQUS Rendering of Mises Stresses for Hydrodynamic Wave Load

8.3.5 Axial Buckle

ABAQUS FEA analysis shows that the required buckling load to reach the bifurcation point is 555KPA. The axial buckling occurs as a local plate buckling, the most desirable form of buckling. This buckling load is applied to the structure in addition to all the loads applied to the structure in the quasi static steps outlined above. The location of the buckle is shell plating between the top ring and bulkhead. At the pressure required to cause the structure to buckle the material would have already failed due to plate bending. Therefore buckling will not be observed for this particular load in the cylinder as designed.

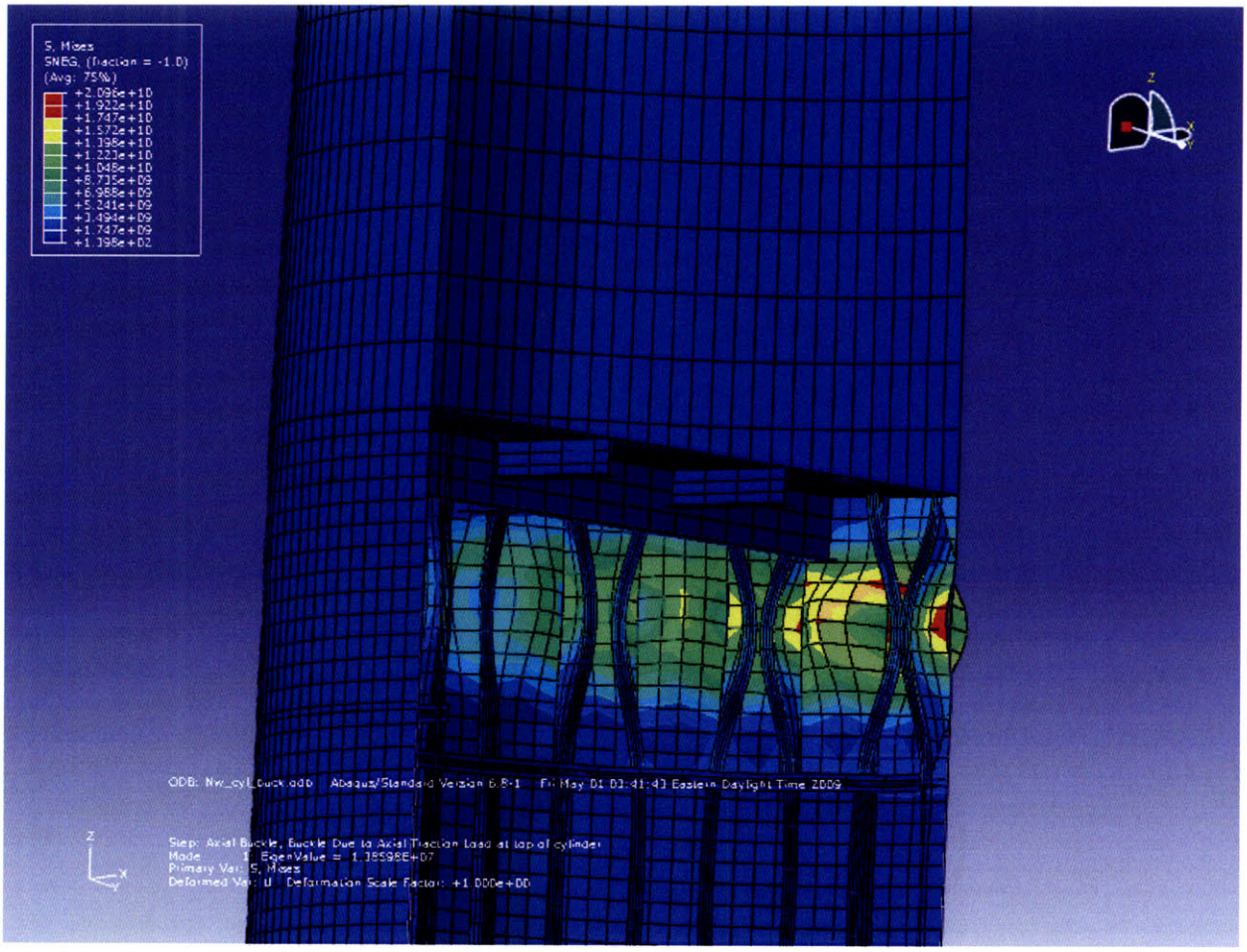

Figure 8.11-ABAQUS Rendering of Mises Stresses for Axial Buckle Load

8.3.6 Hydrostatic Buckle

ABAQUS FEA analysis shows that the additional load required for instability is 8.27 MPA. This buckling load is applied to the structure in addition to all the loads applied to the structure in the quasi static steps outlined above. The location of the buckle is the platting of the middle compartment between stiffeners. This is local buckling, which is the most desirable type of buckling and which the cylinder was designed to fail in first. At the pressure required to cause the structure to buckle, the material would have already failed due to plate bending. Therefore buckling will not be observed for this particular load in the cylinder as designed.

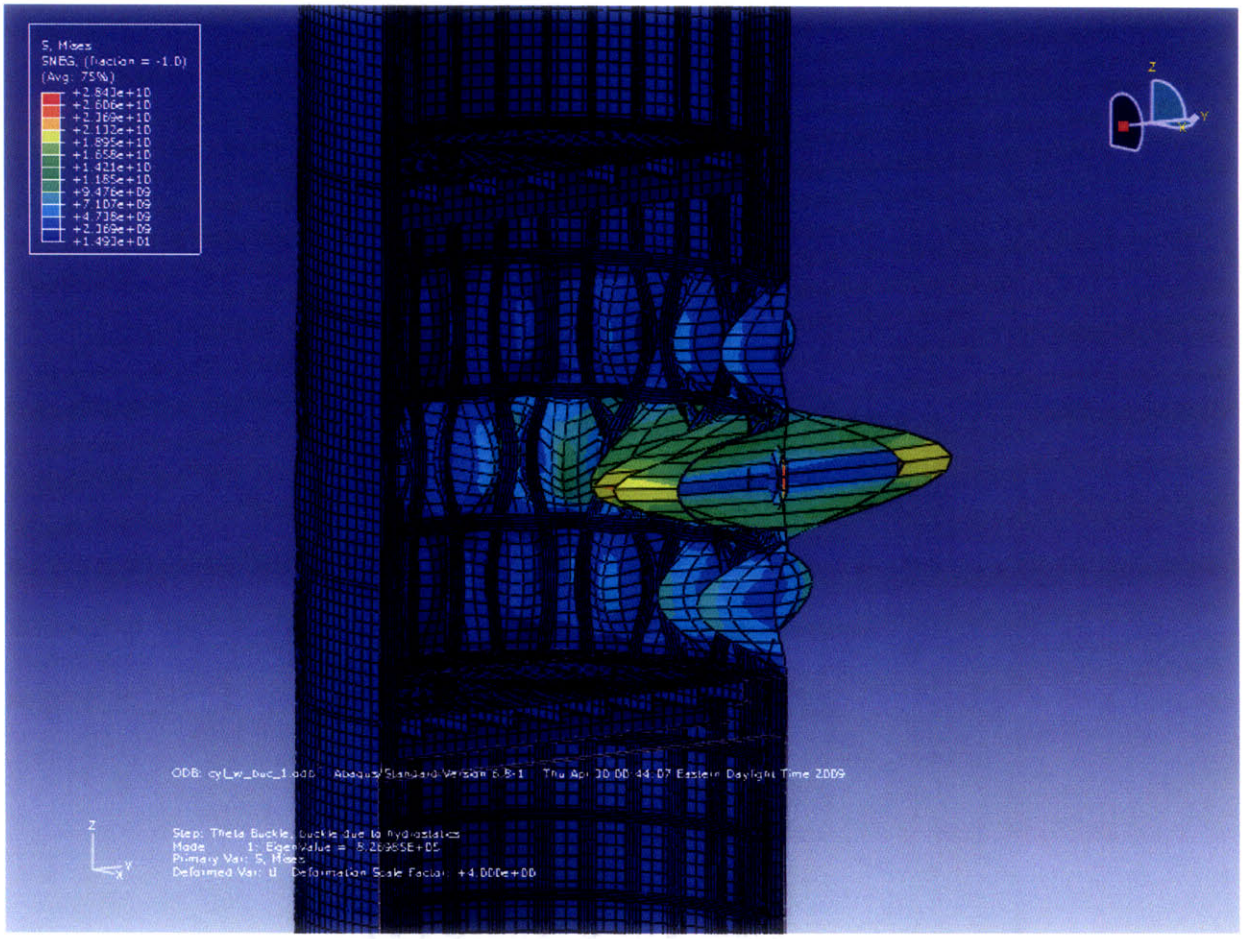

Figure 8.12-ABAQUS Rendering of Mises Stresses for Hydrostatic Buckle Load

8.3.7 Natural Frequency

All natural frequency modes between 0 and 70 rad/sec were calculated; the first 10 are presented below. The frequency range of typical sea spectra is 0-2 rad/sec. The lowest frequency mode of natural frequencies from the ABAQUS analysis was 2.6 rad/sec, which is well outside of the range of sea spectra, so wave excitations at the natural frequencies are highly unlikely. The first six modes listed in Table 9.14 involve primarily the tower as shown by the fact that the generalized mass is approximately equal to the tower mass. For this reason the reader is referred to Chapter 7's discussion of natural frequency for the first 6 natural frequencies. The first resonance mode which involves the tower is mode seven which can be seen in the figure

Natural Frequency Extraction				
Mode NO	EIGENVALUE	FREQUENCY		GENERALIZED MASS
		(RAD/S)	(CYCLES/S)	
1	6.7835	2.6045	0.41452	3.99E+05
2	6.7919	2.6061	0.41478	3.99E+05
3	171.23	13.085	2.0826	1.77E+05
4	171.32	13.089	2.0832	88886
5	257.71	16.053	2.555	75224
6	257.71	16.053	2.555	75251
7	336.76	18.351	2.9207	2.29E+05
8	337.19	18.363	2.9225	2.29E+05
9	530.27	23.028	3.665	61986
10	530.29	23.028	3.665	61999

Table 8.10--First 10 Natural Frequency modes

Figure 8.13-Seventh Natural Frequency mode

8.4 Conclusion

The structure as yielded from the structural optimization routine passes both ABS rules and API recommendations and is validated via FEA in ABAQUS. Its total weight is 342 tons which is an almost 30% reduction from the design produced by similar system analysis and ABS rules alone. Standard plate thickness and stiffeners were used in the design.

The plate bending stress due to quasi hydrostatics was the major driver of the structural design. The first buckling mode for both axial and hydrostatic buckling occurs as local buckling

in the shell. This is the most desirable type of buckling. The structural design has a large amount of reserve stability, this is due in part to the requirement for standard plate thicknesses in the stringers, which decreases the available refinement of the structural optimization. Another factor which contributes to the reserve stability is the conservative techniques presented in Bulletin 2U. As Bulletin 2U is written for a range of types of cylindrical shells, for any application, its conservativeness is necessary and reasonable.

9 Design of Pontoon Leg

9.1 Introduction

The general tenants of the design of the MIT TLP-1 pontoon leg come from the experience of previous mini TLP projects for offshore oil. MIT TLP-1 represents the most extreme case in terms of loads acting on a FWT. This is because it uses the NREL 5 MW turbine and its geometry was Pareto optimized for 14m Sea States. Four legs were selected for this design for symmetry and ease of analysis. The pontoon was designed as a thin walled shell structure in order to house the required ballast for the specific loads expected of MIT TLP-1. Figure 9.1 shows the general dimensions of the four pontoons.

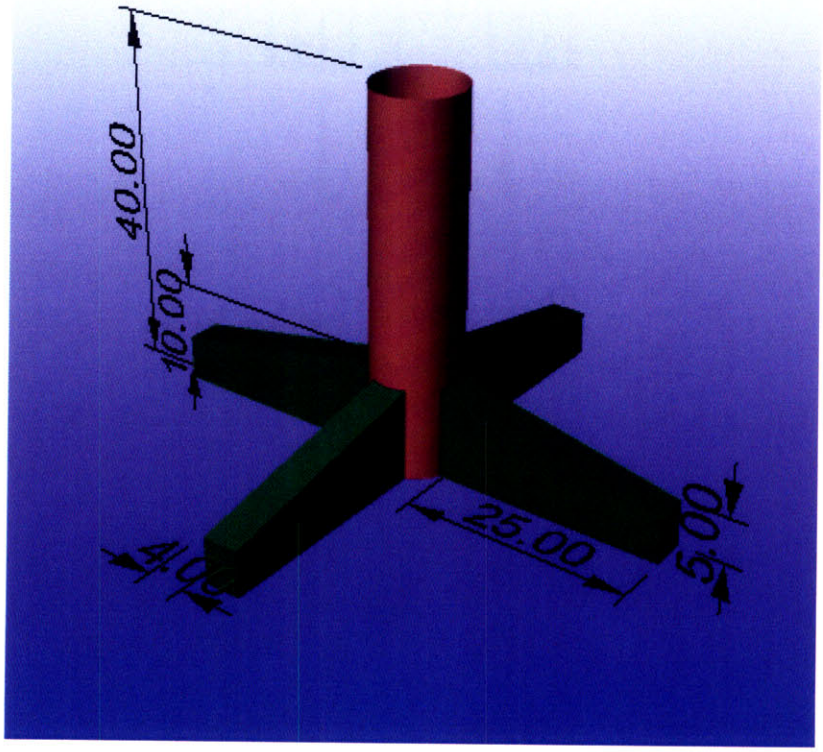

Figure 9.1-General Pontoon Dimensions

The structural design of the MIT TLP-1 pontoon leg was initially created via ABS Publication 82 for Floating Production Instillations. The pertinent section of this publication was 1-4-5 Tension Leg Platforms/13 Scantling Design of Hull Structure.

ABS scantling design rules are based on plate bending and buckling theory and are sufficient to design this structure. As discussed in previous chapters, this technique does not yield optimum designs.

The cylindrical section was structurally optimized since it was a structure that will be used in all foreseeable FWT projects. The shell pontoon on the other hand is one object among others that is being explored as an optional type of structure. The cylinder optimization code does not require intense modifications if the dimensions change drastically, as long as the geometry is still a cylinder. Any code written for the optimization of the pontoon would have to be virtually rewritten for even simple changes to the geometry of the cylinder. Additionally since this is the first attempt at the structural design of the MIT FWT TLP, it may be determined that the general shape is far from optimum once structural effects are considered.

Hence, it was determined that writing a structural optimization code for the pontoon section would not be as beneficial at this stage as would be needed to justify the additional time and work. As the project continues and if the MIT TLP-1 system is selected as the most desirable, then the structural optimization code for the specific external geometry should be written.

Though a structural optimization code is not warranted for the MIT TLP-1, ABS rules should not solely dictate the design of the pontoon, especially as this is the first pontoon TLP design intended for FWTs. ABAQUS FEA software was used to verify that the design produced via ABS was neither overly conservative, nor out of the applicable range of the ABS rules. This

software was then used to adjust the design for better structural efficiency.

9.2 Methodology

9.2.1 Subdivision

Many questions regarding the subdivision of the pontoon are answered in Chapter 6, Feasibility of Dynamic Ballast System. For brevity these points will not be reiterated here. The main conclusion which can be drawn from Chapter 6 is the total flooding of MIT TLP-1's pontoon would have a listing effect which is approximately equal to the rated wind moment. As discussed in Chapter 8, the turbine blades would be feathered in case of any damage, effectively eliminating the wind healing moment. Since, in the case of damage, the wind healing moment would be replaced by a flooding healing moment, the mooring system would be equipped to easily handle this healing moment. Hence the requirement for subdivisions for the pontoon section of MIT TLP-1 will not be dictated by the damaged stability of the pontoon.

There will still be subdivisions present in the pontoon but they will be dictated by the structural strength requirements to be discussed in subsequent sections.

9.2.2 Similar System Analysis

As with the cylindrical section, the Sea Star TLP was used as a similar system for the pontoon section. The reason for this selection can be found in the Cylinder Section chapter. Table 8.1 includes key properties of the SEA STAR TLP.

9.2.3 Plate Aspect Ratio and Stiffener Spacing

The scantling spacing of the Sea Star can be seen in Figure 8.2; this spacing was obtained from Ref [20]. The scantling spacing was used to determine an aspect ratio for the plating of the Sea Star. This aspect ratio was then modified to efficiently withstand the particular stresses experienced by the MIT TLP-1 pontoon.

If a frame spacing of less than 2.5 meters were used, the spacing between frames and the spacing between longitudinal stiffeners would be too small and the structure would become very difficult to fabricate. For this particular geometry, initial analysis and similar system analysis suggest that a more efficient structure would have a spacing of less than 2.5 meters. So for the purposes of producibility, the frame spacing was set to 2.5 meters as this was the most efficient producible design. The frame spacing divided by the aspect ratio gives the longitudinal stiffener spacing of .66 meters; this was modified to .625 meters as this was the closest stiffener spacing which resulted in an integer amount of stiffeners.

9.2.4 Rules Based Design

Rules based design was conducted via ABS Publication 82 for Floating Production Instillations; Section 1-4-5 Tension Leg Platforms/13 Scantling Design of Hull Structure. The rules state that TLP should first be designed for the local load effects as these loads are most likely the limiting case. The subsequent design should then be verified to withstand global loads. The local loads effects are plate and girder bending and buckling due to hydrostatic pressure

effects.

The plating thickness was first determined with scantling spacing, aspect ratio, and water depth as inputs, as obtained in the above section. Equation 9.1 shows the calculation of the plate thickness.

(9.1) $$t = \frac{sk\sqrt{qh}}{290}$$

Where	
t	thickness in mm
s	spacing of stiffeners in mm
k	$(3.075\,\alpha - 2.077)/(\alpha + 0.272)$ for $1 \leq \alpha \leq 1.0$ for $\alpha > 2$
α	aspect ratio of the panel (longer edge/shorter edge)
q	235/Y
Y	specified minimum yield point or yield strength, in N/mm2
h	distance, in m, from the lower edge

The minimum required thickness determined from this calculation was 13.96 mm. As this is not a standard plate thickness the pontoon thickness was chosen as the standard plate thickness of 15mm.

Equations 9.2 and 9.3 calculated the required section modulus for the longitudinal stiffeners and frame girders respectively and are presented below.

(9.2) $$SM = Qfchsl^2$$

Where

Q	$49.92/(Y + 2U/3)$
f	7.8
c	0.56 for stiffeners with ends attached 0.60 for stiffeners with no end attachment
h	distance, in m, from the middle of l to a point defined in 1-4 -5/13.1
s	the spacing of stiffeners, in m
l	the length of stiffeners, in m; where brackets are fitted with a

slope of approximately 45 degrees and thickness given in 3-2-2/Table 2 of the *MODU Rules*, the length of l may be measured to a point on the bracket equal to 25% of the length of the bracket.

Y specified minimum yield strength, in kgf/mm2

U specified minimum tensile strength of the higher-strength material, in kgf/mm2 (psi)

(9.3) $$SM = Qfchsl^2$$

Where

f 4.74 (0.0025)

c 1.5

h distances, in m, from the middle of the area supported to a point defined in 1-4-5/13.1

s sum of half lengths, in m (on each side of girder or web), of the stiffeners or beams supported

l length, in m, between supports, where brackets are fitted at shell, deck or bulkhead supports, and the brackets are in accordance with 3-2-2/Table 2 of the *MODU Rules* and have a slope of approximately 45 degrees, the length, l, may be measured to a point on the bracket located at the distance from the toe equal to 25% of the length of the bracket.

Q factor defined in Equation 9.2

The minimum required section modulus for this configuration was calculated for the top, bottom, and sides. The required section modulus values were different due to the different heights of each of these sections. The height input is a measure of the quasi hydrostatic load. The bottom and sides section heights were modified to account for the internal pressure of the ballast counteracting the external hydrostatic pressure. The approximation of the ballast as an invicid fluid is conservative as it ignores any structural strength aspects of the ballast. This approximation was made in order to allow for different types of ballast besides concrete, such as olivine sand, to be considered.

After the modification for the ballast pressures, the required SMs were calculated. For the longitudinal stiffener the required SMs were 732 cm^3 for the sides and bottom and 695cm^3 for

the top. Since these SM are so close to each other, one type of stiffener was used for all sections. The stiffener type was chosen from common structural tee's found in American Institute of Steel Construction (AISC) Manual of Steel construction; Table 9.1 lists its properties. Though the chosen stiffener exceeds required SM considerably, the weight properties of this stiffener are better than other adequate stiffeners with smaller SMs.

Structural Tees (Cut from W shapes) from *Manual of Steel Construction (9th Edition) p.1-67*												
			Designation 18 X 75									
Units	A	depth of T	stem t	stem A	flange w	flange thick	Ix		SMx	y	Iy	Smy
in	22.1	17.775	0.6	10.7	11.95	0.79	636	49.7	4.78	135	22.5	
SI(cm)	143	45	1.52	143	30.353	2.007	2.65E+04	814	12.14	5.62E+03	369	

Table 9.1: Longitudinal Stiffener Properties

The front face of the pontoon is the location of the tension leg attachments and will have to be stiffened for these additional local load effects. The specific method of tension leg attachment is an involved and complex design which has received much focus in the oil industry. The specific structural design for the FWT tension leg attachment has no attribute which should make it different from the structural design of petroleum TLP, hence the detail design was not considered in this project. For simplicity in design the top bottom and side stiffeners were wrapped around the structure to create an orthogonally stiffened structure which is overly conservative based on preliminary and FEA analysis.

The required section modulus of the frame was calculated for the top, bottom and sides via equation 9.3. It was found that the top and bottom frame web heights required were much smaller than 1 meter, but in order to reduce the length of the side girders, they were set to 1 meter. This is associated with a substantial weight savings as the side girder averages twice the length of the top and bottom girder and the L term is squared in the required section modulus

calculation, so increasing the web depth of the top and bottom decreases the length of the sides and decreases the overall weight. The required side SM and total weight of frames are presented in Table 9.2, where frame 1 is closest to the center of the structure.

Frame Properties						
Section	1	2	3	4	5	6
SM req (cm^3)	32325	24179	17213	14757	9444	7231
Frm Weight (kg)	11606.4	8255.5	5133.96	4141.8	3182.4	2669.16

Table 9.2

Following the design of the pontoon structure for local load effects, the design was verified for global strength. The chosen factor of safety of this design was 1.25. As an unmanned structure with no hazardous chemicals, the loss of this structure would be less catastrophic then a structure engaged in the petroleum industries which the selected ABS rules were written for. For this safety factor, and the loads on the pontoon presented in Chapter 5, the global section modulus required is well below the design section modulus as see in figure 9.1.

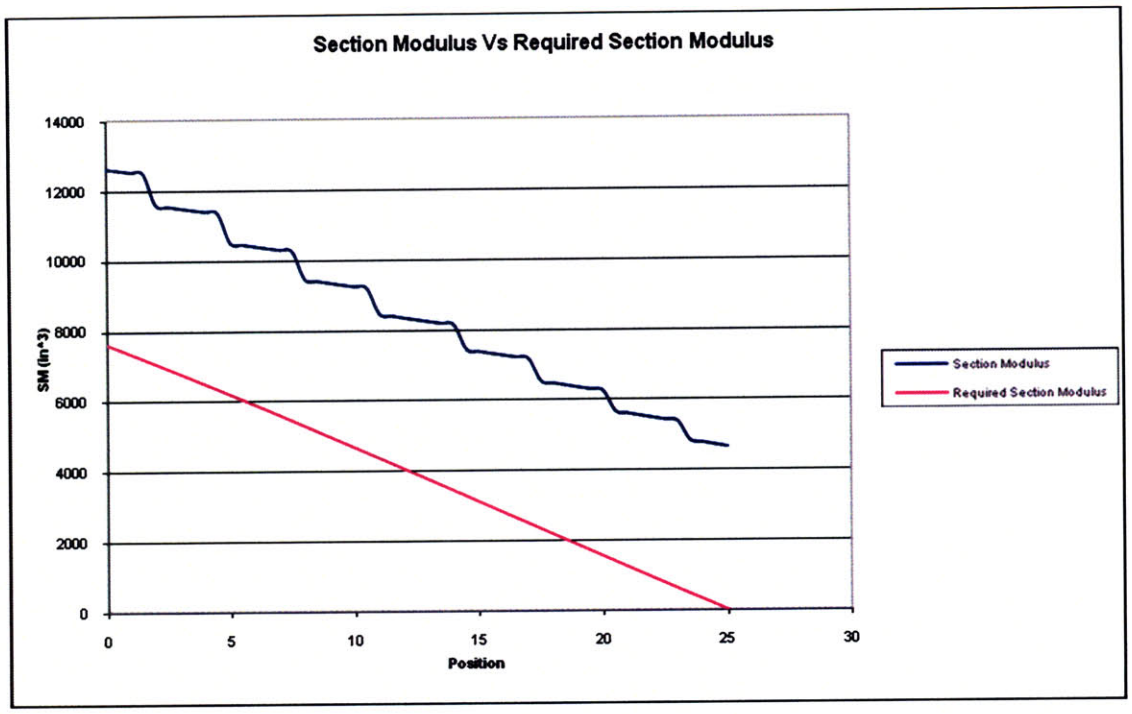

Figure 9.1

The global strength analysis also considered shear stress, bending stress and principle stress, all of which were well below permissible stress levels. This verified the assumption that the local stress effects were the driving design factor which if designed for would automatically satisfy global strength requirements.

After the verification of adequate global strength, the total weight of the structural steel as designed to ABS standards was found to be 227 tons. Table 9.3 shows the weights of each specific element of the structure.

Group Weights (tons)						
Plating	Stiffeners	Girders	Blkhd	Blkhd Stiff	Blkhd Gird	Total
75.5	86	35	14.5	11	5	227

Table 9.4

9.2.5 FEA Analysis via ABAQUS

The ABS design was then evaluated via the FEA program ABAQUS to ensure the structural adequacy of the design. The analysis was a quasi static analysis run in ABAQUS Standard. All elements were entered into ABAQUS as thin shells. All elements were linear quadratic 4 –node with reduced integration and hourglass control. The material was assumed to be mild steel, the properties of which are presented in Chapter 5. The assembly consisted of 10 parts: plate, bulkhead, longitudinal stiffener web, longitudinal stiffener flange, frame web, frame flange, bulkhead girder web, bulkhead girder flange, bulkhead stiffener web and bulkhead stiffener flange. These different structural elements were connected via the Tie keyword, with 5 degrees of freedom. The approximate global size of each element was .15625 meters.

The pontoon was loaded from the environmental load results presented in Chapter 5. The environmental loads were included in three distinct steps during the analysis.

9.2.5.1 Analysis Steps

9.2.5.1.1 Gravity Load

This was a static step with two loads, the self weight of the structure and the pressure acting on the structure due to the weight of the ballast. There was one boundary condition imposed in this step at the cylinder end of the pontoon, this was a clamped boundary condition along the pontoon side top and bottom plate. The assumption is made that subsequent detailed design of the structure will be significantly rigid to justify this boundary condition assumption. The loads and boundary condition created in this step, as with all general static analysis steps, propagated

to all future steps.

9.2.5.1.2 Hydrostatic Load

The hydrostatic load step was also run as a static step. The loads from the previous step were propagated. The hydrodynamic and hydrostatic pressures were taken into account in combination by assuming the loading was quasi-static and equal to the draft at a given point plus the significant wave height.

9.2.5.1.3 Tension Leg Load

The last static step was the tension leg step. All previous loads were propagated into this step. The maximum load due to the tension leg would occur on the windward side of the system, and is equal to twice the pre-tension (presented in Chapter 5). This is because the ΔT due to wind is added to the pretension of the windward side and subtracted from the leeward side. The pretension is set equal to the ΔT in order to prevent a slack cable condition. This load was added as a surface traction load to the far face of the pontoon. In the interest of reducing computational capital, the axial direction component of the tension load was ignored; this is a conservative approximation because this component of the tension leg load would only alleviate stresses induced by hydrostatic pressure acting on the far face of the pontoon.

The total quasi static loading resulting from the first three steps can be seen in Figure 9.2.

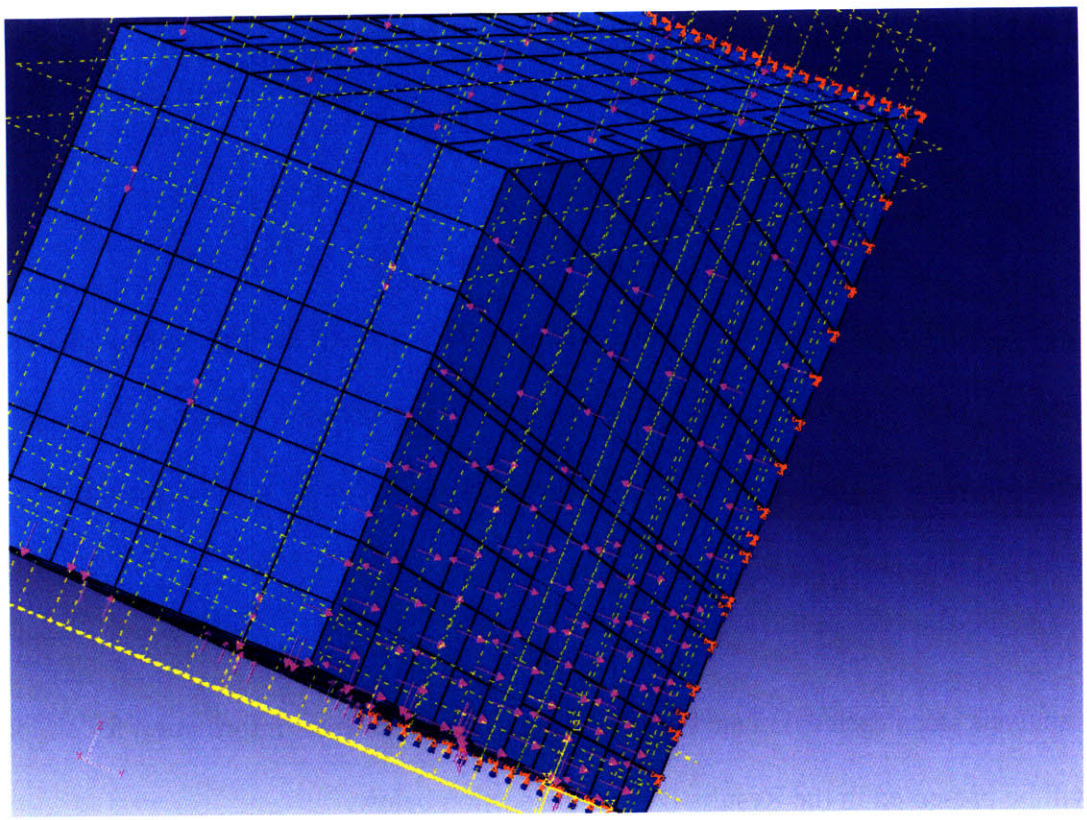

Figure 9.2-Quasi-statically Loaded Pontoon

9.2.5.1.4 Buckling

The next 3 steps were the buckling steps. In these steps the pontoon, loaded with the above mentioned loads, was subjected to a linear perturbation step. In this step an Eigenvalue buckling analysis using the Lanczos method was conducted. The three buckling steps investigated the onset of buckling due to three separate buckling loads which were applied as hydrostatic pressure. The first buckling step applied the buckling load on the sides of the structure, the next applied the load on the top and bottom, and the last step applied a load on the front face. The buckling steps serve as a check to ensure that the buckling loads were not exceeded when the pontoon was loaded with the maximum environmental loads, and to determine the additional

required load, above the maximum loads, required to initiate buckling.

9.2.5.1.5 Natural Frequency Extraction

The last step investigates the natural frequencies of vibration of the pontoon via the linear perturbation frequency extraction step. This uses a linear perturbation Lanczos eigenvalue extraction technique. All eigenvalues for all natural frequency modes were extracted from 0-70 rad/sec.

The analysis steps each calculated displacement, stress and strain information for all loads which will be presented in the Results/Discussion section below.

9.3 Results/Discussion

Once all components were added, connected and subjected to boundary conditions and loads, the analysis was run. The mesh was refined in a mesh convergence test, in the same manner as described in the Tower Design chapter. The mesh was determined to be converged and the average global element size of 0.15625m was used. The results of tests on the initial model built to ABS rules indicated that the actual achieved safety factor exceeded the required safety factor. The sizes of the stiffeners were adjusted to bring the safety factor down to approximately 1.25. This safety margin was chosen based on the relatively lower consequences of structural failure of a wind turbine as compared to the loss of a petroleum handing, manned platform. The total new mass of the slightly adjusted tower was 209 tons.

The maximum loading of each component in each of the quasi static conditions is presented below, the tables are broken into global and bulkhead components.

	Max Global Component σ (Mpa)				
Load Case	Stiffener Flange	Stiffener Web	Frame Flange	Frame Web	Shell
Gravity	51.5	59.2	11.0	21.7	70.9
Hydro	127.5	199.4	140.0	196.5	187.0
Tension Leg	136.8	202.0	135.5	191.1	194.8

Table 9.5

	Max Bulkhead Component σ (Mpa)				
Load Case	Stiffener Flange	Stiffener Web	Frame Flange	Frame Web	Bulkhead
Gravity	6.9	2.7	19.1	17.9	19.0
Hydro	110.0	27.5	58.1	87.5	113.0
Tension Leg	111.0	30.1	71.2	87.8	128.3

Table 9.6

The sections below present a summary of the stresses of the deformed pontoon for each loading condition.

9.3.1 Gravity Load

The maximum gravity load stress is 70.9 MPa; this is experienced in the shell plating. This stress is located at the bottom cylinder end corner of the pontoon.

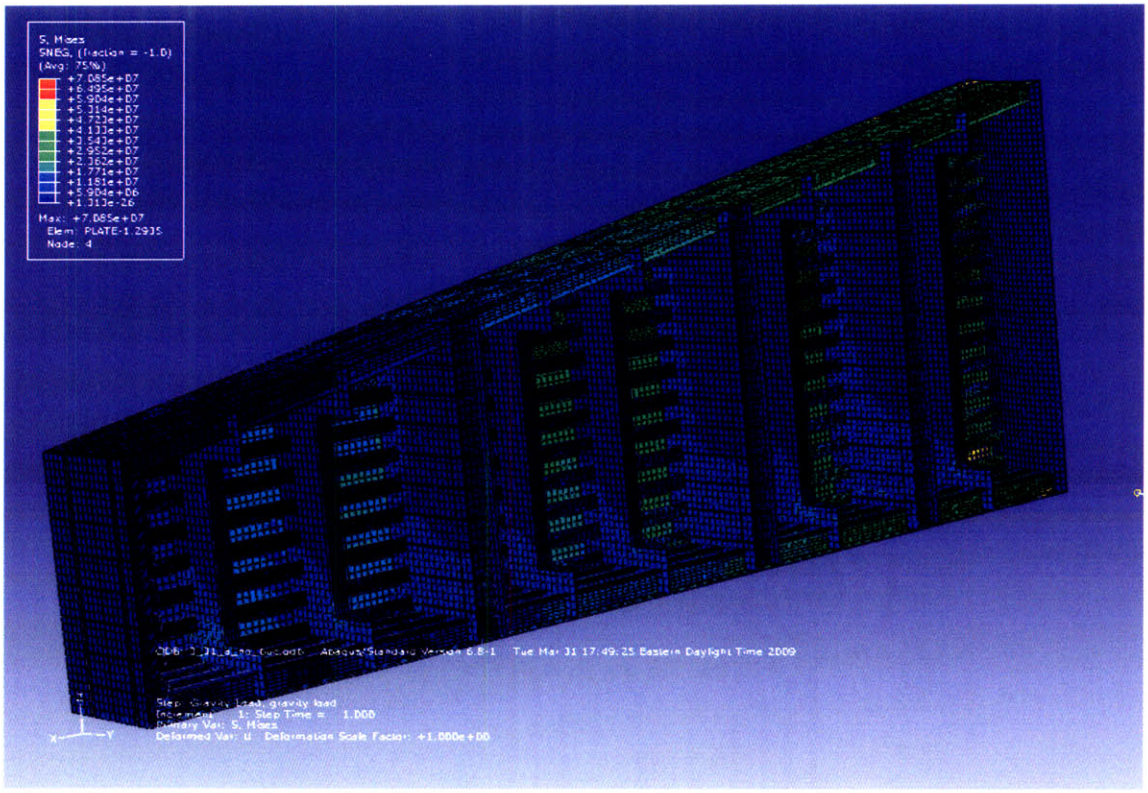

Figure 9.8-ABAQUS Rendering of Mises Stresses for Gravity Load

9.3.2 Quasi Hydrostatic Load

The maximum hydrostatic load stress is 199.4 MPa; this is experienced in the global stiffener web. This stress is located half way up the side of the pontoon at the cylinder to pontoon connection.

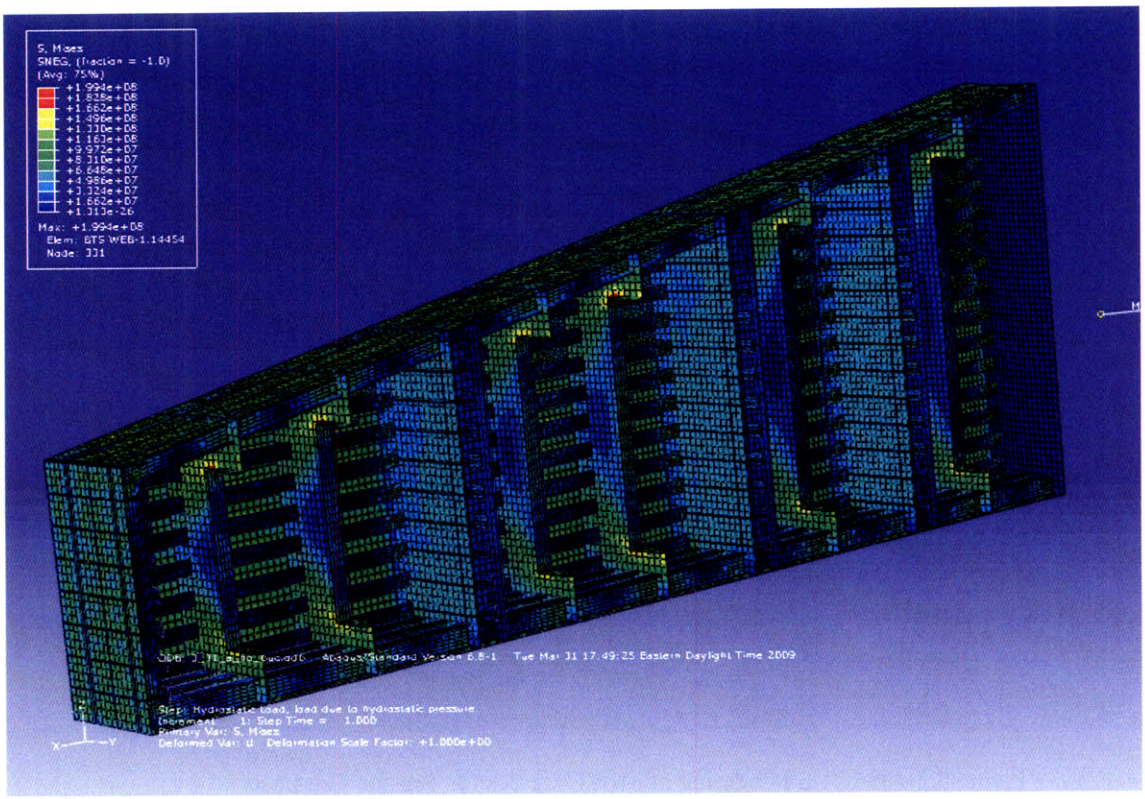

Figure 9.9-ABAQUS Rendering of Mises Stresses for Hydrostatic Load

9.3.3 Tension Leg Load

The maximum tension leg load stress is 202.4 MPa; this is experienced in the global stiffener web. This stress is located half way up the side of the pontoon at the cylinder to pontoon connection.

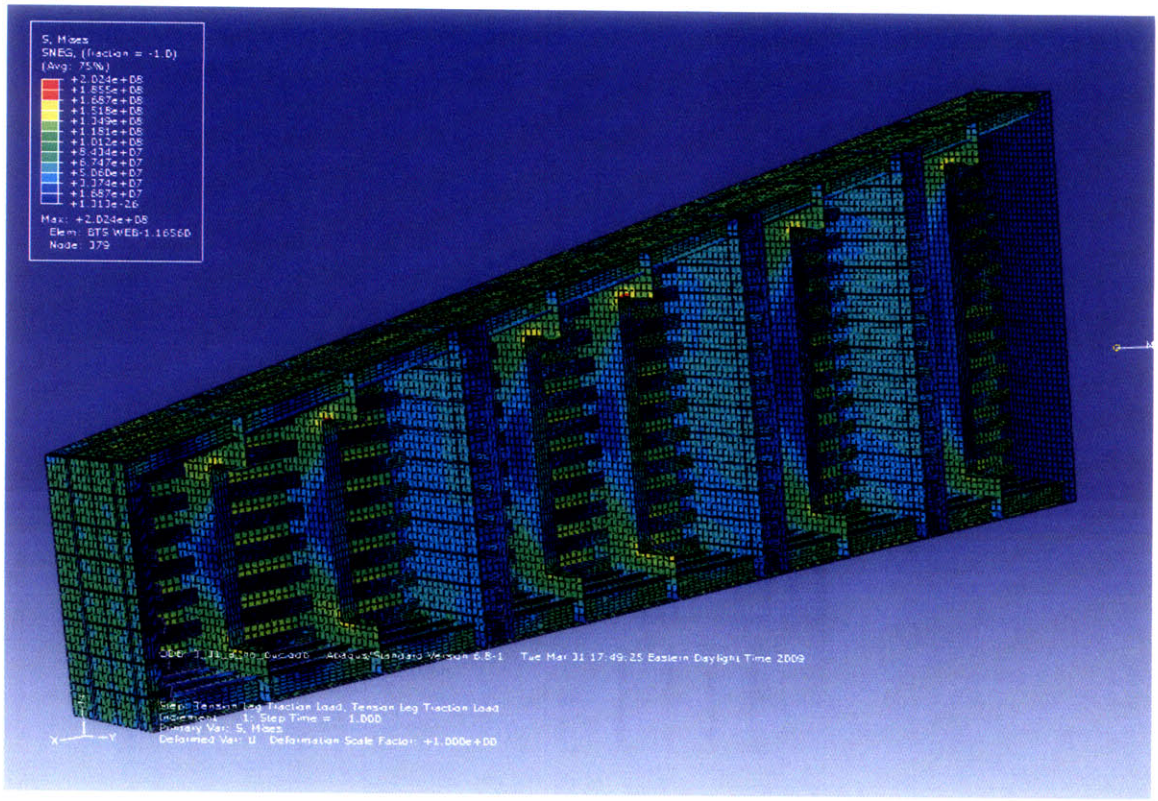

Figure 9.3-ABAQUS Rendering of Mises Stresses for Tension Leg Load

9.3.4 Side Buckle

ABAQUS FEA analysis shows that the required buckling load to reach the bifurcation point is 555KPA. This buckling load is applied to the structure in addition to all the loads applied to the structure in the quasi static steps outlined above. The location of the buckle is the top and bottom of the 5th frame from the cylinder to pontoon connection. At the pressure required to cause the structure to buckle the material would have already failed due to plate bending. Therefore buckling will not be observed for this particular load in the pontoon as designed.

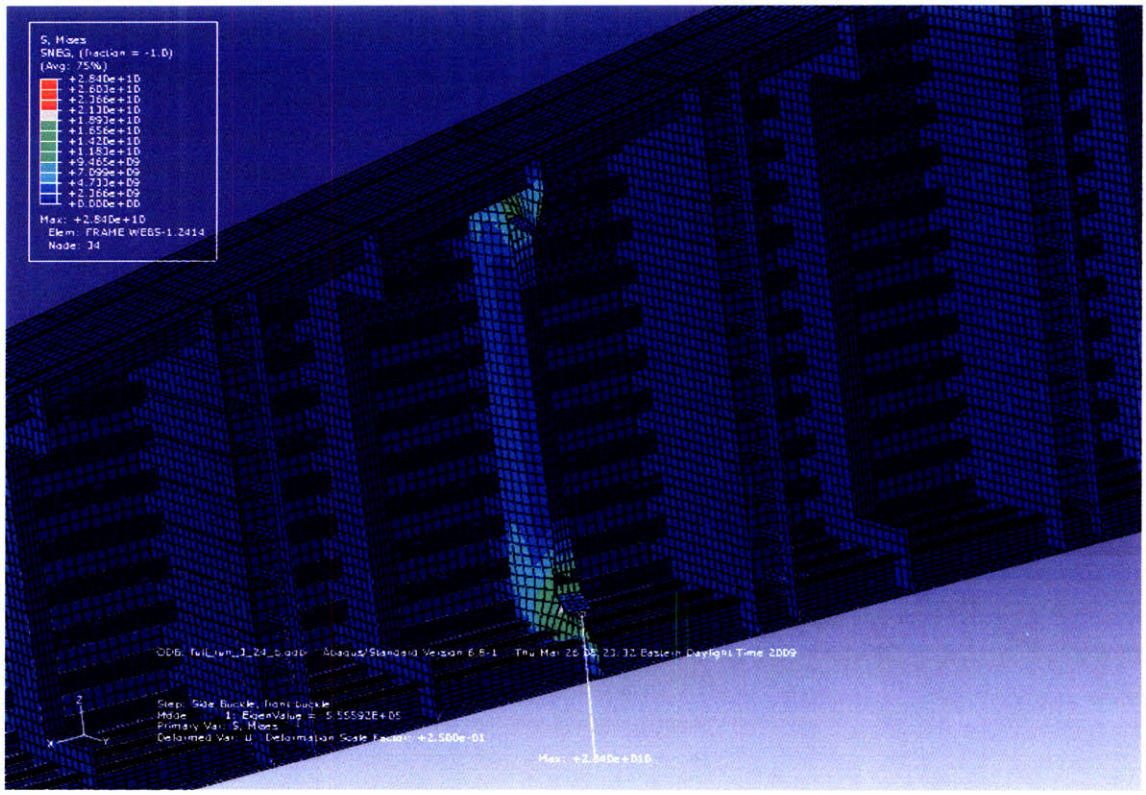

Figure 9.4-ABAQUS Rendering of Mises Stresses for Side Buckle Load

9.3.5 Front Buckle

ABAQUS FEA analysis shows that the required buckling load to reach the bifurcation point is 6MPA. This buckling load is applied to the structure in addition to all the loads applied to the structure in the quasi static steps outlined above. The location of the buckle is the platting at the tension leg end of the pontoon. At the pressure required to cause the structure to buckle the material would have already failed due to plate bending. Therefore buckling will not be observed for this particular load in the pontoon as designed.

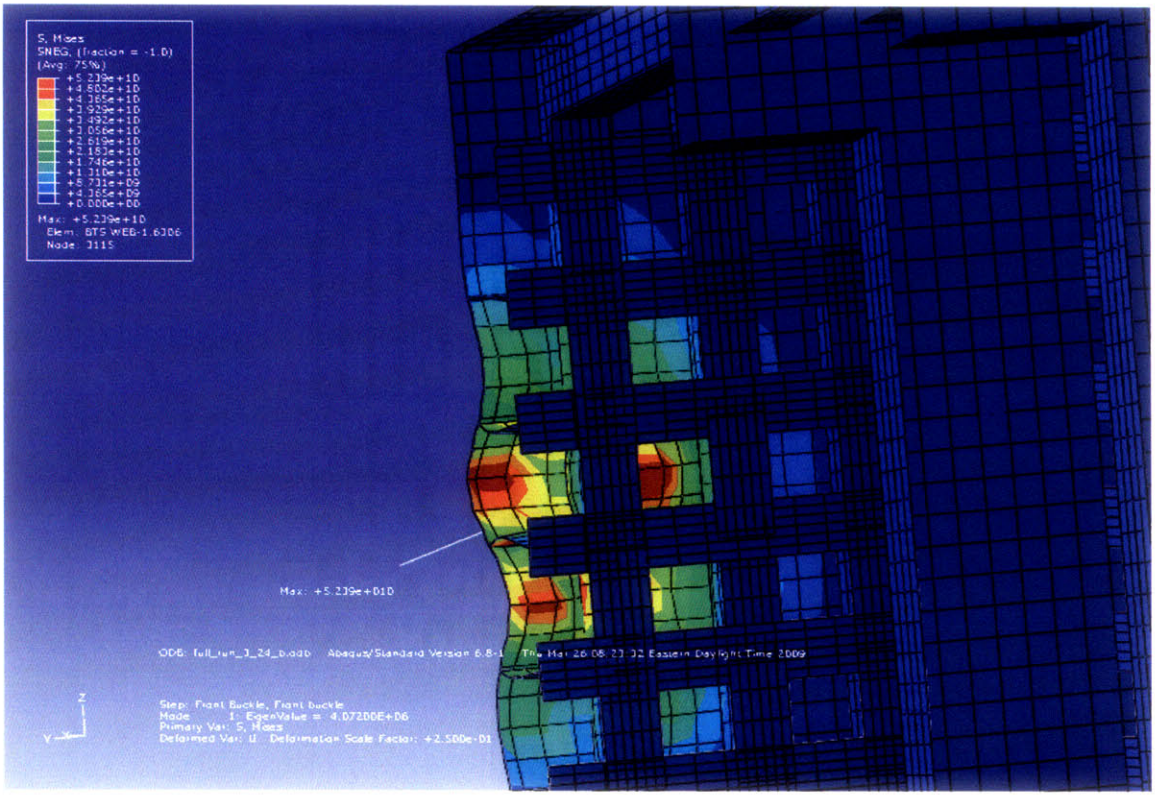

Figure 9.5-ABAQUS Rendering of Mises Stresses for Front Buckle Load

9.3.6 Top and Bottom Buckle

ABAQUS FEA analysis shows that the required buckling load to reach the bifurcation point is 945KPA. This buckling load is applied to the structure in addition to all the loads applied to the structure in the quasi static steps outlined above. The location of the buckle is the bulkhead plating of the first bulkhead as measured from the cylinder to pontoon connection. This is local shell buckling; it is desirable to have local shell buckling be the first mode of buckling to occur in a structure. At the pressure required to cause the structure to buckle the material would have already failed due to plate bending. Therefore buckling will not be observed for this particular load in the pontoon as designed.

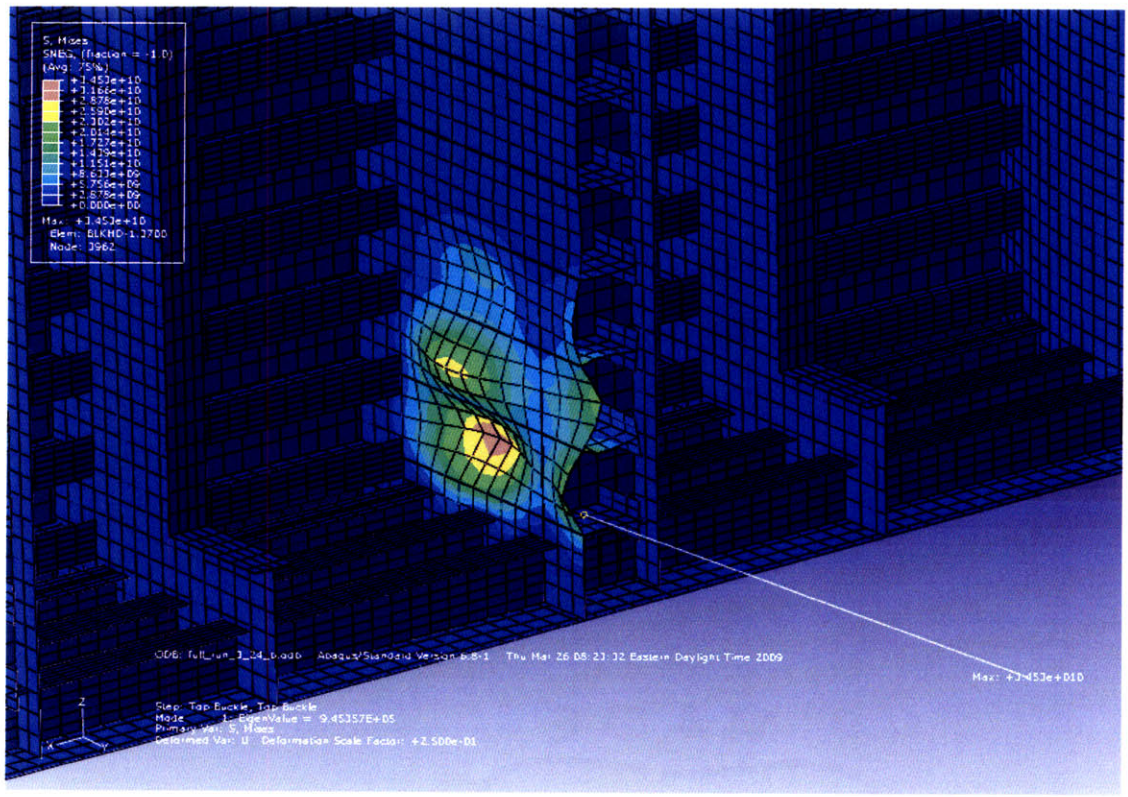

Figure 9.6-ABAQUS Rendering of Mises Stresses for Top and Bottom Load

9.3.7 Natural Frequency

All natural frequency modes between 0 and 70 rad/sec were calculated the first 2 are presented below. The frequency range of typical sea spectra is 0-2 rad/sec. The lowest frequency mode of natural frequencies from the ABAQUS analysis was 36 rad/sec, which is well outside of the range of sea spectra, so wave excitations at the natural frequencies are highly unlikely.

EIGENVALUE OUTPUT				
MODE NO	EIGENVALUE	FREQUENCY (RAD/SEC)	FREQUENCY (CYCLES/SEC)	GENERALIZED MASS
1	1323.6	36.381	5.7902	52799
2	4577.1	67.654	10.767	49582

Figure 9.7-First 2 Natural Frequency modes

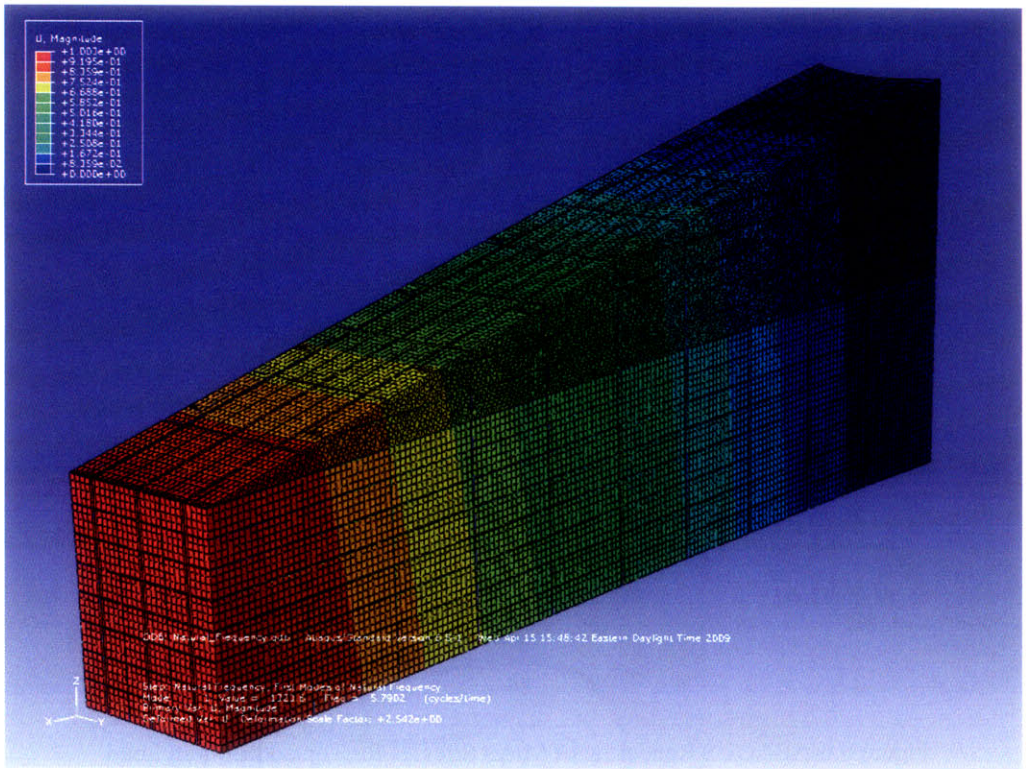

Figure 9.8-First Natural Frequency mode

9.4 Conclusion

The structure as designed by ABS rules passes both ABS rules and FEA via ABAQUS. Its total weight is 209 tons. Standard plate thickness and stiffeners were used in the design.

The plate bending stress due to quasi hydrostatics was the major driver of the structural design. As predicted by ABS rules, by selecting a stiffener layout and properties which are designed to prevent local failure, the global structural requirements are automatically fulfilled. Buckling is not a concern in this structure as the buckling loads are much higher than the experienced loads, and the inception of failure due to plate bending will happen before the buckling loads can be reached.

The structural weight required to resist the given environmental loads was much higher than originally anticipated. This was because of the structural requirements imposed by having such a tall pontoon. Adjusting the overall geometry of the pontoon to decrease the height of the pontoon should be considered.

As a preliminary investigation let a rectangular pontoon with the overall dimensions below be considered.

Height	5 m
Width	5 m
Length	25m

This decreased the unsupported length of the frames significantly. Since in Equation 9.3, unsupported length is the only squared term, this decrease has a profound impact on the required structure and its corresponding weight.

As the pontoon height decreases, the pontoon moves away from the free surface which

decreases the wave influence. A leg geometry change of this kind would have little impact on the submerged volume of the cylinder as the total volume would change by only 16%. Since the height of the pontoon would be lower, its center of gravity would be lower; this requires less ballast and hence compensates for the decrease in volume.

10 Conclusion

The initial structural design presented here provides valuable information as to the approximate weight of the as-designed MIT FWT1. This data will allow the refinement of weight assumptions made in hydrodynamic Pareto optimization codes. Additionally the conclusions drawn from this study provide valuable insight into the best external geometry in terms of structural design, these insights can be combined with conclusions about efficient external geometry in terms of hydrodynamics. For clarity major conclusions from each chapter are listed below.

10.1 Dynamic Water Ballast

This feasibility study shows that for the MIT TLP-1 pontoon proportions and lengths exceeding 22.16m, active dynamic ballasting will reduce the required wind pre-tension. Tension drives the structural steel requirements of the pontoons, the strength of the tension legs, and the size of the mooring system. All of these contribute to the cost of the FWT system. The maximum tension will be reduced significantly for all pontoon lengths which exceed the threshold length, and even be reduced albeit less significantly for lengths not above the threshold. Potential tension reductions versus pontoon lengths are shown below in Figure 10.1.

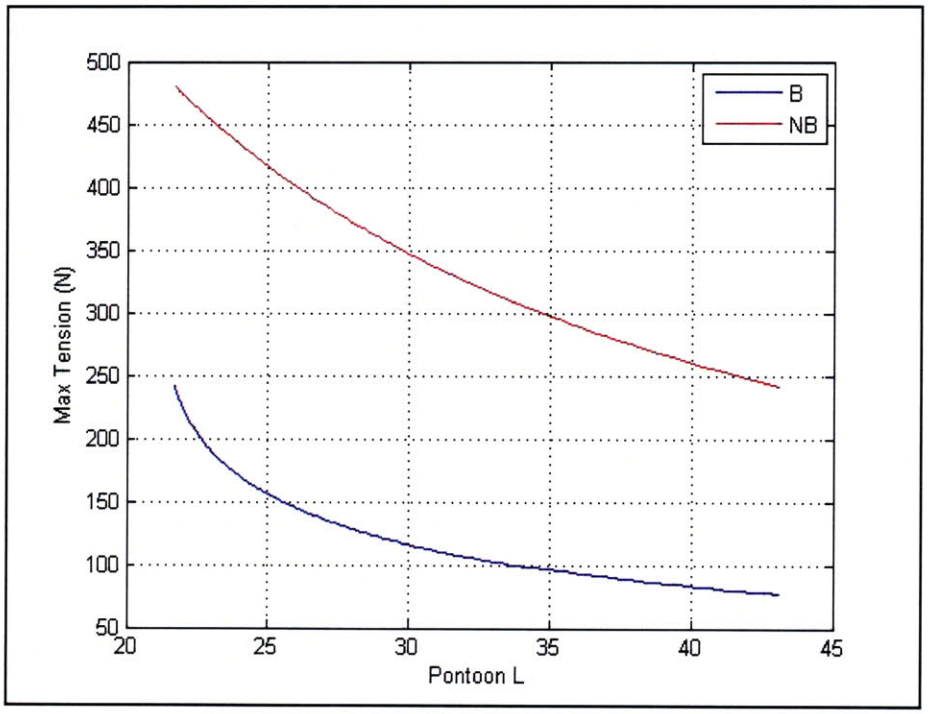

Figure 10.1 Maximum tension versus Pontoon Length

10.2 Tower Design

The API Bulletin 2U and ABAQUS analysis agree in predicting that the tower structure as designed exceeds structural requirements. The maximum stresses for the design are well below the allowable stresses for all failure modes. Eigenvalue frequency extraction analysis shows that the lowest natural frequency mode is below any expected excitation frequency due to typical sea spectrum; however blade passage frequency is higher than the lowest natural frequency mode. Due to weight limitations it is impossible to design the tower as a monocoque cylinder with the lowest natural frequency higher than the blade passage frequency.

The as designed tower has a plate thickness of 20mm, is a monocoque truncated conical cylinder with a maximum diameter of 10m and a minimum diameter of 6 m. The total mass of the tower and nacelle are 700,000 kg.

10.3 Cylinder Design

The structure as yielded from the structural optimization routine passes both ABS rules and API recommendations and is validated via FEA in ABAQUS. Its total weight is 342 tons which is an almost 30% reduction from the design produced by similar system analysis and ABS rules alone. Standard plate thickness and stiffeners were used in the design.

The plate bending stress due to quasi hydrostatics was the major driver of the structural design. The first buckling mode for both axial and hydrostatic buckling occurs as local buckling in the shell. The natural frequencies of the cylindrical section are above any potential exciting frequency.

The table below outlays the specific structural arrangement of the cylindrical section. The overall moment of inertia is 1.02 X 10^8 M^4.

Optimized Properties				
Parameter	Section			Unit
	Bottom	Middle	Top	
Mass/Length	12404.65	10058.99	8594.23	kg/m
Section Mass	78562.78	103942.9	114589.8	kg
N of Vert Stiff	32	32	32	
Vert Flng Thick	0.030	0.030	0.030	m
Vert. Wb Thick	0.015	0.015	0.015	m
Vert Flng Wdth	0.300	0.225	0.150	m
Vert Wb Hght	0.413	0.413	0.413	m
N of Rng Stiff	3	3	3	
Rng Flng Thick	0.020	0.020	0.020	m
Rng Wb Thick	0.020	0.020	0.020	m
Rng Flng Wdth	0.200	0.250	0.200	m
Rng Wb Hght	0.551	0.551	0.551	m
Compartment L	6.333	10.333	13.333	m
Shell thickness	0.020	0.020	0.020	m

Table 8.9- Optimized Cylinder Properties

10.4 Pontoon Design

The structure as designed by ABS rules passes both ABS rules and FEA via ABAQUS. Its total weight is 209 tons. Standard plate thickness and stiffeners were used in the design. The structural weight required to resist the given environmental loads was much higher than originally anticipated. This was because of the structural requirements imposed by having such a tall pontoon. Since in the Equation 9.3, reprinted below, unsupported length is the only squared term, any decrease in the height of the pontoon would have a profound impact on the required structure and its corresponding weight.

(9.3) $$SM = Qfchsl^2$$

Adjusting the overall geometry of the pontoon to decrease the height of the pontoon should be reconsidered. This adjustment is shown to have little effect on the submerged volume of the pontoon for rectangular geometry.

10.5 Natural Frequency of Design

Natural Frequency of the floater design is not a concern in any element. Any section which is subjected to hydrostatic forces requires such extensive reinforcement to resist plate bending and buckling that the structure is sufficiently rigid to exhibit natural frequencies which are much higher than any possible excitation frequencies. Care should be taken during the detailed connection design, to maintain the high rigidity of the rest of the submerged structure.

10.6 Total Weight of Design

The only remaining element of the structural design is the detailed design of the cylinder to pontoon connection. This will require a combination of detail design best practices and FEA calculations. The results of this current thesis will be necessary for the FEA calculations and detailed design of this connection.

If the similar ship analyses cylinder to pontoon design presented in Chapter 8 is used to estimate this section, a first order total structural weight is possible. The total weight of the cylinder to pontoon section of the cylinder is estimated at 200 tons. Based on this weight

estimation, the total MIT TLP-1 structural weight for all elements as currently design is 2078 tons.

11 Future Work

The first step in any future work should be to conduct cost estimation. This cost estimation will provide a bevy of other opportunities for valuable future research. The cost estimation of the FWT must take into account the total instillation cost. This means that an entire installation procedure must be determined and decided on prior to the cost estimation. The cost of the FWT is one of the last great unknowns facing the FWT, and is the most important. The end goal of the MIT FWT project is to show that FWTs can be cost competitive on an industrial scale with fossil fuel energy converters.

The LSPF is currently completing a SPAR FWT design. This design will be structurally optimized via the program written and presented in this thesis for the optimization of the cylindrical section. Cost estimation for the SPAR FWT should be preformed following the structural design. The FWT design ultimately which is ultimately the most promising can then be determined.

Appendix 1-API Bulletin 2U Calculations for Tower

The procedure that was followed is best outlined in the figure below from Bulletin 2U.

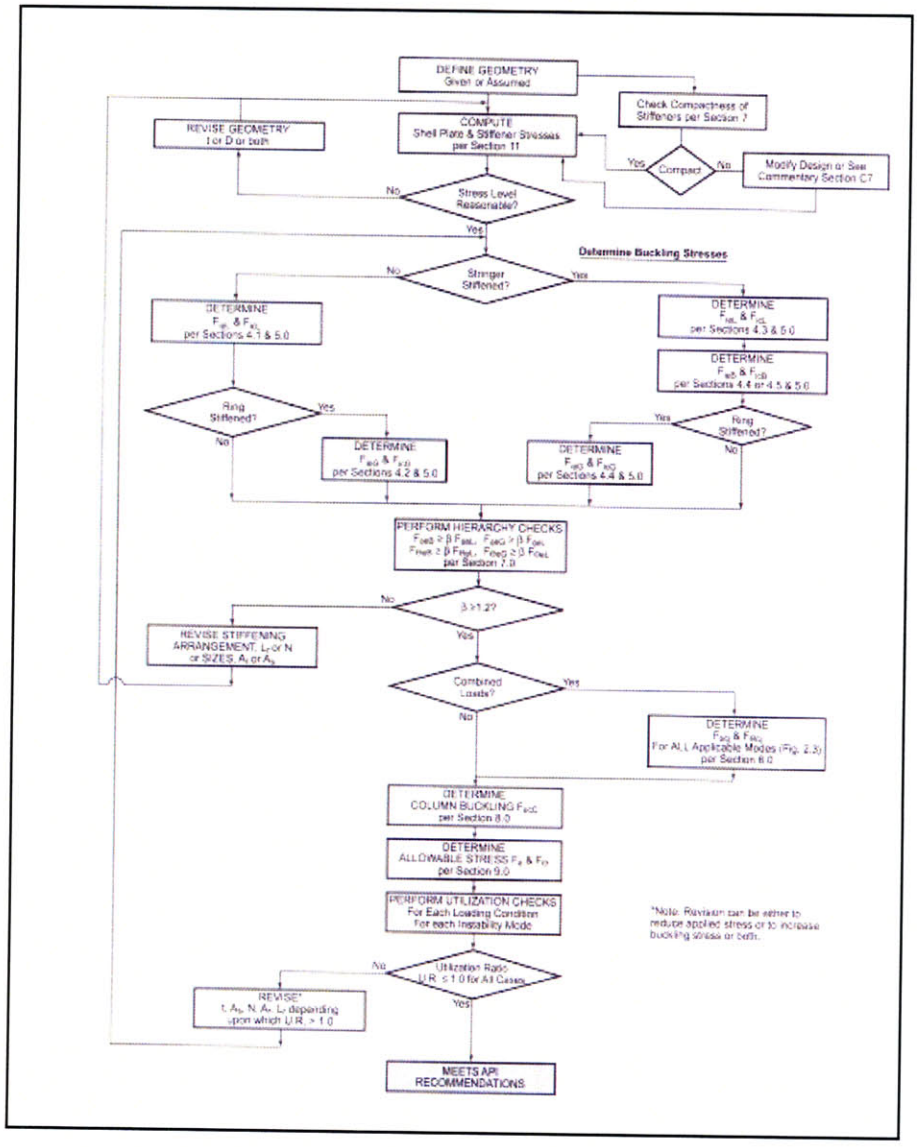

Flow Chart for Meeting API Recommendations

Stress Calculations

The first step in the analysis for a monocoque (un-stiffened) cylinder is to ensure that the bending and yield stress due to the environmental loads are not exceeded in the tower. As recommended by Bulletin 2U this was conducted via ABAQUS. As can be seen in Figure X, the maximum stress experienced in the tower due to all loads was X which is well below the yield stress of mild steel.

Local Shell Buckling

The next analysis step for the monocoque cylinder is to determine the shell elastic and plastic buckling, (F_{ieL}) and (F_{icL}) respectively via equations AX1-AX5.

$$F_{xeL} = C_{xl}\frac{\pi^2 E}{12(1-v^2)}(t/L_r)^2 \qquad \text{AX1}$$

Where the buckling coefficient is defined as

$$C_{xL} = [1+(\frac{150}{(D/t)})(\alpha_{xL})^2(M_x{}^4)]^5 \qquad \text{AX2}$$

Which is a function of the D/t ratio and the geometric curvature parameter, M_x, and imperfection factor, α_{xL}; respectively shown below

$$M_x = L_r/(Rt)^5 \qquad \text{AX3}$$

$$\alpha_{xL} = 9.0 / (300 + D / t)^{.4} \qquad \text{AX4}$$

For the tower, the elastic buckling stress F_{xeL} is 362.4 MPa.

Since $F_{ieL} > .5F_y$ the elastic buckling stress must be reduced via the Plasticity Reduction Factors presented in Section 5 of API 2U.

The plasticity reduction factor, η , is .531 and can be calculated as shown below.

$$\eta = (F_y / F_{xeL}) \left[\frac{1}{\left\langle 1.0 + 3.75(F_y / F_{xeL})^2 \right\rangle} \right]^{1/4} \qquad \text{AX5}$$

Where the corrected Local Shell Buckling stress, F_{xcL} , is equal to 192 MPa and can be calculated via the equation:

$$F_{xcL} = \eta F_{xeL} \qquad \text{AX6}$$

Column Buckling

The next step analysis step for the monocoque cylinder is to determine column buckling. The tower end conditions can be considered to be clamped-free, which means the effective length factor, K, is 2. Where the elastic column buckling, $F_{\phi eC}$, equal to 443MPa for the tower and is given by:

$$F_{\phi eC} = \alpha_{xC} \frac{\pi^2 E}{(KL/r)^2} \qquad \text{AX7}$$

Where r is the radius of vibration given by:

$$r = (.5R^2 + .125t^2)^{1/2} \qquad \text{AX8}$$

Allowable Stresses

The allowable stresses portion applies factors of safety to the structural analysis for the shell buckling and column buckling mode shown below respectively. This is the last portion of the design procedure applicable to monocoque cylinders.

For this cylinder, since the shell buckling stress exceeds yield stress, the factor of safety, FS, specified for local buckling is 1.67. Hence the stress calculated in ABAQUS must not exceed the local buckling stress, F_{xcL} divided by this factor of safety. This requirement is easily met

since the maximum ABAQUS combined bending and axial stress is equal to 40MPa which is less than 114Mpa due to the above safety factor applied to F_{xcL}.

The allowable stresses for column buckling can be from the below equations

$$F_a = \frac{F_{\phi eC}}{FS} \qquad \text{AX9}$$

$$F_b = \frac{F_{xcL}}{FS} \qquad \text{AX10}$$

$$\frac{f_a}{F_a} + \frac{f_b}{F_b} \leq 1.0 \qquad \text{AX11}$$

Where f_a and f_b are the bending and axial strain due to environmental loads, and the FS is the same as defined above. The left side of equation AX11 was calculated at approximately .5 which is well within tolerance.

12 References

1. Jonkman, J.M., Scalvounos, P.D., "Development of Fully Coupled Aeroelastic and Hydrodynamic Models for Offshore Wind Turbines." *AIAA Aerospace Sciences Meeting and Exhibit*, January, 2006.

2. Sclavounos, P. D., *Surface Waves and Their Interaction with Floating Bodies, Lecture Notes,* Massachusetts Institute of Technology, Cambridge, MA

3. Tracy, C., *Parametric Design of Floating Wind Turbines,* Master of Science Thesis, Massachusetts Institute of Technology, 2007

4. Lee, Sungho, *Dynamic Response Analysis of Spar Buoy Floating Wind Turbine Systems,* Masters of Science Thesis, Massachusetts Institute of Technology, 2008

5. Sclavounos, Paul, Chris Tracy, Sungho Lee. "Floating Offshore Wind Turbines: Responses in a Sea State Pareto Optimal Design and Economic Assessment." Proceedings of the 27th Offshore Mechanics and Arctic Engineering OMAE 2008 Conference. June 15-20, 2008, Lisbon, Portugal

6. Musial, W.D.; Butterfield, C.P. "Future for Offshore Wind Energy in the United States" NREL/CP-500-36313 – Energy Ocean Proceedings, Palm Beach, FL, June 2004.

7. Jonkman, J, Butterfield, S., Musial, W., and Scott, G., "Definition of a 5-MW Reference Wind Turbine for Offshore System Development," NREL/TP-500-38060, Golden, CO: National Renewable Energy Laboratory, January 2006

8. Research Reports International, *Offshore Wind Power,* February 2008

9. Wayman, E.N., *Coupled Dynamics and Economic Analysis of Floating Wind Turbine Systems,* Master of Science Thesis, Massachusetts Institute of Technology, 2006

10. Faltiensen, O.M. *Sea Loads on Ships and Offshore Structure, Cambridge,* UK: Cambridge University Press, 1999.

11. Lee, K. H., *Responses of Floating Wind Turbines to Wind and Wave Excitation,* Master of Science Thesis, Massachusetts Institute of Technology, 2004

12. Lee, K. H., Sclavounos, P. D., Wayman, E. N., "Floating Wind Turbines," Workshop on Water Waves and Floating Bodies, May 29, 2005

13. Newman, J. N., *Marine Hydrodynamics,* Cambridge, MA: The MIT Press, 1977

14. Wayman, E.N., Sclavounos P.D., Butterfield S., Jonkman J., Musial W., "Coupled Dynamic Modeling of Floating Wind Turbine Systems," *Offshore Technology Conference,* May, 2006

15. C.H. Lee, *WAMIT THEORY* (Page 1~38) , *Research Project Report to Chevron, Conoco, Exxon, Mobil, Offshore Technology Research Center*, Dept of Ocean Engineering, Massachusetts Institute of Technology, 1995

16. WAMIT® (Chapter 1~7), *version 5.4*, Massachusetts Institute of Technology, 1998

17. Wierzbicki, T., *Structural Mechanics, Lecture Notes,* Massachusetts Institute of Technology, Cambridge, MA

18. Wierzbicki, T., *Plates and shells, Lecture Notes,* Massachusetts Institute of Technology, Cambridge, MA

19. Hughes, O., Ship Structural Design: A Rationally-Based, Computer-Aided Optimization Approach. Jersey City, NJ: SNAME, 1988

20. Kibbe, Stephen. "TLP Technology-Sea Star Minimal Platform for Small Deepwater Reserves" Offshore. Vol 56 issue 6 June 1996

21. Terebushko, O.I., To the buckling analysis and design of stiffened cylindrical shells, Analysis of Thin-Walled Structures, vol. 7, pp. 119–133 (1962)

22. Burns, B. and Almroth, B. "Structural Optimization of Axially Compressed Ring-Stringer Stiffened Cylinders," AIAA Journal of Spacecraft January 1966: 3-1

23. Burns, B. "Structural Optimization of Axially Compressed Cylinders, Considering Ring-Stringer Eccentricity Effects" AIAA Journal of Spacecraft August 1966: 3-8

24. Burns, B. "Optimum Stiffened Cylinders for Combined Axial Compression and Internal or External Pressure," AIAA Journal of Spacecraft January 1968: 5-6

25. "Bulletin on Stability Design of Cylindrical Shells," American Petroleum Institute. June 2004.

26. Block, D.L., Card, M.F., and Mikulas, M. M., "Buckling of Eccentrically Stiffened Orthotropic Cylinders," NASA TN-2960, August 1965

27. Faulkner, D., Chen, Y. N. and deOliveira, J. G., "Limit State Design Criteria for Stiffened Cylinders of Offshore Structures," ASME 4th National Congress of Pressure Vessels and Piping Technology, Portland, Oregon, June 1983.